Leading proton production in deep inelastic scattering at HERA

JHEP06(2009)074

(http://iopscience.iop.org/1126-6708/2009/06/074)

Published by IOP Publishing for SISSA

Received: *December 19, 2008*
Revised: *March 26, 2009*
Accepted: *June 3, 2009*
Published: *June 24, 2009*

JHEP06(2009)074

Leading proton production in deep inelastic scattering at HERA

ZEUS collaboration

E-mail: tobias.haas@desy.de

Abstract: The semi-inclusive reaction $e^+p \to e^+Xp$ was studied with the ZEUS detector at HERA with an integrated luminosity of 12.8 pb^{-1}. The final-state proton, which was detected with the ZEUS leading proton spectrometer, carried a large fraction of the incoming proton energy, $x_L > 0.32$, and its transverse momentum squared satisfied $p_T^2 < 0.5\,\mathrm{GeV}^2$; the exchanged photon virtuality, Q^2, was greater than $3\,\mathrm{GeV}^2$ and the range of the masses of the photon-proton system was $45 < W < 225\,\mathrm{GeV}$. The leading proton production cross section and rates are presented as a function of x_L, p_T^2, Q^2 and the Bjorken scaling variable, x.

Keywords: Lepton-Nucleon Scattering

ArXiv ePrint: 0812.2416v1

doi:10.1088/1126-6708/2009/06/074

Contents

JHEP06(2009)074

1 Introduction

Hadron-hadron collisions predominantly give rise to leading particles of the same type as those in the incoming beams and carrying a large fraction of the momentum of incoming particles. The spectrum of leading particles approximately scales with the centre-of-mass energy, a property known as limiting fragmentation [1]. The properties of the accompanying final state are also universal when studied as a function of the centre-of-mass energy available after excluding the leading particles [2, 3].

Events with a final-state proton carrying a large fraction of the available energy, x_L, but a small transverse momentum, p_T, have been studied in detail in high-energy hadron-proton collisions [4–6]. More recently, the HERA experiments reported measurements of

the production of leading protons in ep collisions [7, 8]. Several mechanisms have been suggested to explain the production of leading protons. None of them are, as yet, amenable to calculations based on perturbative quantum chromodynamics (pQCD). This is, in part, a consequence of the small values of p_T of the leading proton which necessitates a non-perturbative approach. Some models [9–13] are based on the Regge formalism, with leading proton production occurring through t-channel exchanges, both isoscalar and isovector, notably of the Pomeron, pion and Reggeon trajectories. These exchanges mediate the interaction between the proton and the hadronic fluctuations of the virtual photon. Other models retain quarks and gluons as fundamental entities, but add non-perturbative elements, such as soft-colour interactions (SCI) [14]. Alternatively, the concept of fracture functions [15] offers a QCD framework in which to describe the leading baryon momentum spectra.

This paper presents measurements of leading proton production in e^+p collisions, $e^+p \to e^+Xp$, with a four-fold increase in statistics compared to an earlier measurement [7]. High-energy protons with low transverse momentum carrying at least a fraction x_L=0.32 of the incoming-proton momentum were measured in the ZEUS leading proton spectrometer (LPS) [16]. All the six LPS stations are used, for the first time, to perform the measurements presented in this paper. The cross sections are presented as a function of the proton variables x_L and p_T^2. The dependence on the Bjorken variable, x, and on the photon virtuality, Q^2, was also studied and compared to that of the inclusive deep inelastic scattering (DIS) reaction $e^+p \to e^+X$. The measurements cover the kinematic range $Q^2 > 3\,\mathrm{GeV}^2$ and $45 < W < 225\,\mathrm{GeV}$, where W is the total mass of the photon-proton system. The data for $x_L > 0.93$ were used in an earlier study [17] to extract the diffractive structure function of the proton.

The leading proton structure function, F_2^{LP}, defined in section 3, which can be identified with a fracture function, is also presented. The latter parameterises the momentum spectra of leading particles through parton distribution functions in the proton. This approach can be incorporated in Monte Carlo (MC) programs simulating hadronic final states in pp interactions at the LHC [18] and extended cosmic-ray showers [19, 20].

2 Experimental set-up

The measurements were performed with data collected in 1997 at the ep collider HERA using the ZEUS detector, when HERA operated with a proton beam energy $E_p = 820\,\mathrm{GeV}$ and a positron beam energy $E_e = 27.5\,\mathrm{GeV}$.

A detailed description of the ZEUS detector can be found elsewhere [21]. A brief outline of the components which are most relevant for this analysis is given below.

Charged particles were tracked in the central tracking detector (CTD) [22], which operated in a magnetic field of 1.43 T provided by a thin superconducting coil. The CTD consisted of 72 cylindrical drift chamber layers, organized in 9 superlayers covering the polar angle[1] region $15° < \theta < 164°$. The transverse-momentum resolution for full-length

[1] The ZEUS coordinate system is a right-handed Cartesian system, with the Z axis pointing in the proton beam direction, referred to as the "forward direction", and the X axis pointing left towards the center of HERA. The coordinate origin is at the nominal interaction point.

JHEP06(2009)074

tracks was $\sigma(p_T)/p_T = 0.0058 p_T \oplus 0.0065 \oplus 0.0014/p_T$, with p_T in GeV.

The high-resolution uranium-scintillator calorimeter (CAL) [23] consisted of three parts: the forward (FCAL), the barrel (BCAL) and the rear (RCAL) calorimeters. Each part was subdivided transversely into towers and longitudinally into one electromagnetic section (EMC) and either one (in RCAL) or two (in BCAL and FCAL) hadronic sections (HAC). The smallest subdivision of the calorimeter is called a cell. The CAL energy resolutions, as measured under test-beam conditions, were $\sigma(E)/E = 0.18/\sqrt{E}$ for electrons and $\sigma(E)/E = 0.35/\sqrt{E}$ for hadrons, with E in GeV.

The position of the scattered positron was determined by combining information from the CAL, the small-angle rear tracking detector [24] and the hadron-electron separator [25].

The LPS [16] was used during the data-taking period 1994−2000 to detect positively charged particles scattered at very small angles and carrying a large fraction of the longitudinal momentum of the incoming proton. It consisted of 54 planes of silicon microstrip detectors grouped into six stations, S1 to S6, and located along the outgoing proton beam line between $Z = 20$ m and $Z = 90$ m.

The reconstruction program built tracks considering S1, S2, S3 and S4, S5, S6 as two independent spectrometers, called s123 and s456, respectively. Among all hit combinations in s123 and s456, the track with more planes was chosen, with the requirement that the track passed in at least two stations of the same spectrometer. Because of the different phase space covered by the two spectrometers, a track cannot pass through pairs of stations in both s123 and s456. Hence a track is assigned to only one spectrometer.

The alignment procedure is identical for s123 and s456 as far as relative alignment of single planes in a pot is concerned. The spectrometer s456 was aligned first [16]. A small sample of s456 tracks passing through S1 was used to fix S1 position. The remaining stations S2 and S3 were independently aligned by using coincidences with S1. Their positions were fitted by requiring the extrapolated vertex position to be at the nominal ZEUS interaction point and by requiring the diffractive peak to be at $x_L = 1$.

During data taking, the stations were inserted very close to the proton beam (typically a few mm). Charged particles inside the beampipe were deflected by the magnetic field of the proton-beamline magnets and measured in the LPS with a resolution better than 1% on the longitudinal momentum and of 5 MeV on the transverse momentum. The beam transverse momentum spread at the interaction point was ≈ 40 MeV in the horizontal plane and ≈ 90 MeV in the vertical plane and dominated the transverse-momentum resolution which is 20% on average.

A forward neutron calorimeter (FNC) [26] was installed in the HERA tunnel at $\theta = 0^\circ$ and at $Z = 106$ m from the interaction point in the proton-beam direction. The FNC, a lead-scintillator calorimeter, had an energy resolution for hadrons $\sigma(E)/E = 0.70/\sqrt{E}$, with E in GeV, as measured in a test beam. The calorimeter was segmented vertically into 14 towers. Three planes of veto counters were located in front of the FNC to reject events in which a particle showered in inactive material along the beamline upstream of the FNC.

The luminosity was measured from the rate of the bremsstrahlung process $ep \to e\gamma p$. The resulting small-angle energetic photons were measured by the luminosity monitor [27], a lead-scintillator calorimeter placed in the HERA tunnel at $Z = -107$ m.

JHEP06(2009)074

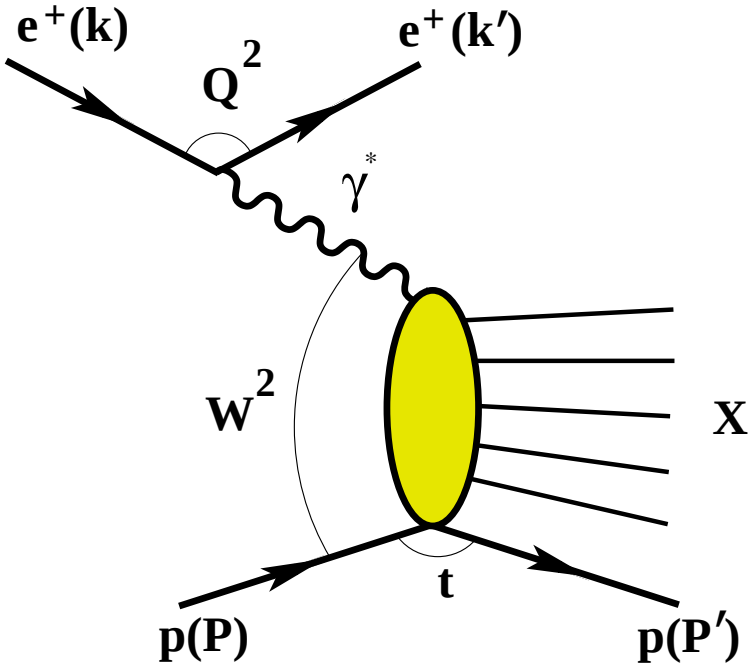

Figure 1. Schematic diagram of the reaction $e^+p \to e^+Xp$.

3 Kinematics and cross sections

Figure 1 illustrates semi-inclusive leading proton production in ep collisions. Four kinematic variables are needed to describe the reaction $e^+p \to e^+Xp$. They are defined in terms of the four-momenta of the incoming and outgoing positron, k and k', and of the incoming and outgoing proton, P and P', respectively.

The Lorentz-invariant kinematic variables used in inclusive studies are $Q^2 = -q^2 = -(k-k')^2$, the virtuality of the exchanged photon; $x = Q^2/(2P\cdot q)$ and the inelasticity, $y = q\cdot P/(k\cdot P) \simeq Q^2/(sx)$; $W^2 = (P+k-k')^2 = m_p^2 + Q^2(1-x)/x$, the square of the photon-proton centre-of-mass energy. In these equations, m_p is the mass of the proton and $\sqrt{s} = 300\,\mathrm{GeV}$ is the e^+p centre-of-mass energy. Among these variables, only two are independent.

Two additional variables are required to describe the leading proton. They are chosen as the momentum fraction carried by the outgoing proton

$$x_L = \frac{P'\cdot k}{P\cdot k}$$

and its transverse momentum with respect to the direction of the incoming proton, p_T. In terms of these variables, the square of the four-momentum transfer from the target proton is given by

$$t = (P-P')^2 \simeq -\frac{p_T^2}{x_L} - \frac{(1-x_L)^2}{x_L}m_p^2,$$

JHEP06(2009)074

where the second term is the minimum kinematically-allowed value of $|t|$ for a given x_L. The variable t is the square of the four-momentum of the exchanged particle.

The differential cross section for inclusive $e^+p \to e^+X$ scattering, in the Q^2 region of this analysis, is written in terms of the proton structure function, $F_2(x, Q^2)$, as

$$\frac{d^2\sigma_{e^+p\to e^+X}}{dxdQ^2} = \frac{4\pi\alpha^2}{xQ^4}\left(1 - y + \frac{y^2}{2}\right) F_2(x, Q^2)(1 + \Delta), \tag{3.1}$$

where Δ is a correction that takes into account the contribution of the longitudinal structure function, F_L, and of electroweak radiative effects. Similarly, the differential cross section for semi-inclusive leading proton (LP) production can be written in terms of the leading proton structure function, $F_2^{\mathrm{LP}(4)}(x, Q^2, x_L, p_T^2)$, as

$$\frac{d^4\sigma_{e^+p\to e^+Xp}}{dxdQ^2dx_Ldp_T^2} = \frac{4\pi\alpha^2}{xQ^4}\left(1 - y + \frac{y^2}{2}\right) F_2^{\mathrm{LP}(4)}(x, Q^2, x_L, p_T^2)(1 + \Delta_{\mathrm{LP}}), \tag{3.2}$$

where Δ_{LP} is the analogue of Δ.

The structure function $F_2^{\mathrm{LP}(4)}(x, Q^2, x_L, p_T^2)$ corresponds to the proton-to-proton fracture function $M_2^{p/p}(x, Q^2, x_L, p_T^2)$ [15], i.e. the structure function of a proton probed under the condition that the target fragmentation region contains a proton with a given x_L and p_T^2.

4 Reconstruction of the kinematic variables

In the Q^2 range of this analysis, DIS events are characterised by the presence of a scattered positron, mostly in RCAL. The scattered positron was reconstructed using an electron finder algorithm based on a neural network [28].

The properties of the hadronic final state in the central detector were derived using the energy flow objects (EFOs) [29] reconstructed from CAL clusters and CTD tracks by combining the CTD and CAL information to optimise the resolution of the reconstructed kinematic variables. The EFOs were additionally corrected for energy loss due to inactive material in front of the CAL.

The DIS variables x, y, Q^2 and W were obtained by using a weighting method [30], which uses a weighted average of the values determined from the electron [31] and double-angle [32] methods. The variable y was also reconstructed using the Jacquet-Blondel method [33], which uses information from the hadronic final state to reconstruct the event kinematics, and is denoted by y_{JB}.

The momentum $p = (p_X, p_Y, p_Z)$ of the leading proton candidate was determined using the LPS. The variable x_L was evaluated as $x_L = p_Z/E_p$ and the squared transverse momentum as $p_T^2 = p_X^2 + p_Y^2$.

5 Data sample and event selection

During 1997, the ZEUS detector collected an integrated luminosity of 27.8 pb^{-1}. However, the experimental conditions allowed the LPS to be operated only for an integrated

JHEP06(2009)074

luminosity of 12.8 pb^{-1}. Of this sample, 4.8 pb^{-1} of data were collected with all the LPS stations. In the remaining part, only the spectrometer s456 was used.

Online, a three-level trigger [34] was used. At the third level, the event variables were reconstructed with an accuracy close to that obtained offline. Final detector calibration and full-event reconstruction were performed offline.

Two sets of events were selected [35]: the inclusive DIS sample and the LPS sample. For a fraction of the inclusive DIS candidate events the trigger was prescaled, thus reducing the effective integrated luminosity of the inclusive DIS sample to 1 pb^{-1}. The selection of the LPS sample was performed with a dedicated LPS trigger.

The LPS trigger was implemented at the third level. The algorithm performed a reconstruction of track segments in each of the detector assemblies inside a pot by geometrically matching the hits on the planes with same strip orientation and by combining them with matching hits in the other projections. A "track quality" was defined for each candidate which reflected the number of hits contributing to a track segment in a pot. All the geometrical cuts as well as a final cut on the minimum track quality were slightly looser than the cuts applied in the offline reconstruction. Studies performed on an unbiased sample of LPS tracks showed a trigger efficiency of 100%.

The presence of a good positron candidate in the CAL was required in the trigger chain used to select the inclusive DIS sample. In addition, the following conditions were applied:

- $|Z_{\rm vtx}| < 50$ cm, where $Z_{\rm vtx}$ is the Z coordinate of the event vertex. This cut is needed to remove background due to proton beam-gas interactions and cosmic rays;
- energy of the scattered positron $E'_e > 10\,\text{GeV}$. The positron position was required to be outside the region close to the rear beampipe hole, where the presence of inactive material reduced the precision of the energy measurement;
- the quantity $E - P_Z$, where the energy E and the longitudinal momentum P_Z are summed over all the EFOs and the scattered positron, in the range $38 < E - P_Z < 65\,\text{GeV}$, to exclude background from photoproduction, proton beam-gas interactions and cosmic rays;
- $y_{\rm JB} > 0.03$ in order to ensure hadronic activity away from the forward direction.

The following cuts define the kinematic region:

- $Q^2 > 3\,\text{GeV}^2$, to select DIS events with large virtuality of the exchanged photon;
- $45 < W < 225\,\text{GeV}$, to ensure a wide kinematic coverage of the hadronic system.

The number of events that passed the inclusive DIS selection cuts was 145447.

The LPS sample was subjected to the same selection as the DIS sample. In addition, the LPS trigger and the following conditions were required:

- a reconstructed track in the LPS with $p_T^2 < 0.5\,\text{GeV}^2$ and $x_L > 0.32$. To reduce the sensitivity of the LPS acceptance to the uncertainties in the location of the beampipe elements, a cut was applied to the variable $\Delta_{\rm pipe}$, the minimum distance between the

JHEP06(2009)074

track and the beampipe anywhere along the beamline. Since the spectrometers s123 and s456 are completely independent (see section 2), different requirements were applied, $\Delta_{\rm pipe} > 0.25$ cm for s123 and $\Delta_{\rm pipe} > 0.04$ cm for s456, in order to exclude regions where the Monte Carlo did not reproduce the data.

The selection of tracks with $\Delta_{\rm pot} > 0.02$ cm, where $\Delta_{\rm pot}$ is the minimum distance of the track from the edge of any LPS detector, ensured that the tracks were well within the active regions of the silicon detectors;

- the sum of the energy and the longitudinal momentum of both the energy deposits in the CAL and the particle detected in the LPS, $E + P_Z$, was required to be smaller than 1655 GeV; this cut rejected most of the random overlays of DIS events with protons from the beam-halo or from a proton beam-gas collision (see section 8).

A total of 73275 events survived the above selection criteria, of which 6008 had a track in s123 and 67267 had a track in s456.

6 Monte Carlo simulation

To determine the acceptance of the apparatus, inclusive DIS events with $Q^2 > 0.5\,\text{GeV}^2$ were generated with DJANGOH [37], which is interfaced to HERACLES [38] for electroweak radiative effects. In order to study the migration of events from low Q^2, a sample of photoproduction events with $Q^2 < 0.5\,\text{GeV}^2$ was generated with PYTHIA [39]. In the MC samples, the hadronic final state was generated with the Matrix Element Parton Shower model (MEPS) [40] for QCD radiation and JETSET [41] for hadronisation. The diffractive events in DJANGOH were generated by means of the soft-colour-interaction mechanism (SCI) [14].

All MC events were passed through the standard simulation of the ZEUS detector, based on GEANT 3.13 [42], and of the trigger and through the same reconstruction and analysis programs as the data. The simulation included the geometry of the beampipe apertures, the magnetic field along the leading proton trajectory and the proton-beam emittance.

To obtain a good description of the data, it was necessary to reweight the leading proton x_L and p_T^2 distributions generated by the MC [35, 43]; the fraction of diffractive events with respect to the total was also reweighted in bins of x_L. In particular, the slope of the exponential p_T^2 distribution, ranging from 2.5 to 4.5 GeV^{-2}, was increased by a constant value $\Delta b = 3.4\,\text{GeV}^{-2}$ and the x_L spectrum was reweighted to a flat distribution below the diffractive peak. The reweighting parameters were chosen according to previous measurements [7]. The reweighting preserved the total MC cross section.

For the LPS sample, the comparison between the data and the sum of the reweighted MC samples (DJANGOH and PYTHIA), for the DIS variables and the LPS specific variables, is shown in figures 2 and 3. The reweighted MC describes the data of the single spectrometers within the systematic uncertainties (see section 9), and the combined plots are shown. The LPS variable $\Delta_{\rm pipe}$ is not perfectly reproduced by the reweighted MC, but the selection cut applied is far from the region in which the disagreement is observed.

JHEP06(2009)074

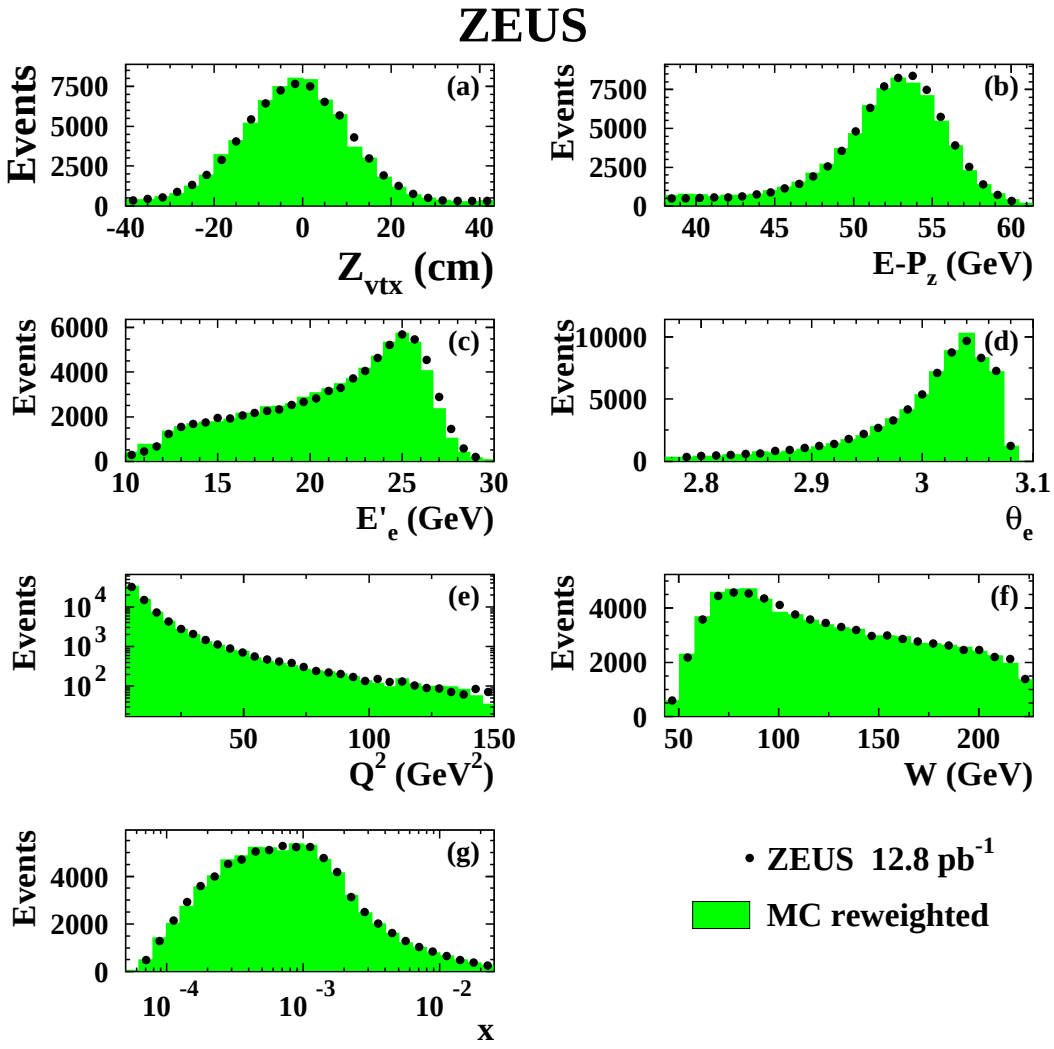

Figure 2. Comparison between data (dots) and reweighted MC (shaded histograms) for DIS quantities for the LPS sample: (a) Z coordinate of the vertex, (b) $E - P_Z$ distribution, (c) energy of the scattered positron, E'_e, (d) polar angle of the scattered positron, θ_e, (e) virtuality of the exchanged photon, Q^2, (f) invariant mass of the hadronic system, W, and (g) Bjorken scaling variable, x.

7 Acceptance

The acceptance was defined as the ratio of the number of reconstructed events in a bin to the number of generated events in that bin. This definition includes the effects of the geometrical acceptance of the apparatus, its efficiency and resolution, and the event selection efficiency. Figure 4 shows the acceptances of the LPS station combinations s123 and s456 as a function of x_L and p_T^2. The maximum acceptance is 10% in the region

JHEP06(2009)074

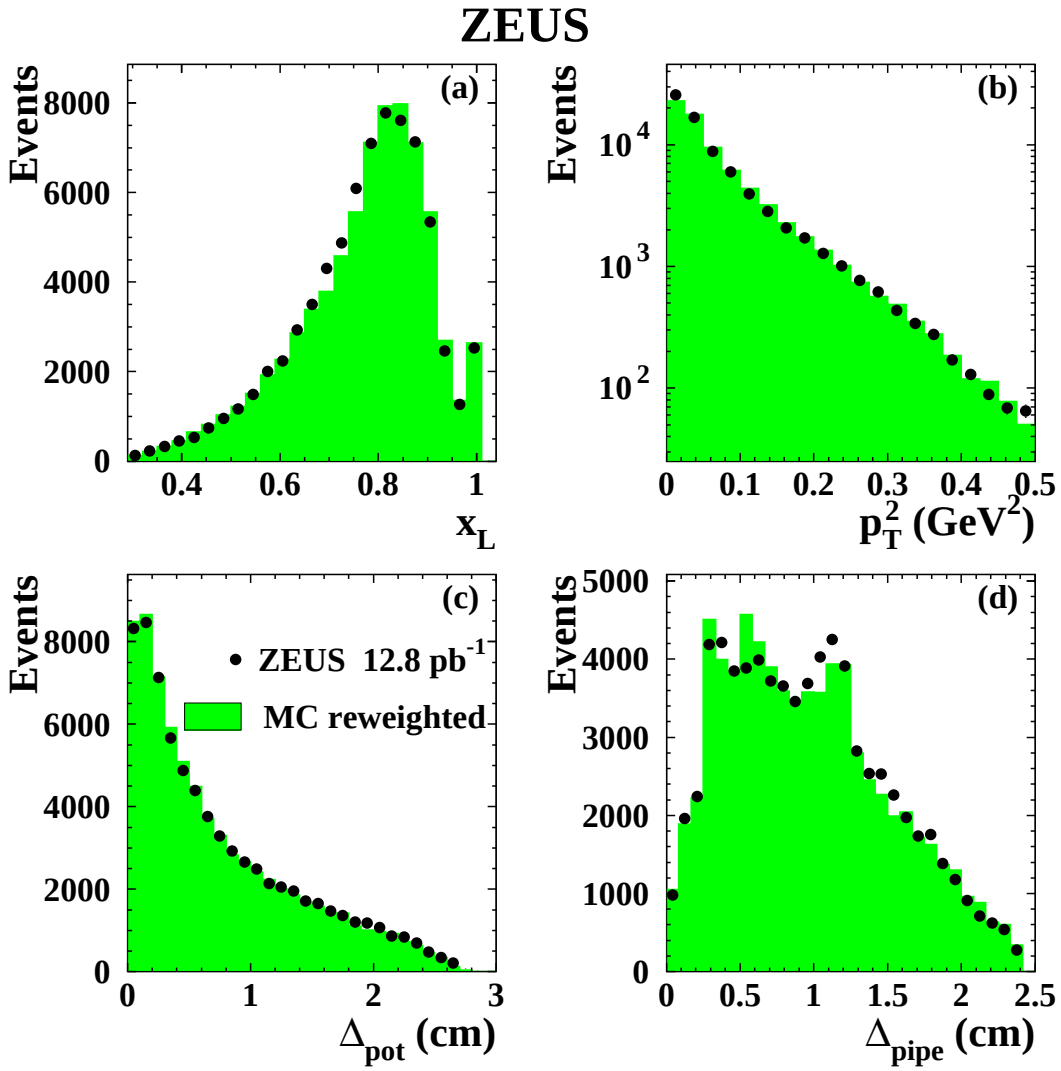

Figure 3. Comparison between data (dots) and reweighted MC (shaded histograms) for LPS specific quantities: (a) fractional longitudinal momentum, x_L, (b) squared transverse momentum, p_T^2, (c) minimum track distance from the edge of the pot, $\Delta_{\rm pot}$, and (d) minimum track distance from the beampipe, $\Delta_{\rm pipe}$.

$0.63 < x_L < 0.65$, $0.05 < p_T^2 < 0.1\,\mathrm{GeV}^2$ for the spectrometer s123 and 52% in the region $0.77 < x_L < 0.8$, $p_T^2 < 0.05\,\mathrm{GeV}^2$ for the spectrometer s456.

The analysis bins were chosen according to the LPS acceptance, resolution (see section 2) and available statistics.

For completeness, also shown in figure 4 are the three regions of p_T^2 used for the cross-section measurements.

JHEP06(2009)074

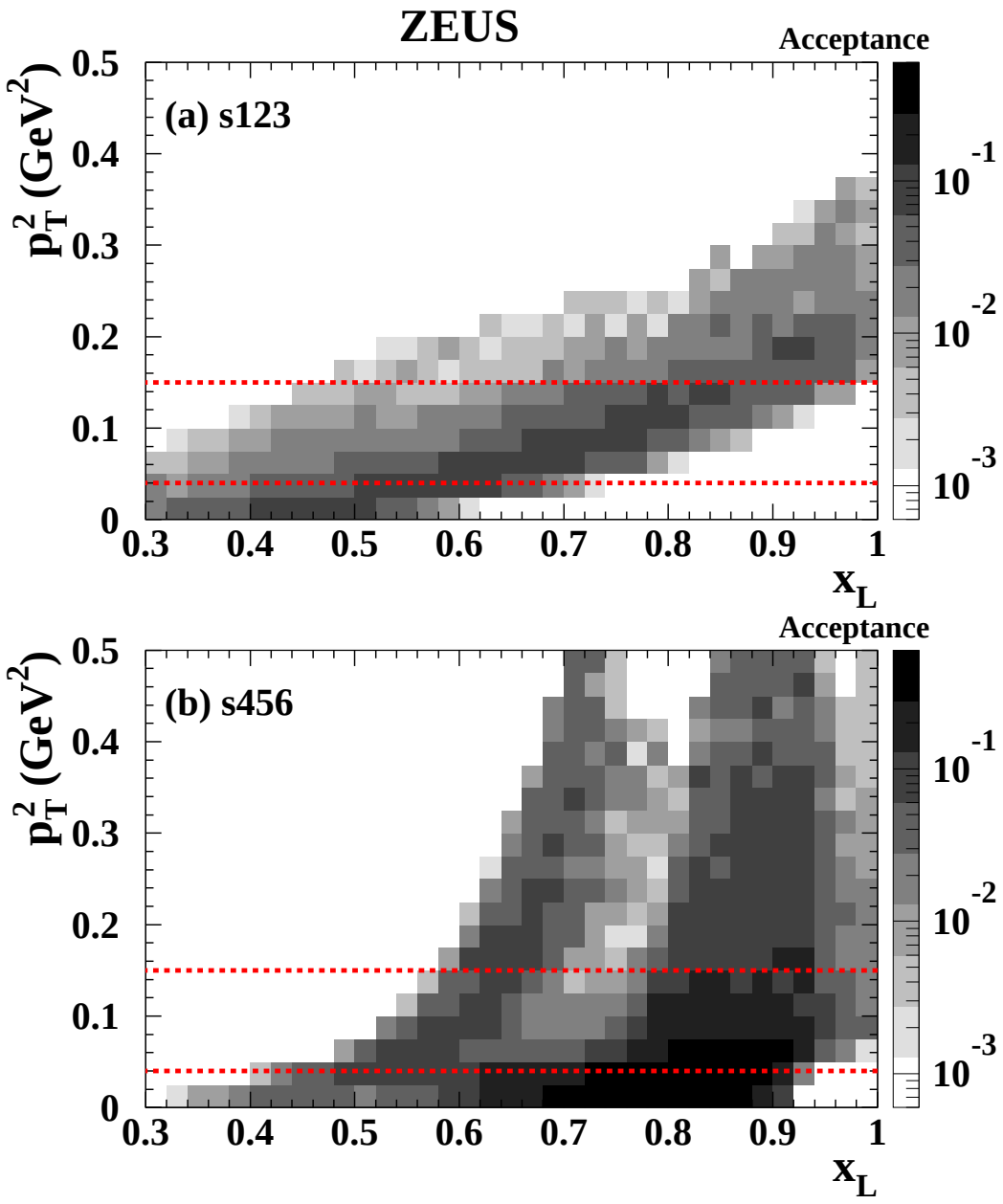

Figure 4. Acceptance of the LPS spectrometers (a) s123 and (b) s456 in the x_L, p_T^2 plane. The dashed lines delimit the three p_T^2 integration ranges.

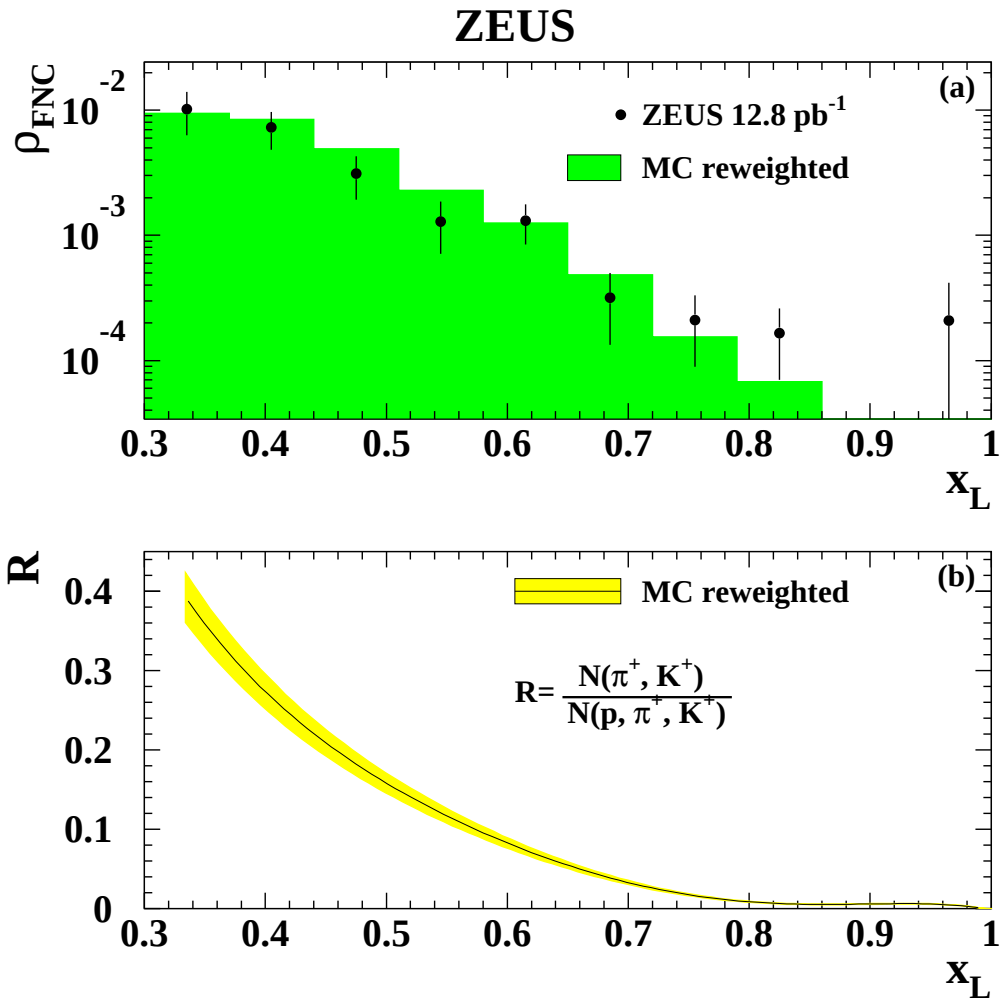

Figure 5. (a) Ratio $\rho_{\rm FNC}$ of the number of events with a track in the LPS and a neutron candidate in the FNC to the number of events with a track in the LPS. The dots represent the data and the shaded histogram the reweighted MC; (b) expected fraction R of positive pions and kaons reconstructed in the LPS as a function of x_L. The error band reflects the statistical uncertainty derived from the LPS-FNC data sample.

8 Background studies

The LPS data sample contains three background contributions,

- non-baryon contributions;
- overlay events;
- misidentified low-Q^2 background.

JHEP06(2009)074

The LPS had no particle identification capability, but MC studies indicate that most high-x_L particles in the LPS are protons. The MC expectations were tested with a subsample of LPS-tagged events where a neutron candidate was found in the FNC [36]. The neutron candidate was required to have a minimum energy deposit of 50 GeV and the total $E + P_Z$ of the event, including the neutron, was required to be below 1750 GeV. A total of 47 events were found. For this class of events the track in the LPS is most likely either a π^+ or a K^+. Figure 5a shows the ratio $\rho_{\rm FNC}$ of the number of events with a track in the LPS and a neutron candidate in the FNC to the number of events with a track in the LPS. The reweighted MC describes the data well and therefore can be used to subtract the background. The fraction R of events with a positive meson reconstructed in the LPS, evaluated with the reweighted MC, is shown in figure 5b as a function of x_L. The fraction R in the MC was found to be independent of p_T^2. It is substantial at low x_L and falls below 10% above $x_L \approx 0.6$. This contribution was subtracted.

The $E + P_Z$ spectrum for the beam-halo events was constructed as a combination of generic DIS events and a beam-halo track reconstructed in the LPS in randomly triggered events. The $E+P_Z$ distribution was normalised to the data for $E+P_Z > 1685$ GeV, which mainly contain beam-halo events. The background remaining after the $E+P_Z < 1655$ GeV cut was negligible for $x_L < 0.9$, and reached $(8 \pm 3)\%$ for $x_L > 0.98$. The expected fraction of overlay events was subtracted.

The acceptance corrections were calculated by means of the reweighted MC generated with $Q^2 > 2$ GeV^2. The contribution of events which migrate from the region $Q^2 < 2$ GeV^2 was found to be independent of x_L and p_T^2 and equal to $(7.3 \pm 0.5)\%$; it was subtracted.

9 Systematic studies

The systematic uncertainties were calculated by varying the cuts and by modifying the analysis procedure. The stability of the DIS selection was checked by varying the selection cuts,

- the $|Z_{\rm vtx}|$ cut was varied by ± 10 cm;
- the cut on the scattered positron energy was varied by $\pm$ 2 GeV and the width of the fiducial region in the rear calorimeter was varied by 0.5 cm in the X and Y directions;
- the $E - P_Z$ cut was changed to $35 < E - P_Z < 68$ GeV and $41 < E - P_Z < 62$ GeV;
- the $y_{\rm JB}$ cut was raised to 0.04.

The observed changes in the cross section were below 1% and neglected. The variation in the LPS selection of the $\Delta_{\rm pipe}$ threshold by $\pm$ 0.03 cm and the $\Delta_{\rm pot}$ threshold by $\pm$ 0.01 led to negligible changes in the cross section ($< 1\%$).

The following checks resulted in non-negligible systematic uncertainties of the cross section (the mean value is given in brackets):

- the reweighting parameter Δb was varied by ± 0.9 GeV^{-2}, compatible with the spread of b versus x_L $(^{+6.8\%}_{-5.9\%})$;

- the subtracted fraction of background from π^+ and K^+ reconstructed in the LPS was varied by the statistical uncertainty derived from the LPS-FNC data (see figure 5) ($^{+1.7\%}_{-1.7\%}$ for $x_L < 0.7$);
- the fraction of overlay events to be subtracted from the data was increased and decreased by its statistical uncertainty ($^{+2.0\%}_{-2.0\%}$ for $x_L > 0.9$);
- the uncertainty on the beam optics was evaluated by varying the transverse momentum spread of the proton beam in the MC by ±10% [17] and led to a change of typically ±1.4%. In addition, the positions of the LPS stations were varied to reflect the actual position of the stations during the data-taking period. This was done because, in the simulation, the MC assumes only one average position ($^{+2.5\%}_{-1.8\%}$). In the diffractive region the uncertainty related to the beam optics increased to ±10%.

The resulting total systematic uncertainty, obtained by adding in quadrature all the individual systematic uncertainties (combining positive and negative contributions separately), excluding an overall normalisation uncertainty of 2% from the luminosity measurement, is shown in the figures as an error band, that includes both a correlated and an uncorrelated component.

10 Results

All measurements were performed separately with the s123 and s456 spectrometers, and were then combined in a weighted average, using only statistical uncertainties. This procedure was repeated for every systematic check. Some measurements are presented as normalised to the inclusive DIS cross section, $\sigma_{\rm inc}$, determined from the inclusive DIS sample described in section 5. All cross-section measurements are averaged over a given bin and quoted at the mean value of the variable in that bin. The measurements for $x_L > 0.93$ are presented here in a different kinematic domain than those previously published [17].

10.1 Transverse-momentum spectra and p_T^2 slopes

x_L range	p_T^2 range (GeV^2)	$d^2\sigma_{\rm LP}/dx_L dp_T^2$ s123 (nb/GeV^2)	$d^2\sigma_{\rm LP}/dx_L dp_T^2$ s456 (nb/GeV^2)	$d^2\sigma_{\rm LP}/dx_L dp_T^2$ Combined (nb/GeV^2)
0.32–0.38	0.00–0.05	$467 \pm 40^{+49}_{-53}$		$467 \pm 40^{+49}_{-53}$
	0.05–0.10	$387 \pm 68^{+45}_{-161}$		$387 \pm 68^{+45}_{-161}$
0.38–0.44	0.00–0.05	$367 \pm 28^{+32}_{-22}$	$502 \pm 41^{+42}_{-83}$	$409 \pm 23^{+28}_{-31}$
	0.05–0.10	$349 \pm 46^{+35}_{-57}$		$349 \pm 46^{+35}_{-57}$
0.44–0.50	0.00–0.05	$362 \pm 25^{+18}_{-40}$	$469 \pm 25^{+46}_{-49}$	$415 \pm 18^{+20}_{-36}$
	0.05–0.10	$332 \pm 40^{+19}_{-38}$		$332 \pm 40^{+19}_{-38}$
	0.10–0.15	$165 \pm 44^{+22}_{-51}$		$165 \pm 44^{+22}_{-51}$
0.50–0.56	0.00–0.05	$403 \pm 26^{+21}_{-26}$	$463 \pm 22^{+128}_{-14}$	$437 \pm 17^{+44}_{-12}$
	0.05–0.10	$317 \pm 33^{+51}_{-17}$	$298 \pm 19^{+52}_{-16}$	$303 \pm 17^{+41}_{-12}$

JHEP06(2009)074

table 1 (cont.)

x_L range	p_T^2 range (GeV^2)	$d^2\sigma_{\rm LP}/dx_L dp_T^2$ s123 (nb/GeV^2)	$d^2\sigma_{\rm LP}/dx_L dp_T^2$ s456 (nb/GeV^2)	$d^2\sigma_{\rm LP}/dx_L dp_T^2$ Combined (nb/GeV^2)
	0.10–0.15	$219 \pm 47^{+40}_{-13}$		$219 \pm 47^{+40}_{-13}$
0.56–0.62	0.00–0.05	$460 \pm 33^{+22}_{-70}$	$463 \pm 19^{+30}_{-26}$	$462 \pm 16^{+20}_{-31}$
	0.05–0.10	$303 \pm 27^{+29}_{-25}$	$306 \pm 16^{+16}_{-30}$	$305 \pm 13^{+16}_{-23}$
	0.10–0.15	$178 \pm 35^{+42}_{-14}$	$210 \pm 17^{+8}_{-46}$	$204 \pm 15^{+7}_{-36}$
	0.15–0.20		$136 \pm 22^{+40}_{-11}$	$136 \pm 22^{+40}_{-11}$
0.62–0.65	0.00–0.05	$410 \pm 53^{+28}_{-56}$	$463 \pm 20^{+19}_{-17}$	$456 \pm 19^{+17}_{-19}$
	0.05–0.10	$296 \pm 29^{+18}_{-12}$	$324 \pm 31^{+16}_{-51}$	$309 \pm 21^{+12}_{-22}$
	0.10–0.15	$189 \pm 43^{+19}_{-51}$	$187 \pm 16^{+13}_{-16}$	$187 \pm 15^{+12}_{-18}$
	0.15–0.20		$148 \pm 17^{+8}_{-27}$	$148 \pm 17^{+8}_{-27}$
	0.20–0.25		$134 \pm 22^{+8}_{-42}$	$134 \pm 22^{+8}_{-42}$
0.65–0.68	0.00–0.05	$421 \pm 74^{+64}_{-71}$	$464 \pm 16^{+27}_{-16}$	$462 \pm 16^{+27}_{-17}$
	0.05–0.10	$320 \pm 29^{+17}_{-43}$	$297 \pm 33^{+24}_{-66}$	$310 \pm 22^{+15}_{-52}$
	0.10–0.15	$181 \pm 36^{+81}_{-19}$	$298 \pm 37^{+20}_{-131}$	$238 \pm 26^{+11}_{-28}$
	0.15–0.20		$118 \pm 13^{+42}_{-6}$	$118 \pm 13^{+42}_{-6}$
	0.20–0.25		$119 \pm 16^{+18}_{-6}$	$119 \pm 16^{+18}_{-6}$
	0.25–0.35		$87 \pm 12^{+7}_{-15}$	$87 \pm 12^{+7}_{-15}$

Table 1. The double-differential cross-section $d^2\sigma_{\rm LP}/dx_L dp_T^2$ as a function of x_L and p_T^2, separately measured with the spectrometers s123 and s456 and the combined result. Statistical uncertainties are listed first, followed by systematic uncertainties.

table 1 (cont.)

x_L range	p_T^2 range (GeV^2)	$d^2\sigma_{\rm LP}/dx_L dp_T^2$ s123 (nb/GeV^2)	$d^2\sigma_{\rm LP}/dx_L dp_T^2$ s456 (nb/GeV^2)	$d^2\sigma_{\rm LP}/dx_L dp_T^2$ Combined (nb/GeV^2)
0.68–0.71	0.00–0.05	$253 \pm 85^{+27}_{-134}$	$500 \pm 15^{+17}_{-17}$	$493 \pm 15^{+16}_{-28}$
	0.05–0.10	$320 \pm 29^{+22}_{-42}$	$366 \pm 41^{+24}_{-138}$	$335 \pm 24^{+17}_{-74}$
	0.10–0.15	$184 \pm 31^{+57}_{-17}$	$259 \pm 47^{+39}_{-55}$	$207 \pm 26^{+47}_{-15}$
	0.15–0.20	$92 \pm 41^{+40}_{-74}$	$155 \pm 24^{+40}_{-11}$	$139 \pm 21^{+33}_{-45}$
	0.20–0.25		$103 \pm 16^{+32}_{-7}$	$103 \pm 16^{+32}_{-7}$
	0.25–0.35		$85 \pm 10^{+6}_{-4}$	$85 \pm 10^{+6}_{-4}$
	0.35–0.50		$44 \pm 9^{+4}_{-9}$	$44 \pm 9^{+4}_{-9}$
0.71–0.74	0.00–0.05		$472 \pm 12^{+28}_{-13}$	$472 \pm 12^{+28}_{-13}$
	0.05–0.10	$279 \pm 27^{+59}_{-16}$	$255 \pm 24^{+51}_{-42}$	$266 \pm 18^{+49}_{-24}$
	0.10–0.15	$217 \pm 33^{+24}_{-38}$	$130 \pm 33^{+85}_{-16}$	$173 \pm 23^{+52}_{-15}$
	0.15–0.20	$114 \pm 43^{+34}_{-58}$	$250 \pm 66^{+51}_{-133}$	$154 \pm 36^{+25}_{-69}$
	0.20–0.25		$116 \pm 27^{+55}_{-15}$	$62 \pm 19^{+55}_{-15}$
	0.25–0.35		$86 \pm 16^{+11}_{-25}$	$86 \pm 16^{+11}_{-25}$
	0.35–0.50		$27 \pm 5^{+2}_{-2}$	$27 \pm 5^{+2}_{-2}$

JHEP06(2009)074

table 1 (cont.)

x_L range	p_T^2 range (GeV^2)	$d^2\sigma_{\mathrm{LP}}/dx_L dp_T^2$ s123 ($\mathrm{nb/GeV}^2$)	$d^2\sigma_{\mathrm{LP}}/dx_L dp_T^2$ s456 ($\mathrm{nb/GeV}^2$)	$d^2\sigma_{\mathrm{LP}}/dx_L dp_T^2$ Combined ($\mathrm{nb/GeV}^2$)
0.74–0.77	0.00–0.05		$467 \pm 10^{+9}_{-28}$	$467 \pm 10^{+9}_{-28}$
	0.05–0.10	$250 \pm 30^{+51}_{-32}$	$325 \pm 21^{+42}_{-14}$	$300 \pm 17^{+42}_{-15}$
	0.10–0.15	$234 \pm 30^{+53}_{-6}$	$199 \pm 40^{+33}_{-19}$	$222 \pm 24^{+40}_{-7}$
	0.15–0.20	$108 \pm 35^{+38}_{-31}$		$108 \pm 35^{+38}_{-31}$
	0.20–0.25		$152 \pm 52^{+18}_{-84}$	$152 \pm 52^{+18}_{-84}$
	0.25–0.35		$121 \pm 34^{+9}_{-80}$	$121 \pm 34^{+9}_{-80}$
	0.35–0.50		$8 \pm 4^{+11}_{-1}$	$8 \pm 4^{+11}_{-1}$
0.77–0.80	0.00–0.05		$452 \pm 10^{+10}_{-17}$	$452 \pm 10^{+10}_{-17}$
	0.05–0.10	$248 \pm 39^{+30}_{-27}$	$297 \pm 14^{+13}_{-38}$	$292 \pm 13^{+13}_{-35}$
	0.10–0.15	$196 \pm 23^{+97}_{-7}$	$241 \pm 20^{+50}_{-9}$	$222 \pm 15^{+62}_{-5}$
	0.15–0.20	$198 \pm 48^{+40}_{-39}$	$203 \pm 32^{+97}_{-9}$	$201 \pm 27^{+56}_{-13}$
	0.20–0.25		$168 \pm 54^{+58}_{-46}$	$168 \pm 54^{+58}_{-46}$
0.80–0.83	0.00–0.05		$451 \pm 10^{+9}_{-19}$	$451 \pm 10^{+9}_{-19}$
	0.05–0.10	$353 \pm 74^{+16}_{-117}$	$266 \pm 11^{+18}_{-8}$	$268 \pm 11^{+18}_{-9}$
	0.10–0.15	$197 \pm 25^{+33}_{-14}$	$210 \pm 14^{+7}_{-16}$	$207 \pm 12^{+5}_{-13}$
	0.15–0.20	$84 \pm 23^{+25}_{-13}$	$178 \pm 17^{+5}_{-75}$	$147 \pm 14^{+9}_{-33}$
	0.20–0.25	$73 \pm 32^{+68}_{-52}$	$136 \pm 16^{+9}_{-33}$	$123 \pm 15^{+22}_{-45}$
	0.25–0.35		$98 \pm 14^{+22}_{-7}$	$98 \pm 14^{+22}_{-7}$
0.83–0.86	0.00–0.05		$434 \pm 10^{+13}_{-19}$	$434 \pm 10^{+13}_{-19}$
	0.05–0.10		$295 \pm 12^{+8}_{-33}$	$295 \pm 12^{+8}_{-33}$
	0.10–0.15	$184 \pm 24^{+79}_{-10}$	$207 \pm 13^{+20}_{-13}$	$202 \pm 11^{+17}_{-5}$
	0.15–0.20	$190 \pm 37^{+33}_{-59}$	$169 \pm 15^{+5}_{-39}$	$172 \pm 14^{+5}_{-39}$
	0.20–0.25	$50 \pm 20^{+22}_{-21}$	$127 \pm 14^{+33}_{-7}$	$102 \pm 11^{+30}_{-19}$
	0.25–0.35		$122 \pm 14^{+7}_{-36}$	$122 \pm 14^{+7}_{-36}$
	0.35–0.50		$49 \pm 8^{+12}_{-6}$	$49 \pm 8^{+12}_{-6}$
0.86–0.89	0.00–0.05		$467 \pm 13^{+24}_{-18}$	$467 \pm 13^{+24}_{-18}$
	0.05–0.10		$309 \pm 12^{+22}_{-20}$	$309 \pm 12^{+22}_{-20}$
	0.10–0.15	$247 \pm 36^{+44}_{-29}$	$232 \pm 14^{+8}_{-20}$	$234 \pm 13^{+7}_{-19}$
	0.15–0.20	$196 \pm 32^{+23}_{-43}$	$180 \pm 15^{+6}_{-35}$	$183 \pm 14^{+6}_{-36}$
	0.20–0.25	$115 \pm 34^{+55}_{-24}$	$136 \pm 14^{+21}_{-16}$	$133 \pm 13^{+20}_{-16}$
	0.25–0.35	$24 \pm 16^{+8}_{-4}$	$81 \pm 8^{+15}_{-11}$	$69 \pm 7^{+24}_{-6}$
	0.35–0.50		$43 \pm 6^{+8}_{-5}$	$43 \pm 6^{+8}_{-5}$
0.89–0.92	0.00–0.05		$481 \pm 19^{+24}_{-19}$	$481 \pm 19^{+24}_{-19}$
	0.05–0.10		$315 \pm 13^{+16}_{-10}$	$315 \pm 13^{+16}_{-10}$
	0.10–0.15	$262 \pm 47^{+68}_{-78}$	$228 \pm 14^{+18}_{-21}$	$231 \pm 13^{+15}_{-24}$
	0.15–0.20	$172 \pm 27^{+28}_{-44}$	$175 \pm 14^{+22}_{-10}$	$174 \pm 12^{+14}_{-11}$
	0.20–0.25	$97 \pm 27^{+58}_{-18}$	$133 \pm 13^{+18}_{-19}$	$126 \pm 12^{+15}_{-11}$
	0.25–0.35	$37 \pm 19^{+18}_{-11}$	$69 \pm 7^{+7}_{-5}$	$65 \pm 6^{+6}_{-5}$

JHEP06(2009)074

table 1 (cont.)

x_L range	p_T^2 range (GeV^2)	$d^2\sigma_{\mathrm{LP}}/dx_L dp_T^2$ s123 ($\mathrm{nb/GeV}^2$)	$d^2\sigma_{\mathrm{LP}}/dx_L dp_T^2$ s456 ($\mathrm{nb/GeV}^2$)	$d^2\sigma_{\mathrm{LP}}/dx_L dp_T^2$ Combined ($\mathrm{nb/GeV}^2$)
	0.35–0.50		$39 \pm 5^{+6}_{-5}$	$39 \pm 5^{+6}_{-5}$
0.92–0.95	0.00–0.05		$820 \pm 145^{+124}_{-432}$	$820 \pm 145^{+124}_{-432}$
	0.05–0.10		$235 \pm 14^{+54}_{-8}$	$235 \pm 14^{+54}_{-8}$
	0.10–0.15	$221 \pm 58^{+212}_{-36}$	$182 \pm 14^{+48}_{-22}$	$184 \pm 13^{+45}_{-21}$
	0.15–0.20	$138 \pm 21^{+47}_{-11}$	$156 \pm 14^{+33}_{-13}$	$150 \pm 12^{+30}_{-9}$
	0.20–0.25	$92 \pm 22^{+38}_{-10}$	$114 \pm 13^{+17}_{-20}$	$109 \pm 11^{+15}_{-11}$
	0.25–0.35	$39 \pm 15^{+9}_{-18}$	$83 \pm 9^{+16}_{-12}$	$72 \pm 8^{+6}_{-13}$
	0.35–0.50		$36 \pm 5^{+16}_{-4}$	$36 \pm 5^{+16}_{-4}$
0.95–0.98	0.05–0.10		$423 \pm 35^{+63}_{-116}$	$423 \pm 35^{+63}_{-116}$
	0.10–0.15		$328 \pm 30^{+84}_{-10}$	$328 \pm 30^{+84}_{-10}$
	0.15–0.20	$280 \pm 39^{+57}_{-16}$	$250 \pm 32^{+142}_{-5}$	$262 \pm 25^{+90}_{-1}$
	0.20–0.25	$254 \pm 46^{+5}_{-116}$	$197 \pm 32^{+60}_{-6}$	$215 \pm 26^{+30}_{-26}$
	0.25–0.35	$50 \pm 17^{+18}_{-30}$	$190 \pm 34^{+60}_{-72}$	$77 \pm 15^{+19}_{-44}$
0.98–1.00	0.05–0.10		$2788 \pm 180^{+466}_{-304}$	$2788 \pm 180^{+466}_{-304}$
	0.10–0.15		$1423 \pm 90^{+188}_{-131}$	$1423 \pm 90^{+188}_{-131}$
	0.15–0.20	$1218 \pm 160^{+182}_{-214}$	$1012 \pm 89^{+132}_{-133}$	$1061 \pm 78^{+85}_{-118}$
	0.20–0.25	$574 \pm 81^{+166}_{-35}$	$848 \pm 93^{+186}_{-41}$	$693 \pm 61^{+174}_{-16}$
	0.25–0.35	$231 \pm 54^{+116}_{-13}$	$588 \pm 69^{+39}_{-93}$	$367 \pm 42^{+147}_{-26}$

JHEP06(2009)074

x_L range	b (GeV^{-2})
0.50–0.56	$6.98^{+1.11+2.99}_{-1.06-1.53}$
0.56–0.62	$8.49^{+0.47+2.18}_{-0.51-1.32}$
0.62–0.65	$7.36^{+0.34+1.12}_{-0.38-0.54}$
0.65–0.68	$6.83^{+0.26+0.78}_{-0.26-0.38}$
0.68–0.71	$7.01^{+0.21+0.15}_{-0.21-0.51}$
0.71–0.74	$7.43^{+0.26+0.63}_{-0.26-0.38}$
0.74–0.77	$7.48^{+0.38+1.23}_{-0.38-1.00}$
0.77–0.80	$6.82^{+0.30+0.90}_{-0.34-1.24}$
0.80–0.83	$6.54^{+0.21+0.52}_{-0.21-0.40}$
0.83–0.86	$5.88^{+0.17+0.75}_{-0.17-0.18}$
0.86–0.89	$6.82^{+0.17+0.82}_{-0.17-0.64}$
0.89–0.92	$7.22^{+0.21+0.72}_{-0.21-0.75}$
0.92–0.95	$6.00^{+0.26+0.48}_{-0.26-1.37}$
0.95–0.98	$4.45^{+0.47+1.69}_{-0.47-0.88}$
0.98–1.00	$8.31^{+0.34+1.05}_{-0.38-0.91}$

Table 2. The p_T^2-slope, b, of the cross-section $d^2\sigma_{\rm LP}/dx_L dp_T^2$, as defined by the parameterisation $A \cdot e^{-b \cdot p_T^2}$ and obtained from a fit to the data in bins of x_L. Statistical uncertainties are listed first, followed by systematic uncertainties.

The double-differential cross-section $d^2\sigma_{\rm LP}/dx_L dp_T^2$ as a function of p_T^2 in bins of x_L is presented in figure 6 and given in table 1. The results obtained with the s123 and s456 spectrometers are shown separately. Within the uncorrelated uncertainties, the two samples lead to consistent results. The lines shown in figure 6 represent the results of a fit of an exponential function $A \cdot e^{-bp_T^2}$ to the combined cross-section $d^2\sigma_{\rm LP}/dx_L dp_T^2$. The band shows the statistical uncertainty of the fit. The slopes are presented as a function of x_L in figure 7 and given in table 2. The slopes show no strong dependence on x_L. The mean value of the slopes is $\langle b \rangle = 6.76 \pm 0.07(\text{stat.})^{+0.63}_{-0.52}(\text{syst.})\,\text{GeV}^{-2}$. The measurements of the p_T^2 slopes at $\langle Q^2 \rangle = 5.1\,\text{GeV}^2$ and $\langle Q^2 \rangle = 30.1\,\text{GeV}^2$, in the range $45 < W < 225\,\text{GeV}$, where x_L bins were combined, are presented in figure 8 and given in table 3. Also shown are the ZEUS 1994 data [16] in the range $Q^2 < 0.02\,\text{GeV}^2$ and $176 < W < 225\,\text{GeV}$ and the ZEUS 1995 [7] data in the range $0.1 < Q^2 < 0.74\,\text{GeV}^2$ and $85 < W < 258\,\text{GeV}$. The p_T^2 slopes are independent of the virtuality of the exchanged photon.

10.2 Longitudinal momentum spectra

The cross section as a function of x_L has been measured in three bins of p_T^2: $0 < p_T^2 < 0.04$, $0.04 < p_T^2 < 0.15$ and $0.15 < p_T^2 < 0.5\,\text{GeV}^2$. The leading proton production rate, $1/\sigma_{\rm inc} \cdot d\sigma_{\rm LP}/dx_L$, for the three p_T^2 ranges is shown in figure 9 and listed in table 4. Due to the LPS acceptance, the accessible x_L range changes as a function of p_T^2, as seen in the figure. The rate as a function of x_L is approximately flat up to the diffractive peak, where it increases by a factor of about six. This behaviour of the cross section as a function of

JHEP06(2009)074

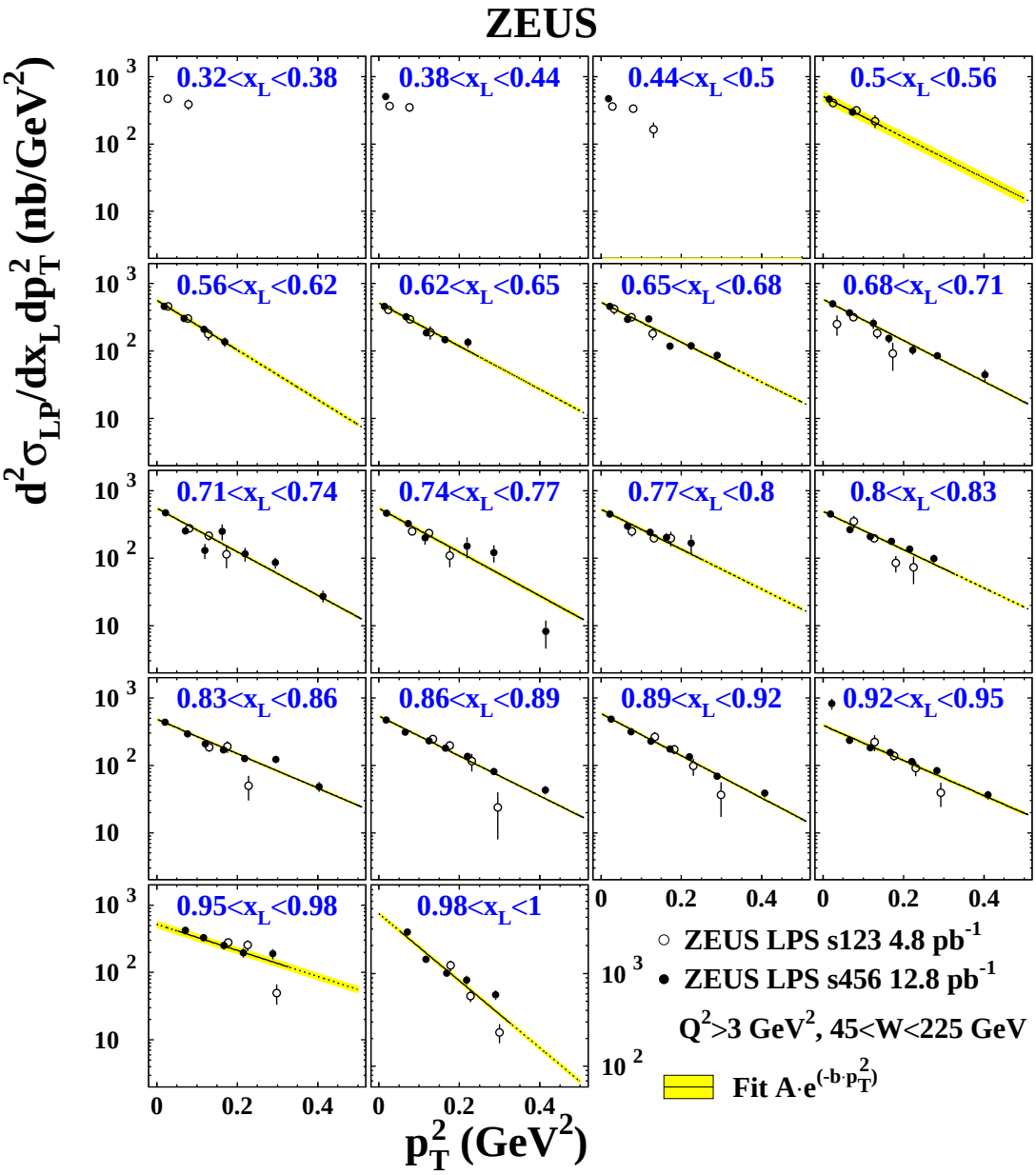

Figure 6. The double-differential cross-section $d^2\sigma_{\rm LP}/dx_L dp_T^2$ for $Q^2 > 3\ GeV^2$ and $45 < W < 225\,$GeV as a function of p_T^2 in bins of x_L. The circles and the dots are the ZEUS data measured with the spectrometers s123 and s456, respectively. For clarity, only the statistical uncertainties are shown. The systematic uncertainties are listed in table 1. The lines are the result of a fit to a function $A \cdot e^{-b\cdot p_T^2}$, as described in the text. The solid lines indicate the range in which the fit was performed. The bands show the statistical uncertainty of the fit.

JHEP06(2009)074

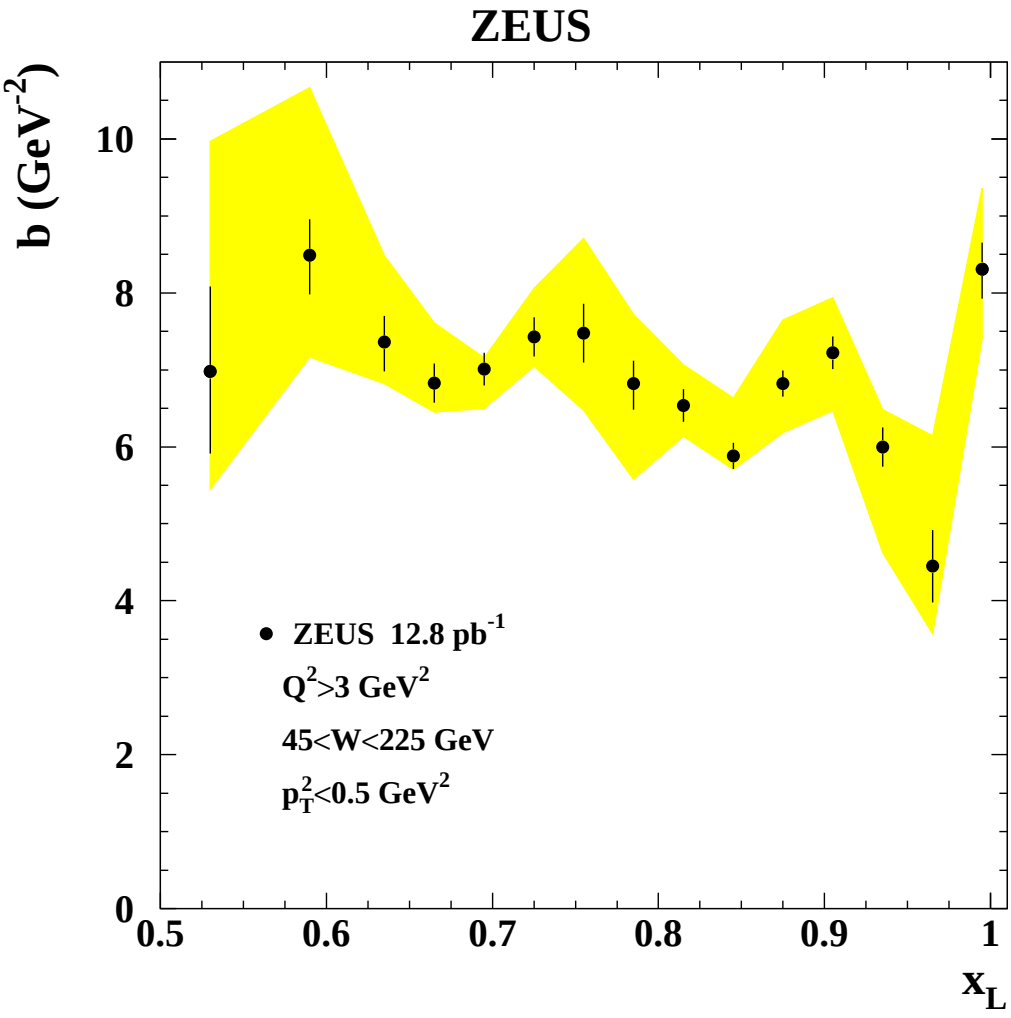

Figure 7. The p_T^2-slope, b, of the cross-section $d^2\sigma_{\rm LP}/dx_L dp_T^2$, as defined by the parameterisation $A \cdot e^{-b \cdot p_T^2}$ and obtained from a fit to the data in bins of x_L, in the kinematic range indicated in the figure. The bands represent the systematic uncertainty.

x_L is essentially independent of p_T^2.

Since, as discussed in the previous section, also the p_T^2 slopes are independent of x_L, the cross section as a function of x_L can be extrapolated to the full $x_L > 0.32$ and $p_T^2 < 0.5\,\text{GeV}^2$ range. The measurement of $1/\sigma_{\rm inc} \cdot d\sigma_{\rm LP}/dx_L$ as a function of x_L, extrapolated to the full $p_T^2 < 0.5\,\text{GeV}^2$ range is shown in figure 10 and given in table 5. For comparison, the ZEUS 1995 data [7] with lower Q^2 are also shown. The two measurements are consistent.

For $p_T^2 < 0.04\,\text{GeV}^2$, the measurement of $1/\sigma_{\rm inc} \cdot d\sigma_{\rm LP}/dx_L$ can also be compared to previous measurements in the photoproduction regime ($Q^2 < 0.02\,\text{GeV}^2$) [7]. The comparison is shown in figure 11. Due to the low p_T^2 values, the diffractive peak is not accessible (see figure 4). The photoproduction data tend to lie systematically below the

JHEP06(2009)074

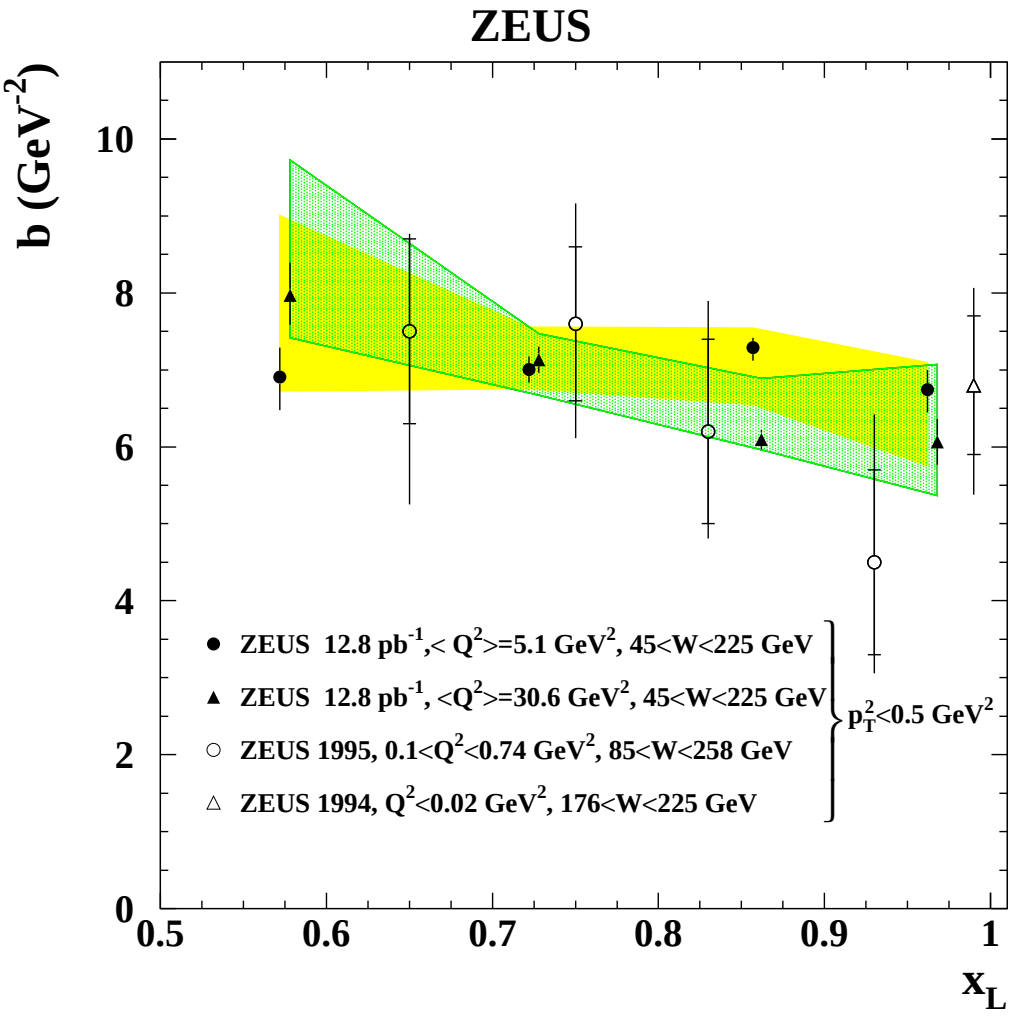

Figure 8. The p_T^2-slope, b, of the cross-section $d^2\sigma_{\rm LP}/dx_L dp_T^2$, as defined by the parameterisation $A\cdot e^{-b\cdot p_T^2}$ and obtained from a fit to the data in bins of x_L, in different kinematic ranges as indicated in the figure. The bands represent the systematic uncertainty (light band for lower Q^2 data and dark band for higher Q^2 data). For the ZEUS 1995 data [7] and the ZEUS 1994 data [16], the inner vertical bars represent the statistical uncertainties, the outer bars the statistical and systematic uncertainties added in quadrature.

higher-Q^2 measurement, though within uncertainties the results are consistent.

10.3 Ratios of leading proton production to inclusive DIS yields

The rate of leading proton production, $r^{\rm LP(3)}(x,Q^2,x_L)$, in e^+p scattering was determined according to

$$r^{\rm LP(3)}(x,Q^2,x_L) = \frac{N^{\rm LPS}(x,Q^2,x_L)}{N^{\rm DIS}(x,Q^2)}\frac{A_{\rm DIS}}{A_{\rm LPS}}\frac{\mathcal{L}^{\rm DIS}}{\mathcal{L}^{\rm LPS}}\frac{1}{\Delta x_L}, \qquad (10.1)$$

x_L range	b (GeV^{-2})	
	$\langle Q^2\rangle = 5.1\,\text{GeV}^2$	$\langle Q^2\rangle = 30.6\,\text{GeV}^2$
0.5–0.65	$6.90^{+0.38\,+1.34}_{-0.43\,-0.18}$	$7.97^{+0.43\,+1.06}_{-0.38\,-0.39}$
0.65–0.8	$7.00^{+0.17\,+0.20}_{-0.17\,-0.21}$	$7.13^{+0.17\,+0.16}_{-0.17\,-0.31}$
0.8–0.92	$7.29^{+0.13\,+0.15}_{-0.17\,-0.49}$	$6.10^{+0.13\,+0.64}_{-0.13\,-0.04}$
0.92–1.0	$6.74^{+0.26\,+0.28}_{-0.30\,-0.33}$	$6.06^{+0.30\,+0.66}_{-0.30\,-0.36}$

Table 3. The p_T^2-slope, b, of the cross-section $d^2\sigma_{\text{LP}}/dx_L dp_T^2$, as defined by the parameterisation $A\cdot e^{-b\cdot p_T^2}$ and obtained from a fit to the data in bins of x_L, measured in two ranges of Q^2. Statistical uncertainties are listed first, followed by systematic uncertainties.

x_L range	$1/\sigma_{\text{inc}}\cdot d\sigma_{\text{LP}}/dx_L$		
	$0 < p_T^2 < 0.04\,\text{GeV}^2$	$0.04 < p_T^2 < 0.15\,\text{GeV}^2$	$0.15 < p_T^2 < 0.5\,\text{GeV}^2$
0.32–0.38	$0.091 \pm 0.008^{+0.009}_{-0.013}$		
0.38–0.44	$0.082 \pm 0.004^{+0.005}_{-0.008}$	$0.156 \pm 0.016^{+0.013}_{-0.024}$	
0.44–0.50	$0.086 \pm 0.004^{+0.003}_{-0.010}$	$0.144 \pm 0.013^{+0.005}_{-0.021}$	
0.50–0.56	$0.091 \pm 0.004^{+0.004}_{-0.006}$	$0.140 \pm 0.006^{+0.026}_{-0.008}$	
0.56–0.62	$0.097 \pm 0.004^{+0.002}_{-0.010}$	$0.143 \pm 0.004^{+0.004}_{-0.014}$	
0.62–0.68	$0.096 \pm 0.003^{+0.003}_{-0.005}$	$0.142 \pm 0.005^{+0.002}_{-0.021}$	$0.126 \pm 0.007^{+0.010}_{-0.011}$
0.68–0.74	$0.100 \pm 0.002^{+0.003}_{-0.005}$	$0.141 \pm 0.005^{+0.004}_{-0.012}$	$0.138 \pm 0.008^{+0.008}_{-0.009}$
0.74–0.80	$0.094 \pm 0.001^{+0.000}_{-0.007}$	$0.145 \pm 0.003^{+0.003}_{-0.006}$	$0.155 \pm 0.015^{+0.010}_{-0.015}$
0.80–0.86	$0.091 \pm 0.001^{+0.001}_{-0.005}$	$0.139 \pm 0.003^{+0.001}_{-0.008}$	$0.146 \pm 0.005^{+0.010}_{-0.023}$
0.86–0.92	$0.099 \pm 0.002^{+0.002}_{-0.007}$	$0.154 \pm 0.003^{+0.005}_{-0.007}$	$0.143 \pm 0.004^{+0.011}_{-0.014}$
0.92–0.98		$0.167 \pm 0.006^{+0.020}_{-0.015}$	$0.179 \pm 0.007^{+0.021}_{-0.013}$
0.97–1.00		$1.126 \pm 0.047^{+0.113}_{-0.092}$	$0.816 \pm 0.036^{+0.088}_{-0.055}$

Table 4. The leading proton production rate, $1/\sigma_{\text{inc}}\cdot d\sigma_{\text{LP}}/dx_L$, as a function of x_L measured in three ranges of p_T^2. Statistical uncertainties are listed first, followed by systematic uncertainties.

where $N^{\text{LPS}}(x, Q^2, x_L)$ is the number of events corresponding to an integrated luminosity, $\mathcal{L}^{\text{LPS}}$, with a proton candidate in the LPS in a given (x, Q^2, x_L) bin and integrated over $0 < p_T^2 < 0.5\,\text{GeV}^2$, and $N^{\text{DIS}}(x, Q^2)$ is the number of DIS events corresponding to an integrated luminosity, $\mathcal{L}^{\text{DIS}}$, in that (x, Q^2) bin. The acceptance A_{DIS} was estimated by applying only the DIS selection cuts and A_{LPS} is the acceptance of the LPS sample. The variable Δx_L is the size of the x_L bin.

The ratio $r^{\text{LP(3)}}$ as a function of x_L in bins of x and Q^2 is shown in figure 12 and given in table 6. The x_L range of the measurement is limited to $0.32 < x_L < 0.92$, as detailed studies of the diffraction region were presented elsewhere [17]. The ratio $r^{\text{LP(3)}}$ has also been measured in the three ranges of p_T^2 and the values are given in tables 7, 8 and 9. The $r^{\text{LP(3)}}$ values are approximately constant over the kinematic range of this analysis, independent of the p_T^2 range.

JHEP06(2009)074

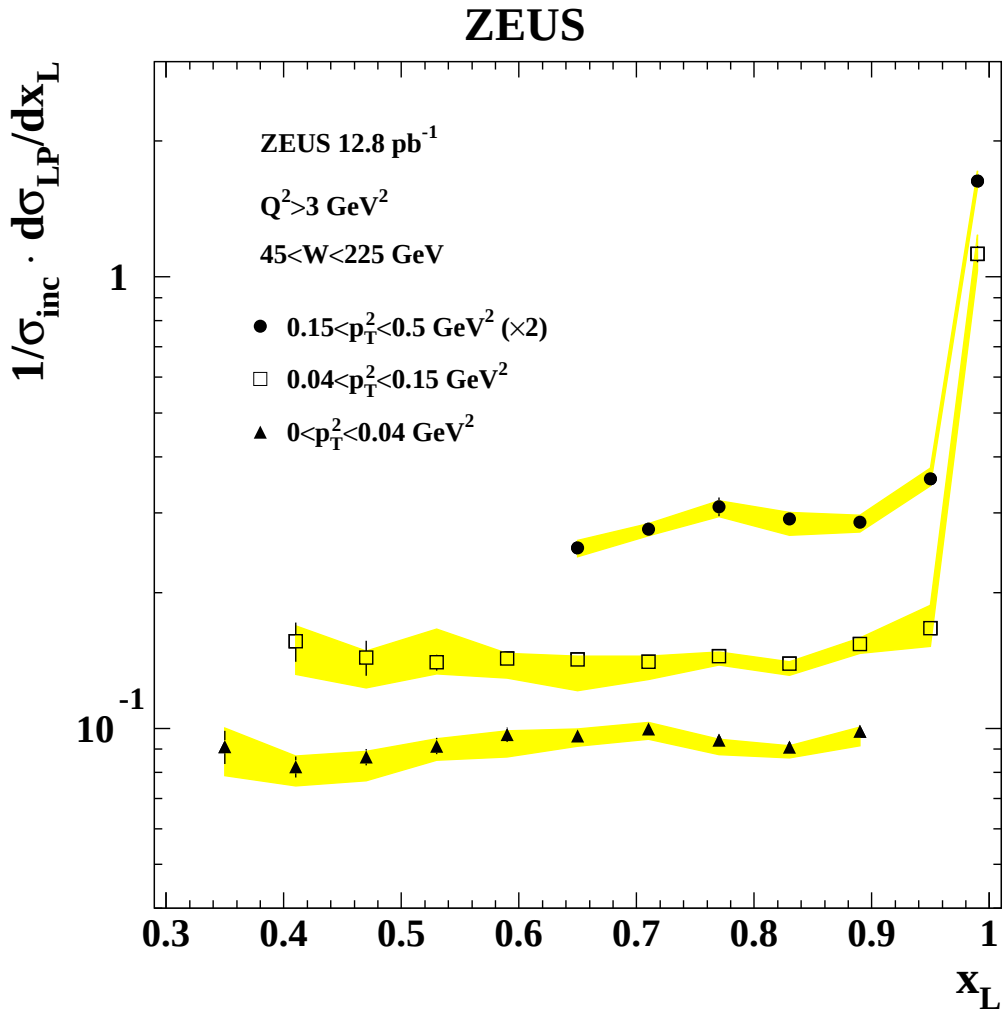

Figure 9. The leading proton production rate, $1/\sigma_{\rm inc} \cdot d\sigma_{\rm LP}/dx_L$, as a function of x_L in three p_T^2 ranges as indicated in the figure. The measurements in the higher p_T^2 range are multiplied by a factor two for visibility. The bands represent the systematic uncertainty.

JHEP06(2009)074

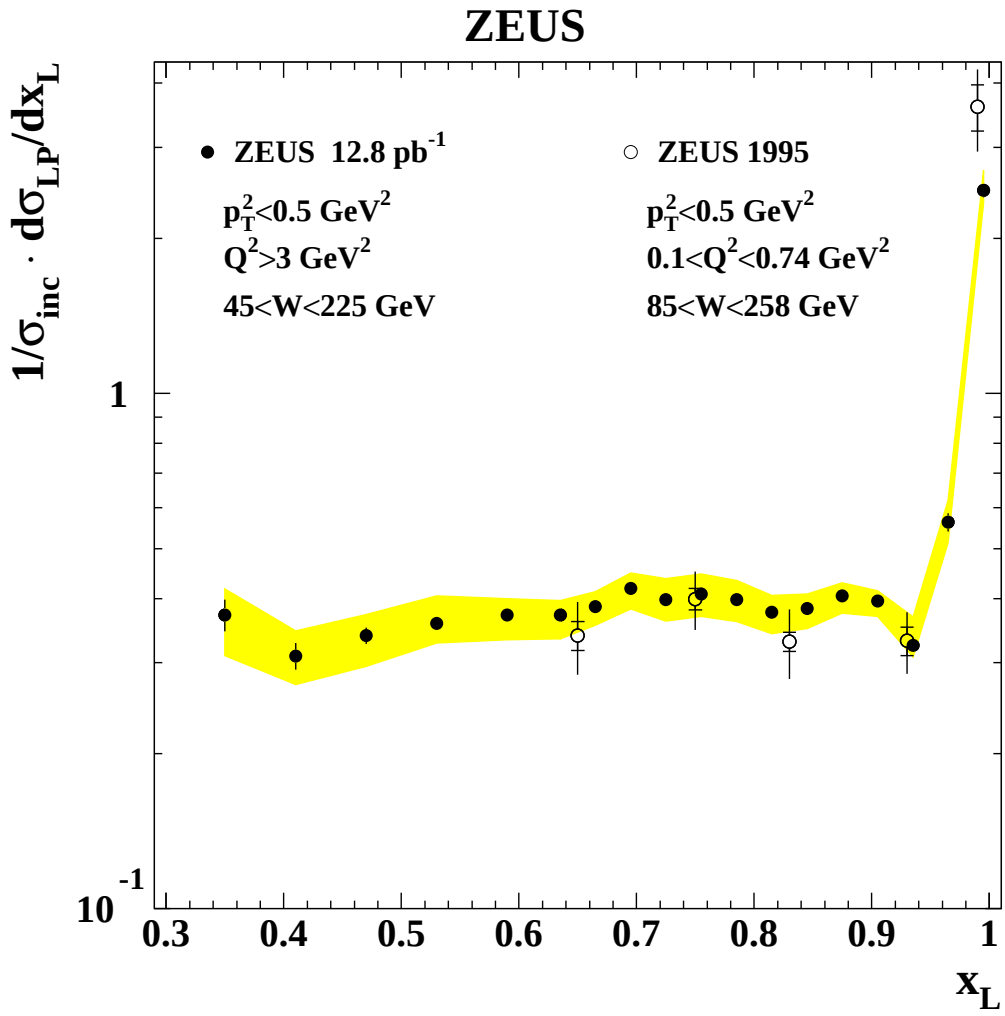

Figure 10. The leading proton production rate, $1/\sigma_{\rm inc} \cdot d\sigma_{\rm LP}/dx_L$, for two ranges of Q^2 as indicated in the figure. The bands represent the systematic uncertainty. For the ZEUS 1995 data [7] the inner vertical bars represent the statistical uncertainties, the outer bars the statistical and systematic uncertainties added in quadrature.

JHEP06(2009)074

x_L range	$1/\sigma_{\rm inc} \cdot d\sigma_{\rm LP}/dx_L$
0.32–0.38	$0.372 \pm 0.026^{+0.046}_{-0.062}$
0.38–0.44	$0.309 \pm 0.018^{+0.037}_{-0.037}$
0.44–0.50	$0.339 \pm 0.012^{+0.033}_{-0.044}$
0.50–0.56	$0.358 \pm 0.010^{+0.047}_{-0.030}$
0.56–0.62	$0.371 \pm 0.009^{+0.029}_{-0.039}$
0.62–0.65	$0.371 \pm 0.011^{+0.025}_{-0.037}$
0.65–0.68	$0.385 \pm 0.010^{+0.027}_{-0.031}$
0.68–0.71	$0.418 \pm 0.010^{+0.030}_{-0.037}$
0.71–0.74	$0.398 \pm 0.009^{+0.039}_{-0.036}$
0.74–0.77	$0.408 \pm 0.008^{+0.038}_{-0.039}$
0.77–0.80	$0.398 \pm 0.007^{+0.036}_{-0.037}$
0.80–0.83	$0.376 \pm 0.006^{+0.029}_{-0.035}$
0.83–0.86	$0.382 \pm 0.006^{+0.026}_{-0.033}$
0.86–0.89	$0.405 \pm 0.007^{+0.024}_{-0.030}$
0.89–0.92	$0.395 \pm 0.008^{+0.019}_{-0.026}$
0.92–0.95	$0.325 \pm 0.010^{+0.044}_{-0.016}$
0.95–0.98	$0.562 \pm 0.023^{+0.058}_{-0.049}$
0.98–1.00	$2.478 \pm 0.076^{+0.235}_{-0.136}$

Table 5. The leading proton production rate, $1/\sigma_{\rm inc} \cdot d\sigma_{\rm LP}/dx_L$, as a function of x_L measured in the region $p_T^2 < 0.5\ GeV^2$. Statistical uncertainties are listed first, followed by systematic uncertainties.

JHEP06(2009)074

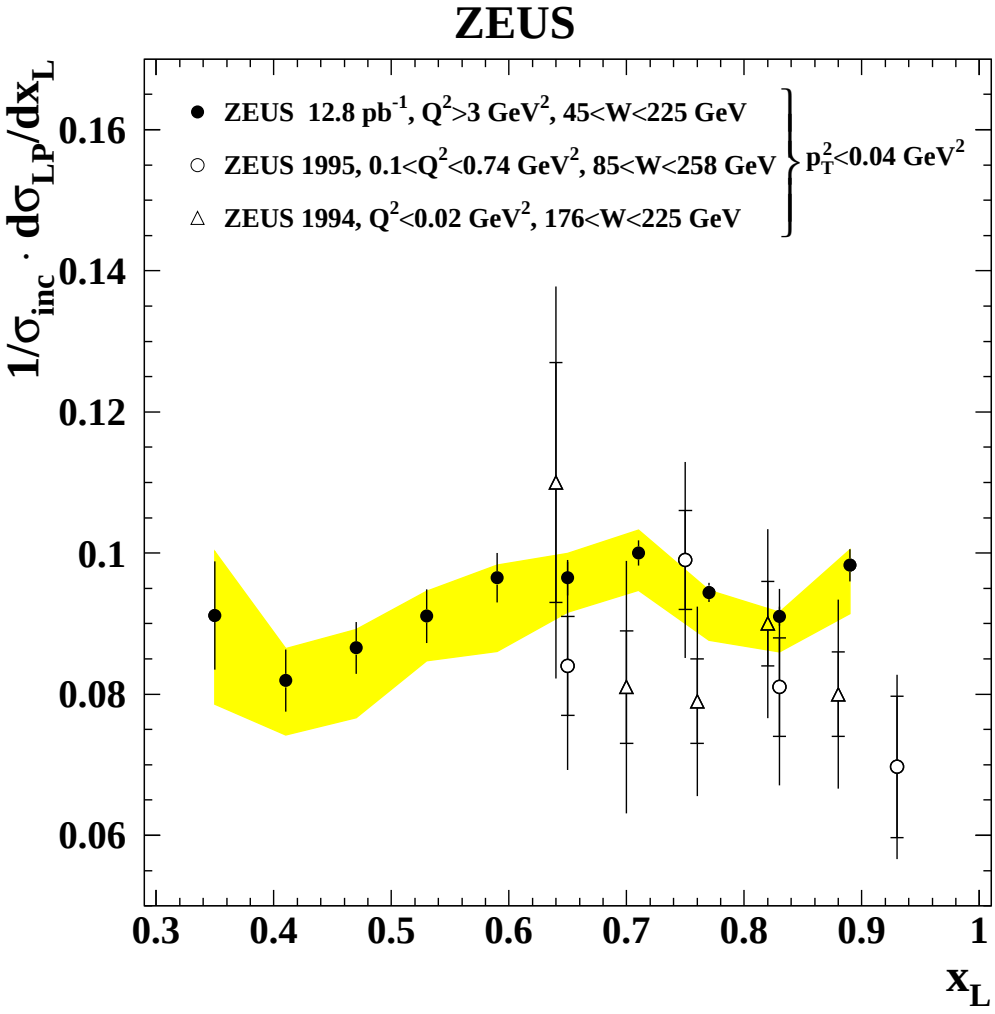

Figure 11. The leading proton production rate, $1/\sigma_{\rm inc} \cdot d\sigma_{\rm LP}/dx_L$, for $p_T^2 < 0.04\ GeV^2$ in the kinematic ranges indicated in the figure. Other details as in figure 8.

JHEP06(2009)074

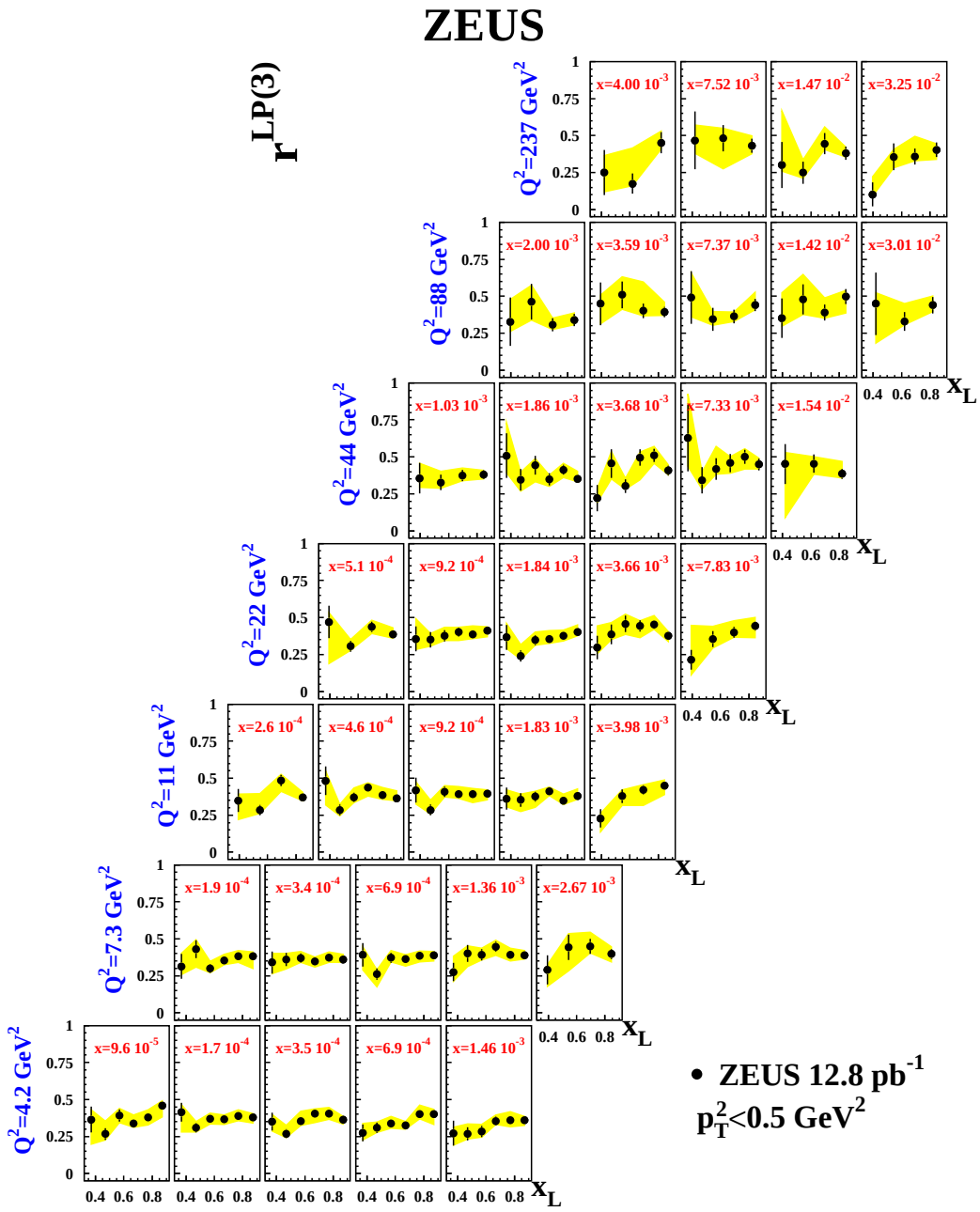

Figure 12. The leading proton production rate, $r^{\mathrm{LP}(3)}$, as a function of x_L in bins of x and Q^2, for $p_T^2 < 0.5\ GeV^2$. The bands represent the systematic uncertainty.

$\langle x \rangle$	$\langle Q^2 \rangle$ (GeV^2)	x_L range	$r^{\mathrm{LP(3)}}$
$9.6 \cdot 10^{-5}$	4.2	0.32–0.42	$0.365 \pm 0.086^{+0.066}_{-0.168}$
		0.42–0.52	$0.268 \pm 0.040^{+0.085}_{-0.041}$
		0.52–0.62	$0.391 \pm 0.041^{+0.050}_{-0.048}$
		0.62–0.72	$0.338 \pm 0.026^{+0.058}_{-0.025}$
		0.72–0.72	$0.378 \pm 0.024^{+0.050}_{-0.049}$
		0.82–0.72	$0.458 \pm 0.027^{+0.032}_{-0.076}$
$1.7 \cdot 10^{-4}$	4.2	0.32–0.42	$0.414 \pm 0.063^{+0.050}_{-0.135}$
		0.42–0.52	$0.310 \pm 0.032^{+0.039}_{-0.029}$
		0.52–0.62	$0.370 \pm 0.026^{+0.037}_{-0.036}$
		0.62–0.72	$0.366 \pm 0.019^{+0.028}_{-0.035}$
		0.72–0.82	$0.390 \pm 0.015^{+0.039}_{-0.034}$
		0.82–0.92	$0.378 \pm 0.014^{+0.026}_{-0.036}$
$3.5 \cdot 10^{-4}$	4.2	0.32–0.42	$0.351 \pm 0.061^{+0.047}_{-0.062}$
		0.42–0.52	$0.269 \pm 0.029^{+0.055}_{-0.028}$
		0.52–0.62	$0.354 \pm 0.025^{+0.067}_{-0.029}$
		0.62–0.72	$0.406 \pm 0.022^{+0.030}_{-0.063}$
		0.72–0.82	$0.405 \pm 0.017^{+0.040}_{-0.038}$
		0.82–0.92	$0.364 \pm 0.014^{+0.023}_{-0.029}$
$6.9 \cdot 10^{-4}$	4.2	0.32–0.42	$0.275 \pm 0.057^{+0.063}_{-0.047}$
		0.42–0.52	$0.308 \pm 0.035^{+0.038}_{-0.031}$
		0.52–0.62	$0.339 \pm 0.027^{+0.045}_{-0.034}$
		0.62–0.72	$0.326 \pm 0.020^{+0.026}_{-0.027}$
		0.72–0.82	$0.400 \pm 0.018^{+0.063}_{-0.031}$
		0.82–0.92	$0.403 \pm 0.017^{+0.030}_{-0.070}$
$1.46 \cdot 10^{-3}$	4.2	0.32–0.42	$0.272 \pm 0.083^{+0.040}_{-0.082}$
		0.42–0.52	$0.268 \pm 0.045^{+0.066}_{-0.035}$
		0.52–0.62	$0.285 \pm 0.038^{+0.047}_{-0.039}$
		0.62–0.72	$0.355 \pm 0.029^{+0.041}_{-0.023}$
		0.72–0.82	$0.362 \pm 0.022^{+0.057}_{-0.046}$
		0.82–0.92	$0.359 \pm 0.021^{+0.025}_{-0.034}$

Table 6. The leading proton production rate, $r^{\mathrm{LP(3)}}$, measured as a function of x_L for protons with $p_T^2 < 0.5\ GeV^2$, in bins of x and Q^2, with averages $\langle x \rangle$ and $\langle Q^2 \rangle$. Statistical uncertainties are listed first, followed by systematic uncertainties.

table 6 (cont.)

$\langle x \rangle$	$\langle Q^2 \rangle$ (GeV^2)	x_L range	$r^{\mathrm{LP(3)}}$
$1.9 \cdot 10^{-4}$	7.3	0.32–0.42	$0.314 \pm 0.084^{+0.087}_{-0.055}$
		0.42–0.52	$0.430 \pm 0.061^{+0.065}_{-0.122}$
		0.52–0.62	$0.299 \pm 0.031^{+0.049}_{-0.027}$
		0.62–0.72	$0.355 \pm 0.027^{+0.041}_{-0.029}$

JHEP06(2009)074

table 6 (cont.)

$\langle x \rangle$	$\langle Q^2 \rangle$ (GeV^2)	x_L range	$r^{\mathrm{LP(3)}}$
		0.72–0.82	$0.382 \pm 0.024^{+0.039}_{-0.042}$
		0.82–0.92	$0.383 \pm 0.022^{+0.028}_{-0.083}$
$3.4 \cdot 10^{-4}$	7.3	0.32–0.42	$0.340 \pm 0.076^{+0.062}_{-0.075}$
		0.42–0.52	$0.360 \pm 0.044^{+0.040}_{-0.062}$
		0.52–0.62	$0.369 \pm 0.032^{+0.044}_{-0.029}$
		0.62–0.72	$0.347 \pm 0.022^{+0.030}_{-0.038}$
		0.72–0.82	$0.374 \pm 0.019^{+0.037}_{-0.033}$
		0.82–0.92	$0.359 \pm 0.016^{+0.037}_{-0.020}$
$6.9 \cdot 10^{-4}$	7.3	0.32–0.42	$0.392 \pm 0.081^{+0.056}_{-0.102}$
		0.42–0.52	$0.261 \pm 0.038^{+0.029}_{-0.086}$
		0.52–0.62	$0.372 \pm 0.034^{+0.048}_{-0.028}$
		0.62–0.72	$0.363 \pm 0.025^{+0.028}_{-0.047}$
		0.72–0.82	$0.385 \pm 0.020^{+0.034}_{-0.040}$
		0.82–0.92	$0.388 \pm 0.019^{+0.027}_{-0.037}$
$1.36 \cdot 10^{-3}$	7.3	0.32–0.42	$0.275 \pm 0.062^{+0.106}_{-0.061}$
		0.42–0.52	$0.401 \pm 0.056^{+0.050}_{-0.088}$
		0.52–0.62	$0.393 \pm 0.039^{+0.043}_{-0.035}$
		0.62–0.72	$0.448 \pm 0.032^{+0.042}_{-0.057}$
		0.72–0.82	$0.394 \pm 0.021^{+0.042}_{-0.043}$
		0.82–0.92	$0.389 \pm 0.020^{+0.033}_{-0.025}$
$2.67 \cdot 10^{-3}$	7.3	0.32–0.47	$0.290 \pm 0.097^{+0.034}_{-0.112}$
		0.47–0.62	$0.442 \pm 0.086^{+0.092}_{-0.159}$
		0.62–0.77	$0.449 \pm 0.050^{+0.094}_{-0.046}$
		0.77–0.92	$0.398 \pm 0.033^{+0.049}_{-0.054}$
$2.6 \cdot 10^{-4}$	11	0.32–0.47	$0.349 \pm 0.078^{+0.042}_{-0.128}$
		0.47–0.62	$0.285 \pm 0.034^{+0.111}_{-0.023}$
		0.62–0.77	$0.485 \pm 0.037^{+0.041}_{-0.074}$
		0.77–0.92	$0.371 \pm 0.021^{+0.033}_{-0.024}$
$4.6 \cdot 10^{-4}$	11	0.32–0.42	$0.482 \pm 0.097^{+0.067}_{-0.162}$
		0.42–0.52	$0.285 \pm 0.036^{+0.037}_{-0.039}$
		0.52–0.62	$0.370 \pm 0.031^{+0.064}_{-0.033}$
		0.62–0.72	$0.435 \pm 0.028^{+0.034}_{-0.054}$
		0.72–0.82	$0.386 \pm 0.019^{+0.051}_{-0.030}$
		0.82–0.92	$0.365 \pm 0.016^{+0.049}_{-0.018}$
$9.2 \cdot 10^{-4}$	11	0.32–0.42	$0.418 \pm 0.084^{+0.056}_{-0.093}$
		0.42–0.52	$0.286 \pm 0.037^{+0.064}_{-0.028}$
		0.52–0.62	$0.408 \pm 0.034^{+0.041}_{-0.035}$
		0.62–0.72	$0.392 \pm 0.024^{+0.052}_{-0.027}$

JHEP06(2009)074

table 6 (cont.)

$\langle x \rangle$	$\langle Q^2 \rangle$ (GeV^2)	x_L range	$r^{\mathrm{LP(3)}}$
		0.72–0.82	$0.392 \pm 0.019^{+0.039}_{-0.056}$
		0.82–0.92	$0.397 \pm 0.018^{+0.024}_{-0.044}$
$1.83 \cdot 10^{-3}$	11	0.32–0.42	$0.361 \pm 0.075^{+0.058}_{-0.056}$
		0.42–0.52	$0.353 \pm 0.047^{+0.039}_{-0.077}$
		0.52–0.62	$0.375 \pm 0.033^{+0.036}_{-0.073}$
		0.62–0.72	$0.411 \pm 0.026^{+0.030}_{-0.027}$
		0.72–0.82	$0.348 \pm 0.017^{+0.043}_{-0.026}$
		0.82–0.92	$0.378 \pm 0.017^{+0.051}_{-0.021}$
$3.98 \cdot 10^{-3}$	11	0.32–0.47	$0.228 \pm 0.063^{+0.033}_{-0.090}$
		0.47–0.62	$0.378 \pm 0.047^{+0.043}_{-0.063}$
		0.62–0.77	$0.421 \pm 0.033^{+0.034}_{-0.105}$
		0.77–0.92	$0.448 \pm 0.026^{+0.038}_{-0.057}$
$5.1 \cdot 10^{-4}$	22	0.32–0.47	$0.470 \pm 0.111^{+0.061}_{-0.281}$
		0.47–0.62	$0.306 \pm 0.037^{+0.045}_{-0.028}$
		0.62–0.77	$0.436 \pm 0.035^{+0.044}_{-0.043}$
		0.77–0.92	$0.388 \pm 0.023^{+0.042}_{-0.027}$
$9.2 \cdot 10^{-4}$	22	0.32–0.42	$0.356 \pm 0.084^{+0.137}_{-0.071}$
		0.42–0.52	$0.350 \pm 0.053^{+0.044}_{-0.044}$
		0.52–0.62	$0.376 \pm 0.039^{+0.058}_{-0.030}$
		0.62–0.72	$0.401 \pm 0.030^{+0.031}_{-0.057}$
		0.72–0.82	$0.386 \pm 0.022^{+0.056}_{-0.029}$
		0.82–0.92	$0.411 \pm 0.022^{+0.026}_{-0.041}$
$1.84 \cdot 10^{-3}$	22	0.32–0.42	$0.367 \pm 0.084^{+0.091}_{-0.075}$
		0.42–0.52	$0.241 \pm 0.038^{+0.075}_{-0.024}$
		0.52–0.62	$0.347 \pm 0.034^{+0.055}_{-0.033}$
		0.62–0.72	$0.353 \pm 0.025^{+0.060}_{-0.027}$
		0.72–0.82	$0.378 \pm 0.021^{+0.036}_{-0.035}$
		0.82–0.92	$0.401 \pm 0.021^{+0.048}_{-0.026}$
$3.66 \cdot 10^{-3}$	22	0.32–0.42	$0.297 \pm 0.078^{+0.145}_{-0.042}$
		0.42–0.52	$0.386 \pm 0.066^{+0.078}_{-0.034}$
		0.52–0.62	$0.457 \pm 0.055^{+0.066}_{-0.071}$
		0.62–0.72	$0.442 \pm 0.038^{+0.035}_{-0.077}$
		0.72–0.82	$0.453 \pm 0.029^{+0.059}_{-0.033}$
		0.82–0.92	$0.377 \pm 0.023^{+0.027}_{-0.040}$
$7.83 \cdot 10^{-3}$	22	0.32–0.47	$0.215 \pm 0.066^{+0.232}_{-0.102}$
		0.47–0.62	$0.354 \pm 0.053^{+0.087}_{-0.060}$
		0.62–0.77	$0.399 \pm 0.036^{+0.079}_{-0.032}$
		0.77–0.92	$0.442 \pm 0.030^{+0.060}_{-0.077}$

JHEP06(2009)074

table 6 (cont.)

$\langle x \rangle$	$\langle Q^2 \rangle$ (GeV^2)	x_L range	$r^{\mathrm{LP(3)}}$
$1.03 \cdot 10^{-3}$	44	0.32–0.47	$0.356 \pm 0.104^{+0.100}_{-0.062}$
		0.47–0.62	$0.327 \pm 0.052^{+0.074}_{-0.039}$
		0.62–0.77	$0.373 \pm 0.038^{+0.051}_{-0.034}$
		0.77–0.92	$0.381 \pm 0.030^{+0.027}_{-0.030}$
$1.86 \cdot 10^{-3}$	44	0.37–0.42	$0.508 \pm 0.150^{+0.221}_{-0.116}$
		0.47–0.52	$0.346 \pm 0.073^{+0.049}_{-0.077}$
		0.57–0.62	$0.444 \pm 0.063^{+0.043}_{-0.112}$
		0.67–0.72	$0.348 \pm 0.041^{+0.027}_{-0.049}$
		0.77–0.82	$0.413 \pm 0.033^{+0.044}_{-0.052}$
		0.87–0.92	$0.352 \pm 0.026^{+0.051}_{-0.021}$
$3.68 \cdot 10^{-3}$	44	0.37–0.42	$0.221 \pm 0.088^{+0.065}_{-0.027}$
		0.47–0.52	$0.456 \pm 0.097^{+0.079}_{-0.105}$
		0.57–0.62	$0.303 \pm 0.046^{+0.052}_{-0.023}$
		0.67–0.72	$0.496 \pm 0.057^{+0.036}_{-0.150}$
		0.77–0.82	$0.511 \pm 0.044^{+0.061}_{-0.056}$
		0.87–0.92	$0.408 \pm 0.033^{+0.041}_{-0.029}$
$7.33 \cdot 10^{-3}$	44	0.37–0.42	$0.628 \pm 0.226^{+0.297}_{-0.190}$
		0.47–0.52	$0.341 \pm 0.090^{+0.053}_{-0.060}$
		0.57–0.62	$0.418 \pm 0.074^{+0.153}_{-0.035}$
		0.67–0.72	$0.458 \pm 0.061^{+0.044}_{-0.070}$
		0.77–0.82	$0.501 \pm 0.048^{+0.055}_{-0.081}$
		0.87–0.92	$0.448 \pm 0.039^{+0.042}_{-0.030}$
$1.54 \cdot 10^{-2}$	44	0.32–0.52	$0.453 \pm 0.135^{+0.078}_{-0.363}$
		0.52–0.72	$0.454 \pm 0.062^{+0.048}_{-0.071}$
		0.72–0.92	$0.385 \pm 0.033^{+0.083}_{-0.027}$
$2.00 \cdot 10^{-3}$	88	0.32–0.47	$0.328 \pm 0.162^{+0.151}_{-0.064}$
		0.47–0.62	$0.462 \pm 0.121^{+0.111}_{-0.122}$
		0.62–0.77	$0.307 \pm 0.045^{+0.045}_{-0.030}$
		0.77–0.92	$0.339 \pm 0.040^{+0.048}_{-0.033}$
$3.59 \cdot 10^{-3}$	88	0.32–0.47	$0.449 \pm 0.145^{+0.058}_{-0.134}$
		0.47–0.62	$0.509 \pm 0.090^{+0.120}_{-0.098}$
		0.62–0.77	$0.402 \pm 0.049^{+0.194}_{-0.034}$
		0.77–0.92	$0.393 \pm 0.034^{+0.068}_{-0.022}$
$7.37 \cdot 10^{-3}$	88	0.32–0.47	$0.491 \pm 0.178^{+0.164}_{-0.131}$
		0.47–0.62	$0.345 \pm 0.078^{+0.050}_{-0.042}$
		0.62–0.77	$0.364 \pm 0.046^{+0.028}_{-0.034}$
		0.77–0.92	$0.440 \pm 0.042^{+0.087}_{-0.032}$
$1.42 \cdot 10^{-2}$	88	0.32–0.47	$0.351 \pm 0.133^{+0.171}_{-0.054}$

JHEP06(2009)074

table 6 (cont.)

$\langle x \rangle$	$\langle Q^2 \rangle$ (GeV^2)	x_L range	$r^{\mathrm{LP(3)}}$
		0.47–0.62	$0.479 \pm 0.101^{+0.169}_{-0.103}$
		0.62–0.77	$0.390 \pm 0.054^{+0.098}_{-0.037}$
		0.77–0.92	$0.498 \pm 0.050^{+0.042}_{-0.112}$
$3.01 \cdot 10^{-2}$	88	0.32–0.52	$0.449 \pm 0.211^{+0.075}_{-0.264}$
		0.52–0.72	$0.330 \pm 0.063^{+0.121}_{-0.023}$
		0.72–0.92	$0.440 \pm 0.056^{+0.062}_{-0.044}$
$4.00 \cdot 10^{-3}$	237	0.32–0.52	$0.250 \pm 0.153^{+0.115}_{-0.129}$
		0.52–0.72	$0.175 \pm 0.068^{+0.241}_{-0.013}$
		0.72–0.92	$0.451 \pm 0.071^{+0.079}_{-0.044}$
$7.52 \cdot 10^{-3}$	237	0.32–0.52	$0.467 \pm 0.195^{+0.105}_{-0.086}$
		0.52–0.72	$0.482 \pm 0.088^{+0.067}_{-0.205}$
		0.72–0.92	$0.430 \pm 0.049^{+0.069}_{-0.053}$
$1.47 \cdot 10^{-2}$	237	0.32–0.47	$0.301 \pm 0.156^{+0.366}_{-0.040}$
		0.47–0.62	$0.249 \pm 0.074^{+0.087}_{-0.037}$
		0.62–0.77	$0.445 \pm 0.070^{+0.112}_{-0.040}$
		0.77–0.92	$0.381 \pm 0.045^{+0.040}_{-0.028}$
$3.25 \cdot 10^{-2}$	237	0.32–0.47	$0.102 \pm 0.082^{+0.119}_{-0.011}$
		0.47–0.62	$0.355 \pm 0.090^{+0.049}_{-0.072}$
		0.62–0.77	$0.359 \pm 0.055^{+0.135}_{-0.028}$
		0.77–0.92	$0.403 \pm 0.049^{+0.041}_{-0.064}$

JHEP06(2009)074

$\langle x \rangle$	$\langle Q^2 \rangle$ (GeV^2)	x_L range	$r^{\mathrm{LP(3)}}$
$9.6 \cdot 10^{-5}$	4.2	0.32–0.47	$0.082 \pm 0.015^{+0.043}_{-0.014}$
		0.47–0.62	$0.091 \pm 0.012^{+0.015}_{-0.019}$
		0.62–0.77	$0.080 \pm 0.006^{+0.005}_{-0.026}$
		0.77–0.92	$0.104 \pm 0.008^{+0.007}_{-0.014}$
$1.7 \cdot 10^{-4}$	4.2	0.32–0.47	$0.103 \pm 0.013^{+0.006}_{-0.026}$
		0.47–0.62	$0.083 \pm 0.008^{+0.009}_{-0.010}$
		0.62–0.77	$0.096 \pm 0.005^{+0.003}_{-0.023}$
		0.77–0.92	$0.089 \pm 0.004^{+0.003}_{-0.008}$
$3.5 \cdot 10^{-4}$	4.2	0.32–0.47	$0.077 \pm 0.010^{+0.009}_{-0.009}$
		0.47–0.62	$0.087 \pm 0.008^{+0.012}_{-0.006}$
		0.62–0.77	$0.108 \pm 0.006^{+0.009}_{-0.007}$
		0.77–0.92	$0.093 \pm 0.004^{+0.004}_{-0.003}$
$6.9 \cdot 10^{-4}$	4.2	0.32–0.47	$0.077 \pm 0.012^{+0.013}_{-0.004}$
		0.47–0.62	$0.085 \pm 0.009^{+0.007}_{-0.007}$
		0.62–0.77	$0.095 \pm 0.006^{+0.009}_{-0.002}$
		0.77–0.92	$0.087 \pm 0.004^{+0.006}_{-0.002}$
$1.46 \cdot 10^{-3}$	4.2	0.32–0.47	$0.074 \pm 0.016^{+0.012}_{-0.015}$
		0.47–0.62	$0.046 \pm 0.008^{+0.011}_{-0.004}$
		0.62–0.77	$0.083 \pm 0.006^{+0.012}_{-0.003}$
		0.77–0.92	$0.086 \pm 0.006^{+0.005}_{-0.007}$

Table 7. The leading proton production rate, $r^{\mathrm{LP(3)}}$, measured as a function of x_L for protons with $p_T^2 < 0.04\ GeV^2$, in bins of x and Q^2, with averages $\langle x \rangle$ and $\langle Q^2 \rangle$. Statistical uncertainties are listed first, followed by systematic uncertainties.

table 7 (cont.)

$\langle x \rangle$	$\langle Q^2 \rangle$ (GeV^2)	x_L range	$r^{\mathrm{LP(3)}}$
$1.9 \cdot 10^{-4}$	7.3	0.32–0.47	$0.093 \pm 0.017^{+0.009}_{-0.015}$
		0.47–0.62	$0.098 \pm 0.012^{+0.008}_{-0.027}$
		0.62–0.77	$0.087 \pm 0.007^{+0.013}_{-0.003}$
		0.77–0.92	$0.092 \pm 0.007^{+0.006}_{-0.015}$
$3.4 \cdot 10^{-4}$	7.3	0.32–0.47	$0.090 \pm 0.015^{+0.012}_{-0.019}$
		0.47–0.62	$0.103 \pm 0.011^{+0.006}_{-0.011}$
		0.62–0.77	$0.079 \pm 0.005^{+0.007}_{-0.002}$
		0.77–0.92	$0.088 \pm 0.005^{+0.004}_{-0.003}$
$6.9 \cdot 10^{-4}$	7.3	0.32–0.47	$0.090 \pm 0.015^{+0.005}_{-0.025}$
		0.47–0.62	$0.093 \pm 0.011^{+0.004}_{-0.017}$
		0.62–0.77	$0.102 \pm 0.007^{+0.004}_{-0.006}$
		0.77–0.92	$0.095 \pm 0.006^{+0.002}_{-0.017}$
$1.36 \cdot 10^{-3}$	7.3	0.32–0.47	$0.075 \pm 0.014^{+0.011}_{-0.006}$

JHEP06(2009)074

table 7 (cont.)

$\langle x \rangle$	$\langle Q^2 \rangle$ (GeV^2)	x_L range	$r^{\mathrm{LP(3)}}$
		0.47–0.62	$0.104 \pm 0.013^{+0.010}_{-0.014}$
		0.62–0.77	$0.113 \pm 0.008^{+0.003}_{-0.017}$
		0.77–0.92	$0.098 \pm 0.006^{+0.006}_{-0.009}$
$2.67 \cdot 10^{-3}$	7.3	0.32–0.47	$0.067 \pm 0.025^{+0.007}_{-0.034}$
		0.47–0.62	$0.112 \pm 0.028^{+0.023}_{-0.036}$
		0.62–0.77	$0.097 \pm 0.015^{+0.017}_{-0.012}$
		0.77–0.92	$0.095 \pm 0.011^{+0.003}_{-0.017}$
$2.6 \cdot 10^{-4}$	11	0.32–0.47	$0.098 \pm 0.024^{+0.006}_{-0.031}$
		0.47–0.62	$0.075 \pm 0.013^{+0.038}_{-0.006}$
		0.62–0.77	$0.129 \pm 0.014^{+0.005}_{-0.011}$
		0.77–0.92	$0.085 \pm 0.008^{+0.003}_{-0.005}$
$4.6 \cdot 10^{-4}$	11	0.32–0.47	$0.114 \pm 0.018^{+0.008}_{-0.027}$
		0.47–0.62	$0.081 \pm 0.009^{+0.014}_{-0.004}$
		0.62–0.77	$0.101 \pm 0.007^{+0.003}_{-0.011}$
		0.77–0.92	$0.099 \pm 0.006^{+0.007}_{-0.003}$
$9.2 \cdot 10^{-4}$	11	0.32–0.47	$0.080 \pm 0.013^{+0.009}_{-0.006}$
		0.47–0.62	$0.110 \pm 0.012^{+0.019}_{-0.004}$
		0.62–0.77	$0.080 \pm 0.006^{+0.009}_{-0.007}$
		0.77–0.92	$0.091 \pm 0.005^{+0.002}_{-0.005}$
$1.83 \cdot 10^{-3}$	11	0.32–0.47	$0.082 \pm 0.015^{+0.008}_{-0.007}$
		0.47–0.62	$0.094 \pm 0.011^{+0.004}_{-0.018}$
		0.62–0.77	$0.100 \pm 0.007^{+0.004}_{-0.006}$
		0.77–0.92	$0.089 \pm 0.005^{+0.008}_{-0.002}$
$3.98 \cdot 10^{-3}$	11	0.32–0.47	$0.041 \pm 0.015^{+0.009}_{-0.020}$
		0.47–0.62	$0.118 \pm 0.021^{+0.010}_{-0.042}$
		0.62–0.77	$0.102 \pm 0.010^{+0.003}_{-0.024}$
		0.77–0.92	$0.107 \pm 0.009^{+0.006}_{-0.014}$
$5.1 \cdot 10^{-4}$	22	0.32–0.47	$0.098 \pm 0.029^{+0.013}_{-0.056}$
		0.47–0.62	$0.081 \pm 0.014^{+0.010}_{-0.006}$
		0.62–0.77	$0.114 \pm 0.014^{+0.021}_{-0.007}$
		0.77–0.92	$0.088 \pm 0.009^{+0.005}_{-0.023}$
$9.2 \cdot 10^{-4}$	22	0.32–0.47	$0.094 \pm 0.018^{+0.007}_{-0.020}$
		0.47–0.62	$0.094 \pm 0.012^{+0.018}_{-0.003}$
		0.62–0.77	$0.100 \pm 0.008^{+0.009}_{-0.008}$
		0.77–0.92	$0.090 \pm 0.006^{+0.008}_{-0.004}$
$1.84 \cdot 10^{-3}$	22	0.32–0.47	$0.089 \pm 0.017^{+0.022}_{-0.008}$
		0.47–0.62	$0.080 \pm 0.010^{+0.007}_{-0.010}$
		0.62–0.77	$0.089 \pm 0.007^{+0.003}_{-0.007}$

JHEP06(2009)074

table 7 (cont.)

$\langle x \rangle$	$\langle Q^2 \rangle$ (GeV^2)	x_L range	$r^{\mathrm{LP(3)}}$
		0.77–0.92	$0.089 \pm 0.006^{+0.010}_{-0.004}$
$3.66 \cdot 10^{-3}$	22	0.32–0.47	$0.078 \pm 0.017^{+0.026}_{-0.005}$
		0.47–0.62	$0.120 \pm 0.019^{+0.009}_{-0.028}$
		0.62–0.77	$0.114 \pm 0.010^{+0.007}_{-0.010}$
		0.77–0.92	$0.099 \pm 0.007^{+0.013}_{-0.002}$
$7.83 \cdot 10^{-3}$	22	0.32–0.47	$0.054 \pm 0.019^{+0.050}_{-0.024}$
		0.47–0.62	$0.087 \pm 0.018^{+0.011}_{-0.043}$
		0.62–0.77	$0.087 \pm 0.010^{+0.041}_{-0.005}$
		0.77–0.92	$0.116 \pm 0.012^{+0.033}_{-0.016}$
$1.03 \cdot 10^{-3}$	44	0.32–0.47	$0.092 \pm 0.031^{+0.020}_{-0.017}$
		0.47–0.62	$0.086 \pm 0.020^{+0.048}_{-0.010}$
		0.62–0.77	$0.105 \pm 0.016^{+0.018}_{-0.031}$
		0.77–0.92	$0.108 \pm 0.013^{+0.015}_{-0.005}$
$1.86 \cdot 10^{-3}$	44	0.32–0.47	$0.096 \pm 0.023^{+0.024}_{-0.010}$
		0.47–0.62	$0.087 \pm 0.016^{+0.005}_{-0.028}$
		0.62–0.77	$0.130 \pm 0.015^{+0.004}_{-0.029}$
		0.77–0.92	$0.102 \pm 0.010^{+0.004}_{-0.016}$
$3.68 \cdot 10^{-3}$	44	0.32–0.47	$0.077 \pm 0.023^{+0.038}_{-0.011}$
		0.47–0.62	$0.079 \pm 0.016^{+0.004}_{-0.019}$
		0.62–0.77	$0.139 \pm 0.017^{+0.005}_{-0.023}$
		0.77–0.92	$0.117 \pm 0.012^{+0.003}_{-0.013}$
$7.33 \cdot 10^{-3}$	44	0.32–0.47	$0.124 \pm 0.039^{+0.021}_{-0.030}$
		0.47–0.62	$0.104 \pm 0.023^{+0.027}_{-0.005}$
		0.62–0.77	$0.107 \pm 0.015^{+0.022}_{-0.004}$
		0.77–0.92	$0.096 \pm 0.011^{+0.023}_{-0.004}$
$1.54 \cdot 10^{-2}$	44	0.32–0.47	$0.076 \pm 0.036^{+0.075}_{-0.017}$
		0.47–0.62	$0.118 \pm 0.034^{+0.020}_{-0.040}$
		0.62–0.77	$0.108 \pm 0.019^{+0.036}_{-0.009}$
		0.77–0.92	$0.101 \pm 0.015^{+0.022}_{-0.015}$
$2.00 \cdot 10^{-3}$	88	0.32–0.52	$0.130 \pm 0.053^{+0.014}_{-0.076}$
		0.52–0.72	$0.128 \pm 0.031^{+0.038}_{-0.049}$
		0.72–0.92	$0.089 \pm 0.014^{+0.021}_{-0.002}$
$3.59 \cdot 10^{-3}$	88	0.32–0.52	$0.126 \pm 0.037^{+0.009}_{-0.046}$
		0.52–0.72	$0.080 \pm 0.014^{+0.035}_{-0.004}$
		0.72–0.92	$0.104 \pm 0.012^{+0.015}_{-0.003}$
$7.37 \cdot 10^{-3}$	88	0.32–0.52	$0.091 \pm 0.031^{+0.034}_{-0.015}$
		0.52–0.72	$0.077 \pm 0.017^{+0.029}_{-0.006}$
		0.72–0.92	$0.090 \pm 0.011^{+0.026}_{-0.004}$

JHEP06(2009)074

table 7 (cont.)

$\langle x \rangle$	$\langle Q^2 \rangle$ (GeV^2)	x_L range	$r^{\mathrm{LP(3)}}$
$1.42 \cdot 10^{-2}$	88	0.32–0.52	$0.075 \pm 0.024^{+0.048}_{-0.005}$
		0.52–0.72	$0.118 \pm 0.027^{+0.051}_{-0.010}$
		0.72–0.92	$0.103 \pm 0.014^{+0.034}_{-0.007}$
$3.01 \cdot 10^{-2}$	88	0.32–0.52	$0.151 \pm 0.075^{+0.022}_{-0.143}$
		0.52–0.72	$0.081 \pm 0.020^{+0.015}_{-0.012}$
		0.72–0.92	$0.099 \pm 0.017^{+0.033}_{-0.004}$
$4.00 \cdot 10^{-3}$	237	0.32–0.52	$0.053 \pm 0.036^{+0.020}_{-0.045}$
		0.52–0.72	$0.092 \pm 0.033^{+0.102}_{-0.006}$
		0.72–0.92	$0.116 \pm 0.025^{+0.022}_{-0.010}$
$7.52 \cdot 10^{-3}$	237	0.32–0.52	$0.116 \pm 0.052^{+0.036}_{-0.015}$
		0.52–0.72	$0.108 \pm 0.030^{+0.016}_{-0.057}$
		0.72–0.92	$0.098 \pm 0.017^{+0.007}_{-0.024}$
$1.47 \cdot 10^{-2}$	237	0.32–0.52	$0.072 \pm 0.036^{+0.053}_{-0.007}$
		0.52–0.72	$0.098 \pm 0.025^{+0.062}_{-0.022}$
		0.72–0.92	$0.128 \pm 0.020^{+0.012}_{-0.025}$
$3.25 \cdot 10^{-2}$	237	0.32–0.52	$0.033 \pm 0.020^{+0.073}_{-0.002}$
		0.52–0.72	$0.071 \pm 0.019^{+0.058}_{-0.013}$
		0.72–0.92	$0.102 \pm 0.017^{+0.014}_{-0.019}$

JHEP06(2009)074

$\langle x \rangle$	$\langle Q^2 \rangle$ (GeV^2)	x_L range	$r^{\mathrm{LP(3)}}$
$9.6 \cdot 10^{-5}$	4.2	0.38–0.56	$0.146 \pm 0.027^{+0.022}_{-0.039}$
		0.56–0.74	$0.125 \pm 0.012^{+0.015}_{-0.013}$
		0.74–0.92	$0.177 \pm 0.013^{+0.017}_{-0.058}$
$1.7 \cdot 10^{-4}$	4.2	0.38–0.56	$0.133 \pm 0.017^{+0.025}_{-0.026}$
		0.56–0.74	$0.145 \pm 0.010^{+0.006}_{-0.026}$
		0.74–0.92	$0.137 \pm 0.006^{+0.009}_{-0.005}$
$3.5 \cdot 10^{-4}$	4.2	0.38–0.56	$0.123 \pm 0.018^{+0.020}_{-0.011}$
		0.56–0.74	$0.140 \pm 0.009^{+0.009}_{-0.013}$
		0.74–0.92	$0.141 \pm 0.007^{+0.008}_{-0.012}$
$6.9 \cdot 10^{-4}$	4.2	0.38–0.56	$0.128 \pm 0.019^{+0.018}_{-0.028}$
		0.56–0.74	$0.128 \pm 0.010^{+0.008}_{-0.018}$
		0.74–0.92	$0.151 \pm 0.008^{+0.006}_{-0.020}$
$1.46 \cdot 10^{-3}$	4.2	0.38–0.56	$0.160 \pm 0.033^{+0.035}_{-0.016}$
		0.56–0.74	$0.156 \pm 0.018^{+0.015}_{-0.019}$
		0.74–0.92	$0.136 \pm 0.010^{+0.017}_{-0.020}$
$1.9 \cdot 10^{-4}$	7.3	0.38–0.56	$0.126 \pm 0.023^{+0.048}_{-0.006}$
		0.56–0.74	$0.123 \pm 0.012^{+0.009}_{-0.016}$
		0.74–0.92	$0.149 \pm 0.011^{+0.004}_{-0.020}$
$3.4 \cdot 10^{-4}$	7.3	0.38–0.56	$0.140 \pm 0.022^{+0.018}_{-0.028}$
		0.56–0.74	$0.144 \pm 0.012^{+0.006}_{-0.026}$
		0.74–0.92	$0.136 \pm 0.008^{+0.008}_{-0.008}$
$6.9 \cdot 10^{-4}$	7.3	0.38–0.56	$0.123 \pm 0.021^{+0.019}_{-0.022}$
		0.56–0.74	$0.122 \pm 0.011^{+0.012}_{-0.004}$
		0.74–0.92	$0.141 \pm 0.008^{+0.009}_{-0.014}$
$1.36 \cdot 10^{-3}$	7.3	0.38–0.56	$0.158 \pm 0.027^{+0.052}_{-0.024}$
		0.56–0.74	$0.140 \pm 0.013^{+0.016}_{-0.009}$
		0.74–0.92	$0.149 \pm 0.010^{+0.013}_{-0.006}$
$2.67 \cdot 10^{-3}$	7.3	0.38–0.56	$0.175 \pm 0.070^{+0.023}_{-0.153}$
		0.56–0.74	$0.193 \pm 0.038^{+0.077}_{-0.054}$
		0.74–0.92	$0.161 \pm 0.021^{+0.032}_{-0.024}$

Table 8. The leading proton production rate, $r^{\mathrm{LP(3)}}$, measured as a function of x_L for protons with $0.04 < p_T^2 < 0.15\ GeV^2$, in bins of x and Q^2, with averages $\langle x \rangle$ and $\langle Q^2 \rangle$. Statistical uncertainties are listed first, followed by systematic uncertainties.

table 8 (cont.)

$\langle x \rangle$	$\langle Q^2 \rangle$ (GeV^2)	x_L range	$r^{\mathrm{LP(3)}}$
$2.6 \cdot 10^{-4}$	11	0.38–0.56	$0.084 \pm 0.021^{+0.033}_{-0.008}$
		0.56–0.74	$0.151 \pm 0.019^{+0.010}_{-0.030}$
		0.74–0.92	$0.140 \pm 0.012^{+0.013}_{-0.006}$
$4.6 \cdot 10^{-4}$	11	0.38–0.56	$0.134 \pm 0.020^{+0.056}_{-0.009}$

JHEP06(2009)074

table 8 (cont.)

$\langle x \rangle$	$\langle Q^2 \rangle$ (GeV^2)	x_L range	$r^{\mathrm{LP(3)}}$
		0.56–0.74	$0.132 \pm 0.011^{+0.009}_{-0.016}$
		0.74–0.92	$0.133 \pm 0.007^{+0.032}_{-0.003}$
$9.2 \cdot 10^{-4}$	11	0.38–0.56	$0.129 \pm 0.021^{+0.008}_{-0.015}$
		0.56–0.74	$0.140 \pm 0.011^{+0.032}_{-0.006}$
		0.74–0.92	$0.150 \pm 0.008^{+0.003}_{-0.022}$
$1.83 \cdot 10^{-3}$	11	0.38–0.56	$0.115 \pm 0.018^{+0.026}_{-0.007}$
		0.56–0.74	$0.165 \pm 0.013^{+0.007}_{-0.036}$
		0.74–0.92	$0.127 \pm 0.007^{+0.022}_{-0.003}$
$3.98 \cdot 10^{-3}$	11	0.38–0.56	$0.110 \pm 0.031^{+0.099}_{-0.013}$
		0.56–0.74	$0.129 \pm 0.018^{+0.007}_{-0.032}$
		0.74–0.92	$0.157 \pm 0.013^{+0.018}_{-0.024}$
$5.1 \cdot 10^{-4}$	22	0.38–0.56	$0.112 \pm 0.029^{+0.079}_{-0.009}$
		0.56–0.74	$0.133 \pm 0.017^{+0.009}_{-0.019}$
		0.74–0.92	$0.148 \pm 0.013^{+0.037}_{-0.003}$
$9.2 \cdot 10^{-4}$	22	0.38–0.56	$0.146 \pm 0.028^{+0.039}_{-0.025}$
		0.56–0.74	$0.153 \pm 0.015^{+0.007}_{-0.025}$
		0.74–0.92	$0.157 \pm 0.010^{+0.004}_{-0.016}$
$1.84 \cdot 10^{-3}$	22	0.38–0.56	$0.101 \pm 0.019^{+0.050}_{-0.006}$
		0.56–0.74	$0.141 \pm 0.013^{+0.009}_{-0.012}$
		0.74–0.92	$0.144 \pm 0.009^{+0.019}_{-0.006}$
$3.66 \cdot 10^{-3}$	22	0.38–0.56	$0.177 \pm 0.036^{+0.042}_{-0.018}$
		0.56–0.74	$0.165 \pm 0.018^{+0.014}_{-0.020}$
		0.74–0.92	$0.156 \pm 0.011^{+0.005}_{-0.020}$
$7.83 \cdot 10^{-3}$	22	0.38–0.56	$0.166 \pm 0.046^{+0.063}_{-0.014}$
		0.56–0.74	$0.185 \pm 0.031^{+0.011}_{-0.065}$
		0.74–0.92	$0.147 \pm 0.015^{+0.007}_{-0.023}$
$1.03 \cdot 10^{-3}$	44	0.38–0.56	$0.128 \pm 0.042^{+0.155}_{-0.008}$
		0.56–0.74	$0.090 \pm 0.016^{+0.052}_{-0.006}$
		0.74–0.92	$0.152 \pm 0.018^{+0.005}_{-0.042}$
$1.86 \cdot 10^{-3}$	44	0.38–0.56	$0.190 \pm 0.048^{+0.059}_{-0.015}$
		0.56–0.74	$0.136 \pm 0.019^{+0.006}_{-0.029}$
		0.74–0.92	$0.115 \pm 0.010^{+0.049}_{-0.003}$
$3.68 \cdot 10^{-3}$	44	0.38–0.56	$0.082 \pm 0.023^{+0.176}_{-0.010}$
		0.56–0.74	$0.156 \pm 0.023^{+0.017}_{-0.031}$
		0.74–0.92	$0.158 \pm 0.015^{+0.021}_{-0.004}$
$7.33 \cdot 10^{-3}$	44	0.38–0.56	$0.138 \pm 0.045^{+0.070}_{-0.011}$
		0.56–0.74	$0.169 \pm 0.028^{+0.027}_{-0.022}$
		0.74–0.92	$0.188 \pm 0.020^{+0.010}_{-0.056}$

JHEP06(2009)074

table 8 (cont.)

$\langle x \rangle$	$\langle Q^2 \rangle$ (GeV^2)	x_L range	$r^{\mathrm{LP(3)}}$
$1.54 \cdot 10^{-2}$	44	0.38–0.56	$0.130 \pm 0.055^{+0.056}_{-0.036}$
		0.56–0.74	$0.195 \pm 0.043^{+0.042}_{-0.078}$
		0.74–0.92	$0.118 \pm 0.016^{+0.052}_{-0.004}$
$2.00 \cdot 10^{-3}$	88	0.38–0.65	$0.092 \pm 0.030^{+0.025}_{-0.018}$
		0.65–0.92	$0.109 \pm 0.018^{+0.020}_{-0.009}$
$3.59 \cdot 10^{-3}$	88	0.38–0.65	$0.236 \pm 0.053^{+0.030}_{-0.098}$
		0.65–0.92	$0.153 \pm 0.018^{+0.018}_{-0.006}$
$7.37 \cdot 10^{-3}$	88	0.38–0.65	$0.190 \pm 0.047^{+0.078}_{-0.030}$
		0.65–0.92	$0.191 \pm 0.024^{+0.022}_{-0.047}$
$1.42 \cdot 10^{-2}$	88	0.38–0.65	$0.153 \pm 0.040^{+0.072}_{-0.018}$
		0.65–0.92	$0.179 \pm 0.026^{+0.004}_{-0.063}$
$3.01 \cdot 10^{-2}$	88	0.38–0.65	$0.137 \pm 0.053^{+0.095}_{-0.010}$
		0.65–0.92	$0.158 \pm 0.032^{+0.030}_{-0.026}$
$4.00 \cdot 10^{-3}$	237	0.38–0.65	$0.051 \pm 0.048^{+0.119}_{-0.003}$
		0.65–0.92	$0.067 \pm 0.027^{+0.069}_{-0.012}$
$7.52 \cdot 10^{-3}$	237	0.38–0.65	$0.162 \pm 0.053^{+0.023}_{-0.048}$
		0.65–0.92	$0.164 \pm 0.027^{+0.094}_{-0.036}$
$1.47 \cdot 10^{-2}$	237	0.38–0.65	$0.161 \pm 0.052^{+0.049}_{-0.048}$
		0.65–0.92	$0.095 \pm 0.015^{+0.056}_{-0.005}$
$3.25 \cdot 10^{-2}$	237	0.38–0.65	$0.179 \pm 0.054^{+0.026}_{-0.056}$
		0.65–0.92	$0.123 \pm 0.019^{+0.017}_{-0.008}$

JHEP06(2009)074

$\langle x \rangle$	$\langle Q^2 \rangle$ (GeV^2)	x_L range	$r^{\mathrm{LP(3)}}$
$9.6 \cdot 10^{-5}$	4.2	0.62–0.72	$0.114 \pm 0.027^{+0.072}_{-0.014}$
		0.72–0.82	$0.116 \pm 0.033^{+0.066}_{-0.026}$
		0.82–0.92	$0.121 \pm 0.016^{+0.054}_{-0.015}$
$1.7 \cdot 10^{-4}$	4.2	0.62–0.72	$0.102 \pm 0.014^{+0.018}_{-0.026}$
		0.72–0.82	$0.105 \pm 0.018^{+0.053}_{-0.034}$
		0.82–0.92	$0.133 \pm 0.012^{+0.036}_{-0.011}$
$3.5 \cdot 10^{-4}$	4.2	0.62–0.72	$0.114 \pm 0.018^{+0.010}_{-0.021}$
		0.72–0.82	$0.212 \pm 0.043^{+0.023}_{-0.172}$
		0.82–0.92	$0.099 \pm 0.010^{+0.010}_{-0.011}$
$6.9 \cdot 10^{-4}$	4.2	0.62–0.72	$0.097 \pm 0.015^{+0.040}_{-0.007}$
		0.72–0.82	$0.166 \pm 0.034^{+0.036}_{-0.048}$
		0.82–0.92	$0.151 \pm 0.016^{+0.011}_{-0.020}$
$1.46 \cdot 10^{-3}$	4.2	0.62–0.72	$0.106 \pm 0.024^{+0.015}_{-0.022}$
		0.72–0.82	$0.090 \pm 0.027^{+0.021}_{-0.039}$
		0.82–0.92	$0.154 \pm 0.022^{+0.043}_{-0.033}$
$1.9 \cdot 10^{-4}$	7.3	0.62–0.72	$0.158 \pm 0.034^{+0.012}_{-0.069}$
		0.72–0.82	$0.068 \pm 0.026^{+0.030}_{-0.040}$
		0.82–0.92	$0.100 \pm 0.017^{+0.019}_{-0.035}$
$3.4 \cdot 10^{-4}$	7.3	0.62–0.72	$0.138 \pm 0.025^{+0.013}_{-0.025}$
		0.72–0.82	$0.149 \pm 0.034^{+0.020}_{-0.077}$
		0.82–0.92	$0.110 \pm 0.013^{+0.012}_{-0.017}$
$6.9 \cdot 10^{-4}$	7.3	0.62–0.72	$0.137 \pm 0.025^{+0.010}_{-0.042}$
		0.72–0.82	$0.098 \pm 0.024^{+0.009}_{-0.035}$
		0.82–0.92	$0.160 \pm 0.018^{+0.012}_{-0.032}$
$1.36 \cdot 10^{-3}$	7.3	0.62–0.72	$0.127 \pm 0.024^{+0.038}_{-0.008}$
		0.72–0.82	$0.170 \pm 0.040^{+0.068}_{-0.066}$
		0.82–0.92	$0.127 \pm 0.016^{+0.009}_{-0.023}$
$2.67 \cdot 10^{-3}$	7.3	0.62–0.77	$0.245 \pm 0.103^{+0.119}_{-0.120}$
		0.77–0.92	$0.113 \pm 0.027^{+0.060}_{-0.018}$

Table 9. The leading proton production rate, $r^{\mathrm{LP(3)}}$, measured as a function of x_L for protons with $0.15 < p_T^2 < 0.5\ GeV^2$, in bins of x and Q^2, with averages $\langle x \rangle$ and $\langle Q^2 \rangle$. Statistical uncertainties are listed first, followed by systematic uncertainties.

table 9 (cont.)

$\langle x \rangle$	$\langle Q^2 \rangle$ (GeV^2)	x_L range	$r^{\mathrm{LP(3)}}$
$2.6 \cdot 10^{-4}$	11	0.62–0.72	$0.170 \pm 0.047^{+0.063}_{-0.036}$
		0.72–0.82	$0.088 \pm 0.048^{+0.225}_{-0.012}$
		0.82–0.92	$0.169 \pm 0.027^{+0.023}_{-0.059}$
$4.6 \cdot 10^{-4}$	11	0.62–0.72	$0.176 \pm 0.030^{+0.015}_{-0.040}$
		0.72–0.82	$0.126 \pm 0.030^{+0.076}_{-0.074}$

JHEP06(2009)074

table 9 (cont.)

$\langle x \rangle$	$\langle Q^2 \rangle$ (GeV^2)	x_L range	$r^{\mathrm{LP(3)}}$
		0.82–0.92	$0.134 \pm 0.015^{+0.020}_{-0.027}$
$9.2 \cdot 10^{-4}$	11	0.62–0.72	$0.142 \pm 0.023^{+0.015}_{-0.039}$
		0.72–0.82	$0.158 \pm 0.040^{+0.026}_{-0.117}$
		0.82–0.92	$0.148 \pm 0.016^{+0.017}_{-0.019}$
$1.83 \cdot 10^{-3}$	11	0.62–0.72	$0.107 \pm 0.018^{+0.018}_{-0.012}$
		0.72–0.82	$0.071 \pm 0.019^{+0.089}_{-0.008}$
		0.82–0.92	$0.145 \pm 0.015^{+0.020}_{-0.017}$
$3.98 \cdot 10^{-3}$	11	0.62–0.77	$0.135 \pm 0.034^{+0.058}_{-0.014}$
		0.77–0.92	$0.199 \pm 0.033^{+0.018}_{-0.050}$
$5.1 \cdot 10^{-4}$	22	0.62–0.72	$0.125 \pm 0.033^{+0.019}_{-0.052}$
		0.72–0.82	$0.179 \pm 0.069^{+0.038}_{-0.121}$
		0.82–0.92	$0.127 \pm 0.020^{+0.053}_{-0.012}$
$9.2 \cdot 10^{-4}$	22	0.62–0.72	$0.127 \pm 0.024^{+0.057}_{-0.016}$
		0.72–0.82	$0.106 \pm 0.027^{+0.014}_{-0.019}$
		0.82–0.92	$0.147 \pm 0.018^{+0.010}_{-0.021}$
$1.84 \cdot 10^{-3}$	22	0.62–0.72	$0.084 \pm 0.017^{+0.028}_{-0.008}$
		0.72–0.82	$0.158 \pm 0.039^{+0.017}_{-0.063}$
		0.82–0.92	$0.157 \pm 0.021^{+0.016}_{-0.036}$
$3.66 \cdot 10^{-3}$	22	0.62–0.72	$0.115 \pm 0.029^{+0.019}_{-0.052}$
		0.72–0.82	$0.112 \pm 0.030^{+0.097}_{-0.011}$
		0.82–0.92	$0.124 \pm 0.020^{+0.018}_{-0.068}$
$7.83 \cdot 10^{-3}$	22	0.62–0.77	$0.110 \pm 0.037^{+0.064}_{-0.024}$
		0.77–0.92	$0.223 \pm 0.044^{+0.015}_{-0.127}$
$1.03 \cdot 10^{-3}$	44	0.62–0.77	$0.171 \pm 0.054^{+0.048}_{-0.039}$
		0.77–0.92	$0.100 \pm 0.023^{+0.014}_{-0.024}$
$1.86 \cdot 10^{-3}$	44	0.62–0.77	$0.124 \pm 0.030^{+0.013}_{-0.024}$
		0.77–0.92	$0.141 \pm 0.022^{+0.068}_{-0.015}$
$3.68 \cdot 10^{-3}$	44	0.62–0.77	$0.170 \pm 0.049^{+0.060}_{-0.058}$
		0.77–0.92	$0.117 \pm 0.022^{+0.026}_{-0.016}$
$7.33 \cdot 10^{-3}$	44	0.62–0.77	$0.185 \pm 0.078^{+0.044}_{-0.103}$
		0.77–0.92	$0.120 \pm 0.024^{+0.037}_{-0.074}$
$1.54 \cdot 10^{-2}$	44	0.62–0.77	$0.196 \pm 0.078^{+0.228}_{-0.020}$
		0.77–0.92	$0.182 \pm 0.050^{+0.041}_{-0.079}$
$2.00 \cdot 10^{-3}$	88	0.62–0.77	$0.156 \pm 0.077^{+0.040}_{-0.081}$
		0.77–0.92	$0.125 \pm 0.034^{+0.011}_{-0.047}$
$3.59 \cdot 10^{-3}$	88	0.62–0.77	$0.208 \pm 0.087^{+0.115}_{-0.044}$
		0.77–0.92	$0.129 \pm 0.027^{+0.067}_{-0.019}$
$7.37 \cdot 10^{-3}$	88	0.62–0.77	$0.061 \pm 0.031^{+0.003}_{-0.022}$

JHEP06(2009)074

table 9 (cont.)

$\langle x \rangle$	$\langle Q^2 \rangle$ (GeV^2)	x_L range	$r^{\mathrm{LP(3)}}$
		0.77–0.92	$0.127 \pm 0.035^{+0.050}_{-0.040}$
$1.42 \cdot 10^{-2}$	88	0.62–0.77	$0.145 \pm 0.056^{+0.338}_{-0.013}$
		0.77–0.92	$0.268 \pm 0.079^{+0.030}_{-0.264}$
$3.01 \cdot 10^{-2}$	88	0.62–0.77	$0.106 \pm 0.063^{+0.200}_{-0.040}$
		0.77–0.92	$0.215 \pm 0.107^{+0.031}_{-0.146}$
$4.00 \cdot 10^{-3}$	237	0.62–0.92	$0.248 \pm 0.107^{+0.024}_{-0.132}$
$7.52 \cdot 10^{-3}$	237	0.62–0.92	$0.183 \pm 0.049^{+0.068}_{-0.027}$
$1.47 \cdot 10^{-2}$	237	0.62–0.92	$0.203 \pm 0.057^{+0.016}_{-0.059}$
$3.25 \cdot 10^{-2}$	237	0.62–0.92	$0.164 \pm 0.045^{+0.061}_{-0.055}$

JHEP06(2009)074

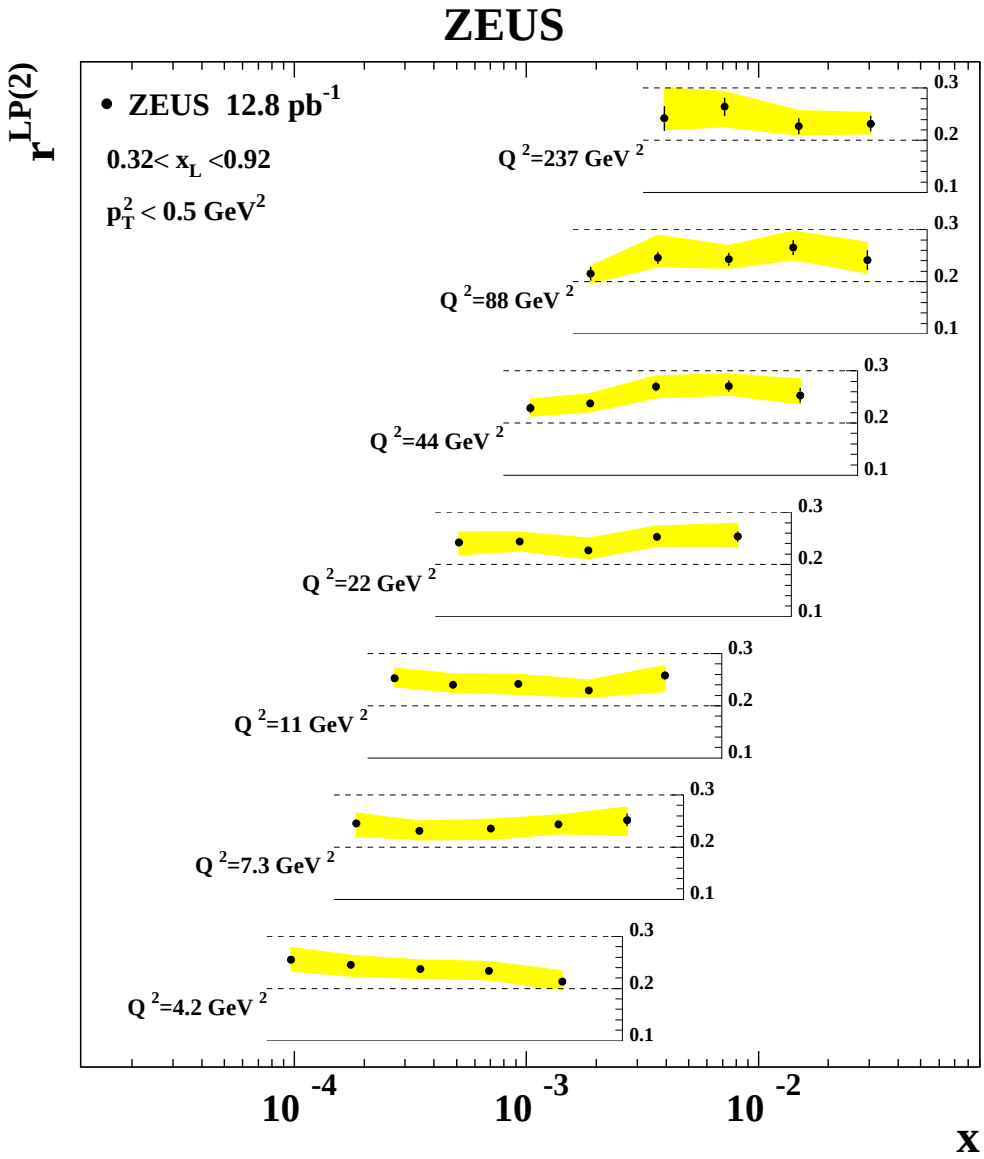

Figure 13. The leading proton production rate, $r^{\mathrm{LP}(2)}$, as a function of x in bins of Q^2, in the kinematic range indicated in the figure. The bands represent the correlated systematic uncertainty.

The rate of leading proton production as a function of x and Q^2, integrated over $0.32 < x_L < 0.92$ and $p_T^2 < 0.5\,\mathrm{GeV}^2$, $r^{\mathrm{LP}(2)}(x, Q^2)$, is shown in figure 13 and given in table 10. The ratio $r^{\mathrm{LP}(2)}$ is approximately constant as a function of x and of Q^2. The mean value $\langle r^{\mathrm{LP}(2)} \rangle = 0.240 \pm 0.001(\mathrm{stat.})^{+0.020}_{-0.018}(\mathrm{syst.})$ means that approximately 24% of inclusive DIS events have a leading proton in the range $0.32 < x_L < 0.92$ with $p_T^2 < 0.5\,\mathrm{GeV}^2$.

The ratio $\langle r^{\mathrm{LP}(2)} \rangle$ averaged over x as a function of Q^2 is shown in figure 14 and given in table 11, in the range $0.32 < x_L < 0.92$, $p_T^2 < 0.5\,\mathrm{GeV}^2$ and $45 < W < 225\,\mathrm{GeV}$.

JHEP06(2009)074

$\langle Q^2 \rangle$ (GeV^2)	x	$r^{\mathrm{LP(2)}}$
4.2	$9.6 \cdot 10^{-5}$	$0.256 \pm 0.006^{+0.023}_{-0.022}$
	$1.7 \cdot 10^{-4}$	$0.245 \pm 0.004^{+0.018}_{-0.021}$
	$3.5 \cdot 10^{-4}$	$0.237 \pm 0.004^{+0.018}_{-0.017}$
	$6.9 \cdot 10^{-4}$	$0.234 \pm 0.004^{+0.018}_{-0.016}$
	$1.46 \cdot 10^{-3}$	$0.214 \pm 0.006^{+0.020}_{-0.016}$
7.3	$1.9 \cdot 10^{-4}$	$0.246 \pm 0.006^{+0.020}_{-0.024}$
	$3.4 \cdot 10^{-4}$	$0.231 \pm 0.005^{+0.019}_{-0.016}$
	$6.9 \cdot 10^{-4}$	$0.236 \pm 0.005^{+0.018}_{-0.021}$
	$1.36 \cdot 10^{-3}$	$0.243 \pm 0.006^{+0.019}_{-0.018}$
	$2.67 \cdot 10^{-3}$	$0.252 \pm 0.012^{+0.025}_{-0.030}$
11	$2.6 \cdot 10^{-4}$	$0.253 \pm 0.007^{+0.020}_{-0.016}$
	$4.6 \cdot 10^{-4}$	$0.241 \pm 0.005^{+0.020}_{-0.015}$
	$9.2 \cdot 10^{-4}$	$0.242 \pm 0.005^{+0.018}_{-0.019}$
	$1.83 \cdot 10^{-3}$	$0.230 \pm 0.005^{+0.019}_{-0.014}$
	$3.98 \cdot 10^{-3}$	$0.258 \pm 0.008^{+0.019}_{-0.030}$
22	$5.1 \cdot 10^{-4}$	$0.242 \pm 0.007^{+0.020}_{-0.023}$
	$9.2 \cdot 10^{-4}$	$0.244 \pm 0.006^{+0.018}_{-0.018}$
	$1.84 \cdot 10^{-4}$	$0.227 \pm 0.005^{+0.022}_{-0.016}$
	$3.66 \cdot 10^{-3}$	$0.253 \pm 0.007^{+0.020}_{-0.018}$
	$7.83 \cdot 10^{-3}$	$0.254 \pm 0.010^{+0.025}_{-0.020}$
44	$1.03 \cdot 10^{-3}$	$0.228 \pm 0.009^{+0.017}_{-0.015}$
	$1.86 \cdot 10^{-3}$	$0.238 \pm 0.008^{+0.019}_{-0.016}$
	$3.68 \cdot 10^{-3}$	$0.270 \pm 0.009^{+0.020}_{-0.021}$
	$7.33 \cdot 10^{-3}$	$0.271 \pm 0.011^{+0.023}_{-0.017}$
	$1.54 \cdot 10^{-3}$	$0.253 \pm 0.014^{+0.031}_{-0.016}$
88	$2.00 \cdot 10^{-3}$	$0.215 \pm 0.013^{+0.015}_{-0.019}$
	$3.59 \cdot 10^{-3}$	$0.245 \pm 0.011^{+0.043}_{-0.017}$
	$7.37 \cdot 10^{-3}$	$0.243 \pm 0.013^{+0.026}_{-0.017}$
	$1.42 \cdot 10^{-2}$	$0.265 \pm 0.015^{+0.032}_{-0.023}$
	$3.01 \cdot 10^{-2}$	$0.241 \pm 0.019^{+0.034}_{-0.024}$
237	$4.00 \cdot 10^{-2}$	$0.242 \pm 0.024^{+0.069}_{-0.021}$
	$7.52 \cdot 10^{-2}$	$0.264 \pm 0.018^{+0.029}_{-0.038}$
	$1.47 \cdot 10^{-2}$	$0.227 \pm 0.015^{+0.029}_{-0.017}$
	$3.25 \cdot 10^{-2}$	$0.232 \pm 0.015^{+0.021}_{-0.019}$

Table 10. The leading proton production rate, $r^{\mathrm{LP(2)}}$, measured as a function of x in bins of Q^2, with average $\langle Q^2 \rangle$, for protons with $0.32 < x_L < 0.92$ and $p_T^2 < 0.5\ GeV^2$. Statistical uncertainties are listed first, followed by systematic uncertainties.

A mild increase with Q^2 cannot be excluded. To further investigate the Q^2 dependence, the rates integrated over $0.6 < x_L < 0.97$ can be compared to the equivalent rates for

JHEP06(2009)074

Q^2 (GeV^2)	$\langle r^{\mathrm{LP}(2)} \rangle$	
	$0.6 < x_L < 0.97$	$0.32 < x_L < 0.92$
5.1	$0.145 \pm 0.001^{+0.010}_{-0.010}$	$0.238 \pm 0.002^{+0.018}_{-0.017}$
15.8	$0.149 \pm 0.001^{+0.011}_{-0.009}$	$0.241 \pm 0.002^{+0.018}_{-0.015}$
81.1	$0.151 \pm 0.002^{+0.011}_{-0.009}$	$0.245 \pm 0.003^{+0.019}_{-0.015}$

Table 11. The leading proton production rate, $\langle r^{\mathrm{LP}(2)} \rangle$, averaged over x, as a function of Q^2, for protons with $p_T^2 < 0.5\ GeV^2$ in two x_L ranges as denoted in the table. Statistical uncertainties are listed first, followed by systematic uncertainties.

$\langle Q^2 \rangle = 0.29\,\mathrm{GeV}^2$ measured by the ZEUS collaboration previously [7]. The result is shown in figure 14 and included in table 11. Assuming that the systematic uncertainties have a similar origin, dominated by the LPS acceptance, a steady rise with Q^2 is observed. A similar effect was observed in leading neutron production [36], where it was attributed to absorption and rescattering effects [44], which disappear when the transverse size of the virtual photon decreases with increasing Q^2.

10.4 The leading proton structure functions

The ratio $r^{\mathrm{LP}(2)}$ can be expressed as the ratio of $F_2^{\mathrm{LP}(2)}$ to F_2,

$$r^{\mathrm{LP}(2)}(x, Q^2) = \frac{F_2^{\mathrm{LP}(2)}(x, Q^2)}{F_2(x, Q^2)}, \tag{10.2}$$

where $F_2^{\mathrm{LP}(2)}$ is obtained from $F_2^{\mathrm{LP}(4)}$ by integrating over x_L and p_T^2. Therefore, the values of $F_2^{\mathrm{LP}(2)}$ can be obtained from the measured $r^{\mathrm{LP}(2)}$ and F_2. The values of F_2 were obtained from the NLO ZEUS-S fit parameterisation of the parton distribution functions of the proton [45].

The structure-function $F_2^{\mathrm{LP}(2)}$ is presented in figure 15, plotted as a function of x at fixed Q^2 values for $0.32 < x_L < 0.92$, $p_T^2 < 0.5\,\mathrm{GeV}^2$ and given in table 12. The curves in the plot show the F_2 parameterisation scaled by the average value $\langle r^{\mathrm{LP}(2)} \rangle = 0.24$ and the bands represent the one-standard-deviation limits of the NLO ZEUS-S parameterisation. A very good description of $F_2^{\mathrm{LP}(2)}$ is obtained, as expected from the approximate x and Q^2 independence of $r^{\mathrm{LP}(2)}$.

10.5 Comparison to leading neutrons

The rate of leading proton production for $p_T^2 < 0.04\,\mathrm{GeV}^2$ can be compared to the recent ZEUS measurement of leading neutrons [36]. The comparison is shown in figure 16. In the range $0.32 < x_L < 0.92$, there are approximately twice as many protons as neutrons. This is consistent with the additive quark model [46], in which the probabilities to have a proton or a neutron in the final state are 2/3 and 1/3, respectively. In a particle exchange model, the exchange of isovector particles would result in half as many protons as neutrons. Thus, exchange of isoscalars must be invoked to account for the observed proton rate, notably

JHEP06(2009)074

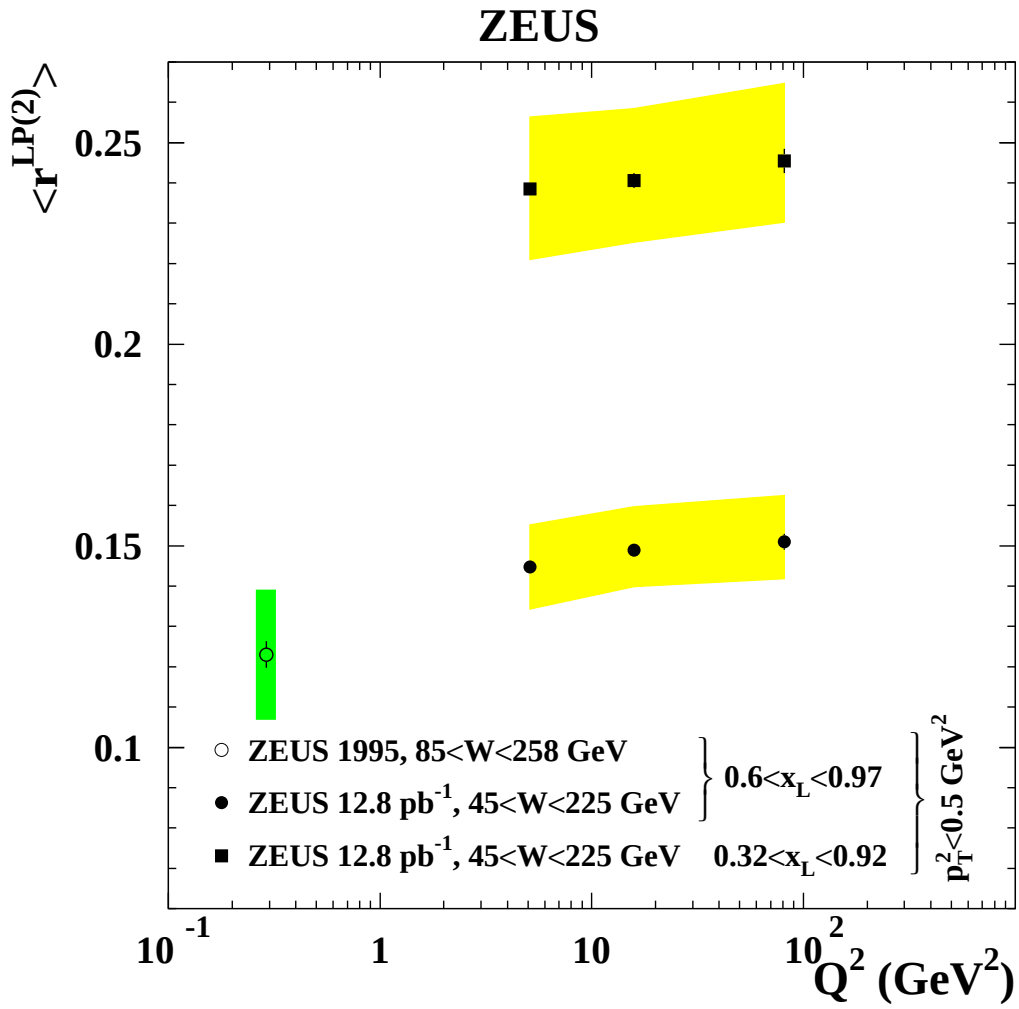

Figure 14. The leading proton production rate averaged over x, $\langle r^{\mathrm{LP}(2)} \rangle$, as a function of Q^2 in two different ranges of x_L, in the kinematic range indicated in the figure. The bands represent the correlated systematic uncertainty.

the f_0 trajectory at intermediate-low x_L and the Pomeron trajectory at high x_L [13]. This contribution is likely also to explain the different behaviour of the rates at large x_L.

The slopes of the p_T^2 distributions for leading protons and neutrons are shown in figure 17. Although the p_T^2 and Q^2 ranges are different, the two slopes have similar values in the region $0.65 < x_L < 0.8$.

10.6 Comparison to models

The predictions of the model of Szczurek et al. [13] are compared to the leading proton production rate $1/\sigma_{\mathrm{inc}} \cdot d\sigma_{\mathrm{LP}}/dx_L$ and the p_T^2 slopes in figure 18. In this model, leading proton production for $0.6 < x_L < 0.9$ is dominated by isoscalar Reggeon exchange. Diffrac-

JHEP06(2009)074

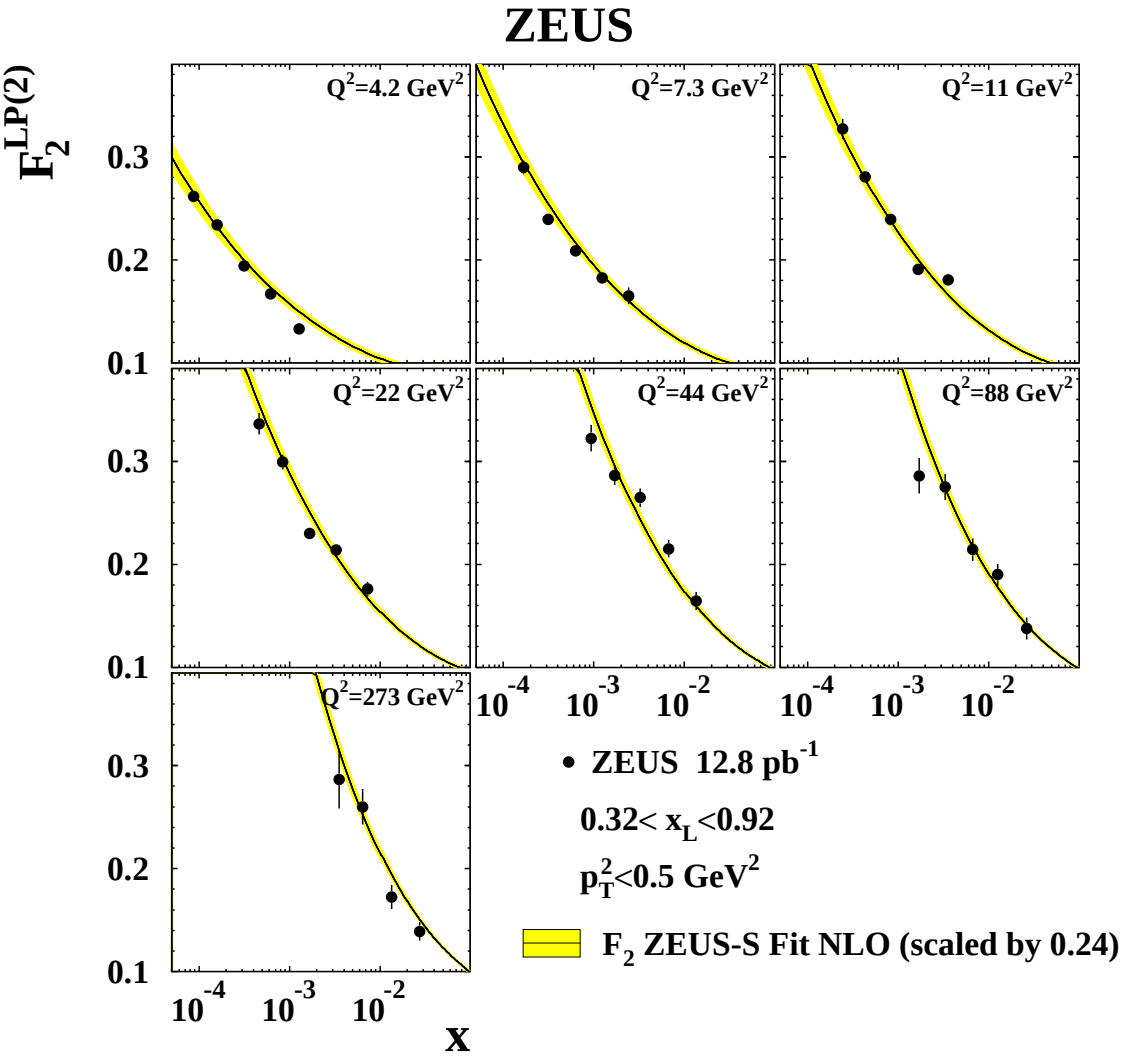

Figure 15. The leading proton structure function, $F^{\mathrm{LP}(2)}$, as a function of x in bins of Q^2, in the kinematic range indicated in the figure. For clarity, only the statistical uncertainties are shown. The systematic uncertainties are listed in table 12. The lines show the F_2 parameterisation scaled by 0.24, the approximate average value of $r^{\mathrm{LP}(2)}$. The bands show the one-standard deviation limits of the F_2 parameterisation.

tive processes due to Pomeron exchange become increasingly important as x_L approaches unity. The contribution of pion exchange plays an important role in the medium x_L range. The model describes the shape of the longitudinal momentum spectrum and of the p_T^2 slopes reasonably well. The normalisation of the Reggeon contribution, which has a large theoretical uncertainty [13], may be constrained by this measurement. The model does not include absorptive corrections and rescattering effects [44], since they are expected to be small in DIS regime.

JHEP06(2009)074

$\langle Q^2 \rangle$ (GeV^2)	x	$F_2^{\mathrm{LP(2)}}$
4.2	$9.6 \cdot 10^{-5}$	$0.262 \pm 0.006^{+0.023}_{-0.024}$
	$1.7 \cdot 10^{-4}$	$0.234 \pm 0.004^{+0.021}_{-0.018}$
	$3.5 \cdot 10^{-4}$	$0.195 \pm 0.003^{+0.015}_{-0.015}$
	$6.9 \cdot 10^{-4}$	$0.167 \pm 0.003^{+0.012}_{-0.013}$
	$1.46 \cdot 10^{-3}$	$0.133 \pm 0.004^{+0.011}_{-0.013}$
7.3	$1.9 \cdot 10^{-4}$	$0.290 \pm 0.007^{+0.030}_{-0.024}$
	$3.4 \cdot 10^{-4}$	$0.239 \pm 0.005^{+0.018}_{-0.020}$
	$6.9 \cdot 10^{-4}$	$0.209 \pm 0.004^{+0.019}_{-0.016}$
	$1.36 \cdot 10^{-3}$	$0.183 \pm 0.004^{+0.014}_{-0.015}$
	$2.67 \cdot 10^{-3}$	$0.165 \pm 0.008^{+0.021}_{-0.018}$
11	$2.6 \cdot 10^{-4}$	$0.327 \pm 0.010^{+0.023}_{-0.027}$
	$4.6 \cdot 10^{-4}$	$0.281 \pm 0.005^{+0.018}_{-0.024}$
	$9.2 \cdot 10^{-4}$	$0.239 \pm 0.005^{+0.020}_{-0.019}$
	$1.83 \cdot 10^{-3}$	$0.191 \pm 0.004^{+0.012}_{-0.017}$
	$3.98 \cdot 10^{-3}$	$0.181 \pm 0.006^{+0.022}_{-0.015}$
22	$5.1 \cdot 10^{-4}$	$0.336 \pm 0.010^{+0.033}_{-0.030}$
	$9.2 \cdot 10^{-4}$	$0.299 \pm 0.007^{+0.023}_{-0.023}$
	$1.84 \cdot 10^{-3}$	$0.230 \pm 0.005^{+0.017}_{-0.023}$
	$3.66 \cdot 10^{-3}$	$0.210 \pm 0.006^{+0.016}_{-0.018}$
	$7.83 \cdot 10^{-3}$	$0.176 \pm 0.007^{+0.015}_{-0.018}$
44	$1.03 \cdot 10^{-4}$	$0.322 \pm 0.013^{+0.025}_{-0.027}$
	$1.86 \cdot 10^{-3}$	$0.286 \pm 0.009^{+0.022}_{-0.025}$
	$3.68 \cdot 10^{-3}$	$0.265 \pm 0.009^{+0.023}_{-0.022}$
	$7.33 \cdot 10^{-3}$	$0.215 \pm 0.008^{+0.016}_{-0.020}$
	$1.54 \cdot 10^{-2}$	$0.164 \pm 0.009^{+0.014}_{-0.022}$
88	$2.00 \cdot 10^{-3}$	$0.286 \pm 0.017^{+0.030}_{-0.027}$
	$3.59 \cdot 10^{-3}$	$0.275 \pm 0.013^{+0.023}_{-0.050}$
	$7.37 \cdot 10^{-3}$	$0.214 \pm 0.011^{+0.018}_{-0.026}$
	$1.42 \cdot 10^{-2}$	$0.190 \pm 0.010^{+0.020}_{-0.025}$
	$3.01 \cdot 10^{-2}$	$0.138 \pm 0.011^{+0.017}_{-0.022}$
273	$4.00 \cdot 10^{-3}$	$0.287 \pm 0.028^{+0.038}_{-0.087}$
	$7.52 \cdot 10^{-3}$	$0.260 \pm 0.017^{+0.041}_{-0.034}$
	$1.47 \cdot 10^{-2}$	$0.173 \pm 0.012^{+0.017}_{-0.025}$
	$3.25 \cdot 10^{-2}$	$0.139 \pm 0.009^{+0.015}_{-0.016}$

Table 12. The leading proton structure function, $F_2^{\mathrm{LP(2)}}$, measured as a function of x in bins of Q^2, with average $\langle Q^2 \rangle$, for protons with $0.32 < x_L < 0.92$ and $p_T^2 < 0.5\ GeV^2$. Statistical uncertainties are listed first, followed by systematic uncertainties.

In figure 19, various DIS Monte Carlo models are compared to the experimental data. The prediction of DJANGOH [37] with SCI [40] and RAPGAP [47] are compared to the leading

JHEP06(2009)074

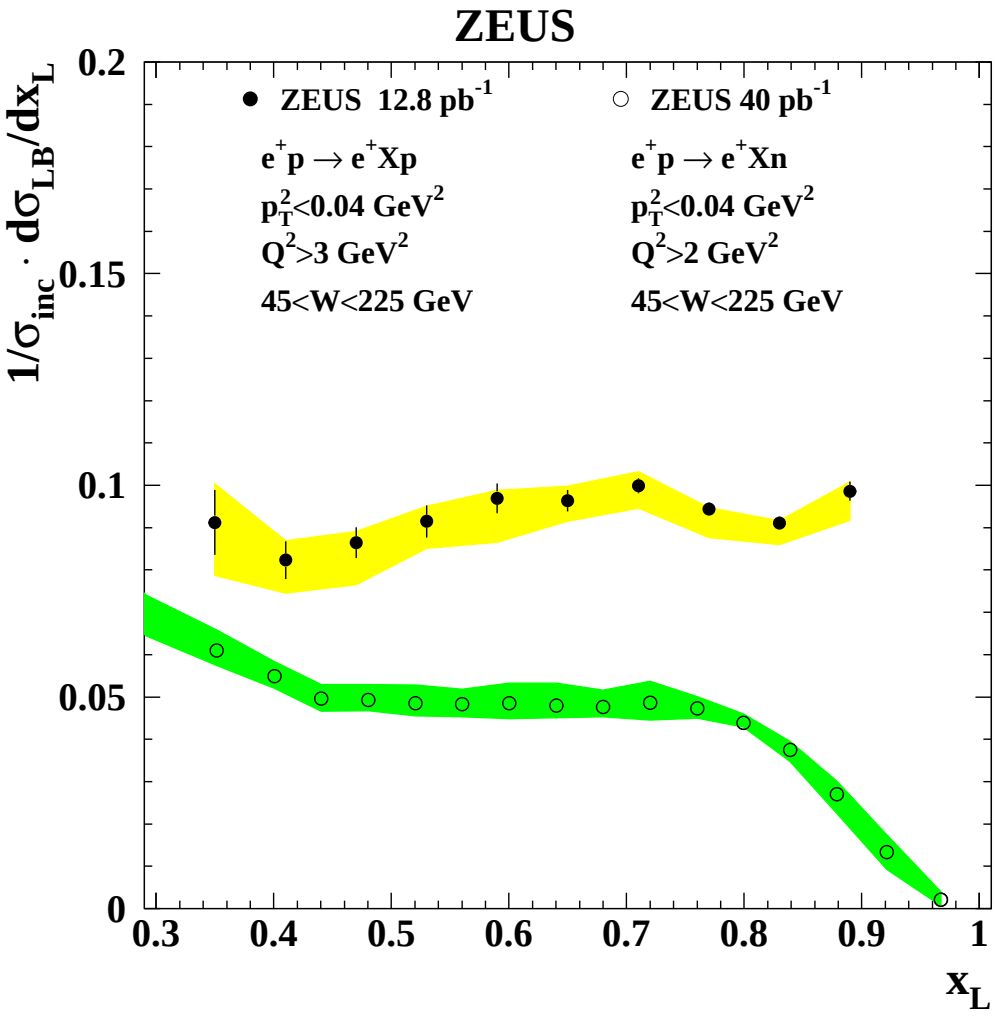

Figure 16. The rate $1/\sigma_{\rm inc} \cdot d\sigma_{\rm LB}/dx_L$ for leading proton (dots) and leading neutron production (circles). The bands show the systematic uncertainties.

proton production rate $1/\sigma_{\rm inc} \cdot d\sigma_{\rm LP}/dx_L$ and to the p_T^2 slopes. In both MC models, the QCD radiation was performed either by the parton shower [40] or colour dipole (CDM) [48] models. None of the DIS Monte Carlo models can reproduce the flat dependence of x_L below the diffractive peak. The MC generator DJANGOH, with SCI and MEPS, reproduces quite well the dependence of b on x_L, although the mean values of the slope are lower than those measured. In the other MC models, the value of the slope is consistent with the measurements only at high x_L.

11 Summary

The cross section of leading proton production for $x_L > 0.32$ and $p_T^2 < 0.5\,\text{GeV}^2$ and its ratio to the inclusive DIS cross section have been measured in the range $Q^2 > 3\,\text{GeV}^2$

JHEP06(2009)074

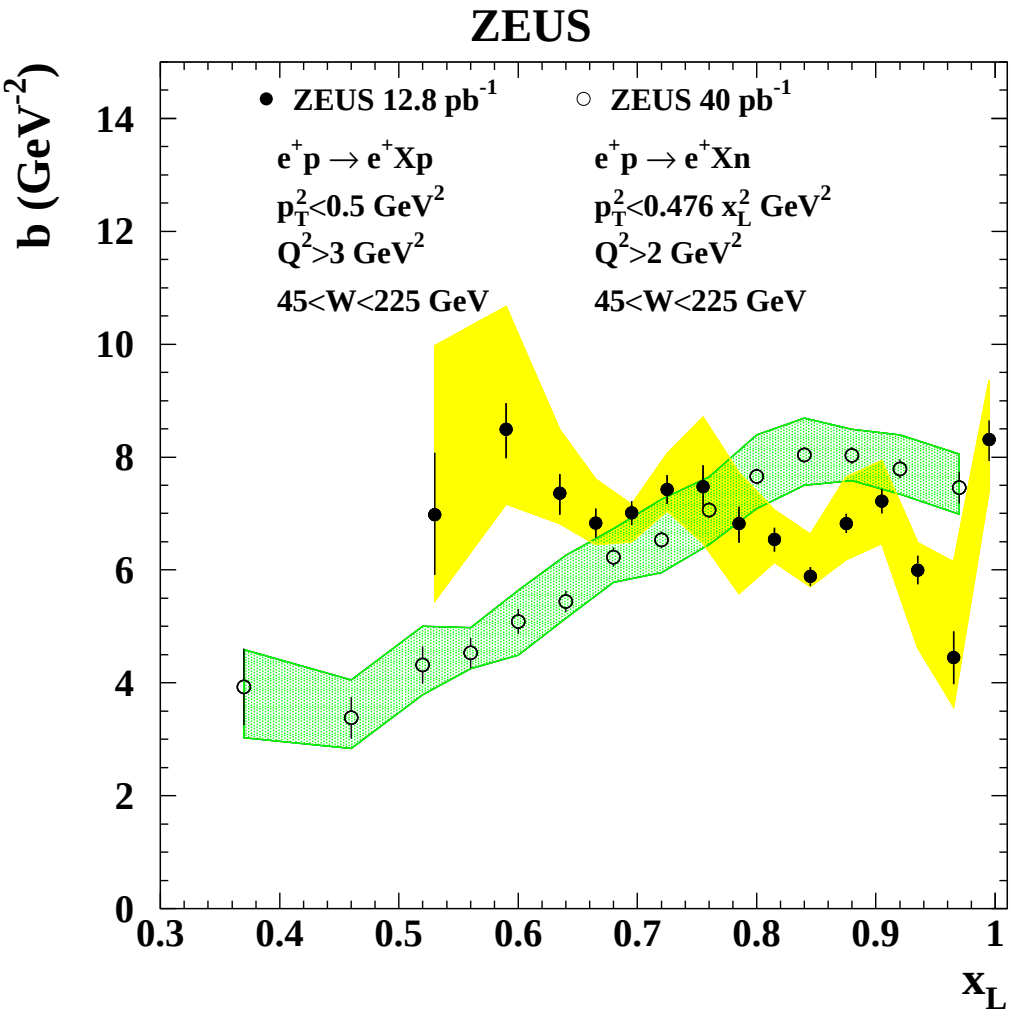

Figure 17. The p_T^2-slope, b, as a function of x_L for leading proton (dots) and leading neutron (circles) production. The bands show the systematic uncertainties.

and $45 < W < 225\,\text{GeV}$, with 12.8 pb^{-1} collected during 1997 with the ZEUS leading proton spectrometer. The leading proton production cross section as a function of p_T^2 falls exponentially with a mean slope $\langle b \rangle = 6.76 \pm 0.07(\text{stat.})^{+0.63}_{-0.52}(\text{syst.})\,\text{GeV}^{-2}$, approximately independently of x_L and of the photon virtuality, Q^2. Below the diffractive peak, the x_L distribution is flat, independent of p_T^2 and Q^2.

The ratios of leading proton production to the inclusive DIS yields, $r^{\text{LP}(2)}$ and $r^{\text{LP}(3)}$, show no strong dependence on x or Q^2. In the range $0.32 < x_L < 0.92$ and $p_T^2 < 0.5\,\text{GeV}^2$, approximately 24% of DIS events have a leading proton. The ratio $\langle r^{\text{LP}(2)} \rangle$ averaged over x rises very slowly with Q^2 in the DIS regime. This trend is further confirmed by measurements at lower Q^2. The dependence of the leading proton structure-function $F_2^{\text{LP}(2)}$ on x and Q^2 is approximately the same as that of F_2.

JHEP06(2009)074

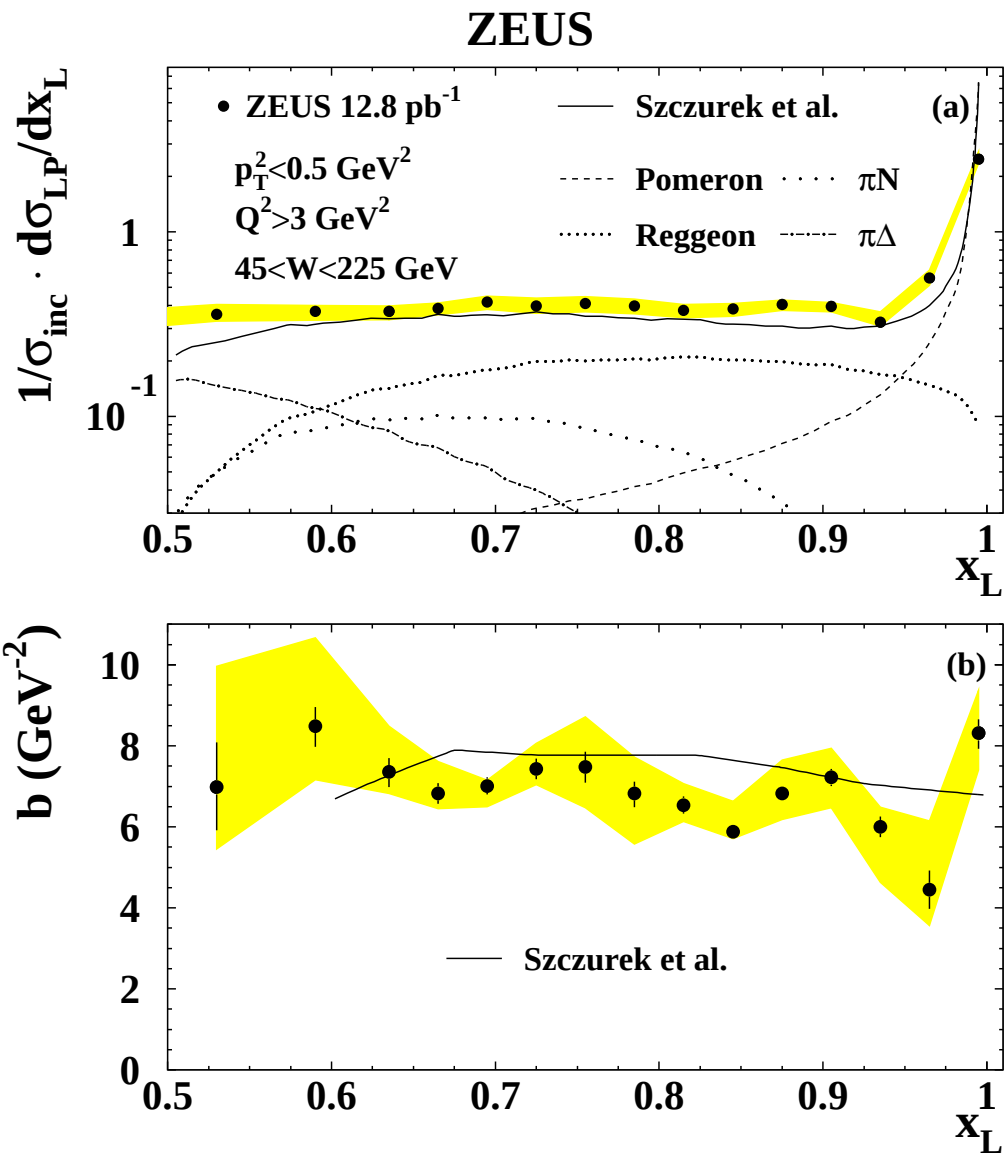

Figure 18. A Regge-based model [13] compared to (a) the measured leading proton production rate, $1/\sigma_{\rm inc} \cdot d\sigma_{\rm LP}/dx_L$, and (b) the p_T^2-slope, b. The bands show the systematic uncertainties.

The yield of leading protons in DIS is almost twice that of leading neutrons. The p_T^2 slopes have a different dependence on x_L, and have compatible values in the range $0.65 < x_L < 0.8$.

The main features of the experimental data are reproduced by a Regge-inspired model. The results of this study are an important ingredient for modelling leading particle production in hadron-hadron interactions, which is not properly reproduced by existing generators.

JHEP06(2009)074

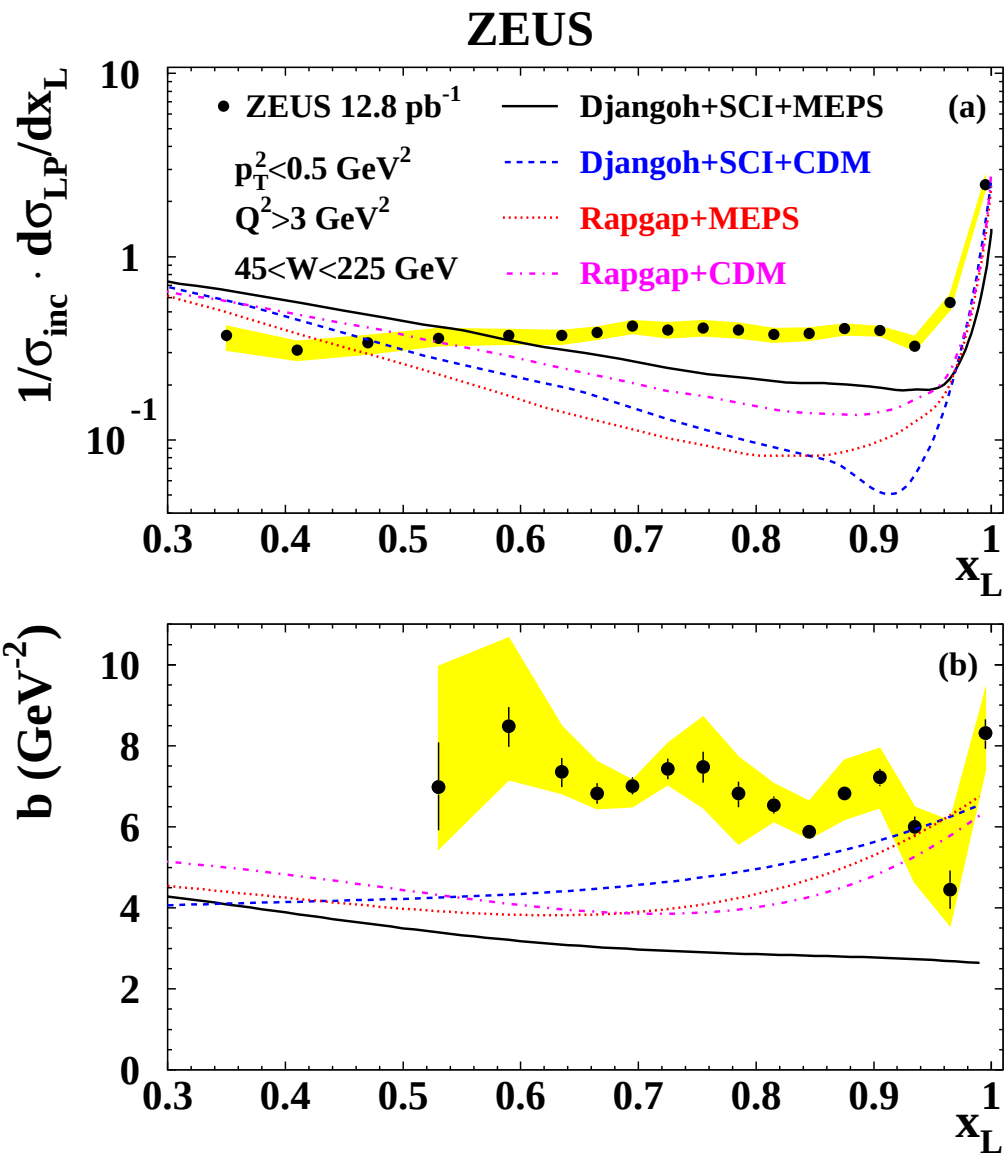

Figure 19. Expectations of various Monte Carlo models of DIS, as described in the figure, compared to (a) the leading proton production rate, $1/\sigma_{\rm inc} \cdot d\sigma_{\rm LP}/dx_L$, and (b) the p_T^2-slope, b. The bands show the systematic uncertainties.

Acknowledgments

We thank the DESY Directorate for their encouragement, and gratefully acknowledge the support of the DESY computing and network services. We are specially grateful to the HERA machine group: collaboration with them was crucial for the successful installation and operation of the leading proton spectrometer. The design, construction and installation

JHEP06(2009)074

of the ZEUS detector have been made possible by the ingenuity and effort of many people from DESY and home institutes who are not listed as authors. Finally, it is a pleasure to thank F. A. Ceccopieri and L. Trentadue for many useful discussions.

Author list

S. Chekanov, M. Derrick, S. Magill, B. Musgrave, D. Nicholass,[1] J. Repond and R. Yoshida
Argonne National Laboratory,
Argonne, Illinois 60439–4815, U.S.A.[n]

M.C.K. Mattingly
Andrews University,
Berrien Springs, Michigan 49104–0380, U.S.A.

P. Antonioli, G. Bari, L. Bellagamba, D. Boscherini, A. Bruni, G. Bruni, G. Cara Romeo F. Cindolo, M. Corradi, P. Giusti, G. Iacobucci, A. Margotti, T. Massam, R. Nania and A. Polini
INFN Bologna,
Bologna, Italy[e]

S. Antonelli, M. Basile, M. Bindi, L. Cifarelli, A. Contin, F. Palmonari, S. De Pasquale,[2] G. Sartorelli and A. Zichichi
University and INFN Bologna,
Bologna, Italy[e]

D. Bartsch, I. Brock, H. Hartmann, E. Hilger, H.-P. Jakob, M. Jüngst, A.E. Nuncio-Quiroz, E. Paul, U. Samson, V. Schönberg, R. Shehzadi and M. Wlasenko
Physikalisches Institut der Universität Bonn,
Bonn, Germany[b]

N.H. Brook, G.P. Heath and J.D. Morris
H.H. Wills Physics Laboratory, University of Bristol,
Bristol, U.K.[m]

M. Kaur, P. Kaur[3] and I. Singh[3]
Panjab University, Department of Physics,
Chandigarh, India

JHEP06(2009)074

M. Capua, S. Fazio, L. Ianotti, A. Mastroberardino, M. Schioppa, G. Susinno and E. Tassi
Calabria University, Physics Department and INFN,
Cosenza, Italy[e]

J.Y. Kim
Chonnam National University,
Kwangju, South Korea

Z.A. Ibrahim, F. Mohamad Idris, B. Kamaluddin and W.A.T. Wan Abdullah
Jabatan Fizik, Universiti Malaya,
50603 Kuala Lumpur, Malaysia[r]

Y. Ning, Z. Ren and F. Sciulli
Nevis Laboratories, Columbia University,
Irvington on Hudson, New York 10027, U.S.A.[o]

J. Chwastowski, A. Eskreys, J. Figiel, A. Galas, K. Olkiewicz, B. Pawlik, P. Stopa and L. Zawiejski
The Henryk Niewodniczanski Institute of Nuclear Physics, Polish Academy of Sciences,
Cracow, Poland[i]

L. Adamczyk, T. Bołd, I. Grabowska-Bołd, D. Kisielewska, J. Łukasik,[4]
M. Przybycień and L. Suszycki
Faculty of Physics and Applied Computer Science, AGH-University of Science and Technology,
Cracow, Poland[p]

A. Kotański[5] **and W. Słomiński**[6]
Department of Physics, Jagellonian University,
Cracow, Poland

O. Behnke, U. Behrens, C. Blohm, A. Bonato, K. Borras, D. Bot, R. Ciesielski, N. Coppola, S. Fang, J. Fourletova,[7] **A. Geiser, P. Göttlicher,**[8] **J. Grebenyuk, I. Gregor, T. Haas, W. Hain, A. Hüttmann, F. Januschek, B. Kahle, I.I. Katkov,**[9] **U. Klein,**[10] **U. Kötz, H. Kowalski, M. Lisovyi, E. Lobodzinska, B. Löhr, R. Mankel,**[11] **I.-A. Melzer-Pellmann, S. Miglioranzi,**[12] **A. Montanari, T. Namsoo, D. Notz,**[11] **A. Parenti, L. Rinaldi,**[13] **P. Roloff, I. Rubinsky, U. Schneekloth, A. Spiridonov,**[14] **D. Szuba,**[15] **J. Szuba,**[16] **T. Theedt, J. Ukleja,**[17] **G. Wolf, K. Wrona, A.G. Yagües Molina, C. Youngman and W. Zeuner**[11]
Deutsches Elektronen-Synchrotron DESY,
Hamburg, Germany

JHEP06(2009)074

V. Drugakov, W. Lohmann and S. Schlenstedt
Deutsches Elektronen-Synchrotron DESY,
Zeuthen, Germany

G. Barbagli and E. Gallo
INFN Florence,
Florence, Italy[e]

P. G. Pelfer
University and INFN Florence,
Florence, Italy[e]

A. Bamberger, D. Dobur, F. Karstens and N.N. Vlasov[18]
Fakultät für Physik der Universität Freiburg i.Br.,
Freiburg i.Br., Germany[b]

P.J. Bussey,[19] **A.T. Doyle, W. Dunne, M. Forrest, M. Rosin, D.H. Saxon and I.O. Skillicorn**
Department of Physics and Astronomy, University of Glasgow,
Glasgow, U.K.[m]

I. Gialas[20] **and K. Papageorgiu**
Department of Engineering in Management and Finance, Univ. of Aegean,
Greece

U. Holm, R. Klanner, E. Lohrmann, H. Perrey, P. Schleper, T. Schörner-Sadenius, J. Sztuk, H. Stadie and M. Turcato
Hamburg University, Institute of Exp. Physics,
Hamburg, Germany[b]

C. Foudas, C. Fry, K.R. Long and A.D. Tapper
Imperial College London, High Energy Nuclear Physics Group,
London, U.K.[m]

T. Matsumoto, K. Nagano, K. Tokushuku,[21] **S. Yamada and Y. Yamazaki**[22]
Institute of Particle and Nuclear Studies, KEK,
Tsukuba, Japan[f]

A.N. Barakbaev, E.G. Boos, N.S. Pokrovskiy and B.O. Zhautykov
Institute of Physics and Technology of Ministry of Education and Science of Kazakhstan,
Almaty, Kazakhstan

JHEP06(2009)074

V. Aushev,[23] O. Bachynska, M. Borodin, I. Kadenko, A. Kozulia, V. Libov, D. Lontkovskyi, I. Makarenko, Iu. Sorokin, A. Verbytskyi and O. Volynets
Institute for Nuclear Research, National Academy of Sciences, Kiev, Ukraine and Kiev National University, Kiev, Ukraine

D. Son
Kyungpook National University, Center for High Energy Physics, Daegu, South Korea[g]

J. de Favereau and K. Piotrzkowski
Institut de Physique Nucléaire, Université Catholique de Louvain, Louvain-la-Neuve, Belgium[q]

F. Barreiro, C. Glasman, M. Jimenez, L. Labarga, J. del Peso, E. Ron, M. Soares, J. Terrón, C. Uribe-Estrada and M. Zambrana
Departamento de Física Teórica, Universidad Autónoma de Madrid, Madrid, Spain[l]

F. Corriveau, C. Liu, J. Schwartz, R. Walsh and C. Zhou
Department of Physics, McGill University, Montréal, Québec, H3A 2T8, Canada[a]

T. Tsurugai
Meiji Gakuin University, Faculty of General Education, Yokohama, Japan[f]

A. Antonov, B.A. Dolgoshein, D. Gladkov, V. Sosnovtsev, A. Stifutkin and S. Suchkov
Moscow Engineering Physics Institute, Moscow, Russia[j]

R.K. Dementiev, P.F. Ermolov †, L.K. Gladilin, Yu.A. Golubkov, L.A. Khein, I.A. Korzhavina, V.A. Kuzmin, B.B. Levchenko,[24] O.Yu. Lukina, A.S. Proskuryakov, L.M. Shcheglova and D.S. Zotkin
Moscow State University, Institute of Nuclear Physics, Moscow, Russia[k]

I. Abt, A. Caldwell, D. Kollar, B. Reisert and W.B. Schmidke
Max-Planck-Institut für Physik, München, Germany

JHEP06(2009)074

G. Grigorescu, A. Keramidas, E. Koffeman, P. Kooijman, A. Pellegrino, H. Tiecke, M. Vázquez[12] and L. Wiggers
NIKHEF and University of Amsterdam,
Amsterdam, Netherlands[h]

N. Brümmer, B. Bylsma, L.S. Durkin, A. Lee and T.Y. Ling
Physics Department, Ohio State University,
Columbus, Ohio 43210, U.S.A.[n]

P.D. Allfrey, M.A. Bell, A.M. Cooper-Sarkar, R.C.E. Devenish, J. Ferrando, B. Foster, C. Gwenlan,[25] K. Horton,[26] K. Oliver, A. Robertson and R. Walczak
Department of Physics, University of Oxford,
Oxford U.K.[m]

A. Bertolin, F. Dal Corso, S. Dusini, A. Longhin and L. Stanco
INFN Padova,
Padova, Italy[e]

P. Bellan, R. Brugnera, R. Carlin, A. Garfagnini and S. Limentani
Dipartimento di Fisica dell' Università and INFN,
Padova, Italy[e]

B.Y. Oh, A. Raval and J.J. Whitmore[27]
Department of Physics, Pennsylvania State University,
University Park, Pennsylvania 16802, U.S.A.[o]

Y. Iga
Polytechnic University,
Sagamihara, Japan[f]

G. D'Agostini, G. Marini and A. Nigro
Dipartimento di Fisica, Università 'La Sapienza' and INFN,
Rome, Italy[e]

J.E. Cole[28] and J.C. Hart
Rutherford Appleton Laboratory, Chilton,
Didcot, Oxon, U.K.[m]

D. Epperson,[29] C. Heusch, H. Sadrozinski, A. Seiden, R. Wichmann[30] and D.C. Williams
University of California,
Santa Cruz, California 95064, U.S.A.[n]

JHEP06(2009)074

H. Abramowicz,[31] **R. Ingbir, S. Kananov, A. Levy and A. Stern**
Raymond and Beverly Sackler Faculty of Exact Sciences, School of Physics, Tel Aviv University,
Tel Aviv, Israel[d]

M. Kuze and J. Maeda
Department of Physics, Tokyo Institute of Technology,
Tokyo, Japan[f]

R. Hori, S. Kagawa,[32] **N. Okazaki, S. Shimizu and T. Tawara**
Department of Physics, University of Tokyo,
Tokyo, Japan[f]

R. Hamatsu, H. Kaji,[33] **S. Kitamura,**[34] **O. Ota**[35] **and Y.D. Ri**
Tokyo Metropolitan University, Department of Physics,
Tokyo, Japan[f]

R. Cirio, M. Costa, M.I. Ferrero, V. Monaco, C. Peroni, M.C. Petrucci, R. Sacchi, V. Sola and A. Solano
Università di Torino and INFN,
Torino, Italy[e]

N. Cartiglia, S. Maselli and A. Staiano
INFN Torino,
Torino, Italy[e]

M. Arneodo and M. Ruspa
Università del Piemonte Orientale,
Novara, Italy and
INFN,
Torino, Italy[e]

S. Fourletov,[7] **J.F. Martin and T.P. Stewart**
Department of Physics, University of Toronto,
Toronto, Ontario, M5S 1A7, Canada[a]

S.K. Boutle,[20] **J.M. Butterworth, T.W. Jones, J.H. Loizides and M. Wing**[36]
Physics and Astronomy Department, University College London,
London, U.K.[m]

JHEP06(2009)074

B. Brzozowska, J. Ciborowski,[37] G. Grzelak, P. Kulinski, P. Łużniak,[38] J. Malka,[38] R.J. Nowak, J.M. Pawlak, W. Perlanski,[38] T. Tymieniecka[39] and A.F. Żarnecki
Warsaw University, Institute of Experimental Physics, Warsaw, Poland

M. Adamus, P. Plucinski[40] and A. Ukleja
Institute for Nuclear Studies, Warsaw, Poland

Y. Eisenberg, D. Hochman and U. Karshon
Department of Particle Physics, Weizmann Institute, Rehovot, Israel[c]

E. Brownson, D.D. Reeder, A.A. Savin, W.H. Smith and H. Wolfe
Department of Physics, University of Wisconsin, Madison, Wisconsin 53706, U.S.A.[n]

S. Bhadra, C.D. Catterall, Y. Cui, G. Hartner, S. Menary, U. Noor, J. Standage and J. Whyte
Department of Physics, York University, Ontario, M3J1P3, Canada[a]

[1] *also affiliated with University College London, U.K.*
[2] *now at University of Salerno, Italy*
[3] *also working at Max Planck Institute, Munich, Germany*
[4] *now at Institute of Aviation, Warsaw, Poland*
[5] *supported by the research grant no. 1 P03B 04529 (2005–2008)*
[6] *This work was supported in part by the Marie Curie Actions Transfer of Knowledge project COCOS (contract MTKD-CT-2004–517186)*
[7] *now at University of Bonn, Germany*
[8] *now at DESY, group FEB, Hamburg, Germany*
[9] *also at Moscow State University, Russia*
[10] *now at University of Liverpool, UK*
[11] *on leave of absence at CERN, Geneva, Switzerland*
[12] *now at CERN, Geneva, Switzerland*
[13] *now at Bologna University, Bologna, Italy*
[14] *also at Institut of Theoretical and Experimental Physics, Moscow, Russia*
[15] *also at INP, Cracow, Poland*
[16] *also at FPACS, AGH-UST, Cracow, Poland*
[17] *partially supported by Warsaw University, Poland*
[18] *partly supported by Moscow State University, Russia*
[19] *Royal Society of Edinburgh, Scottish Executive Support Research Fellow*
[20] *also affiliated with DESY, Germany*

JHEP06(2009)074

[21] *also at University of Tokyo, Japan*
[22] *now at Kobe University, Japan*
[23] *supported by DESY, Germany*
[24] *partly supported by Russian Foundation for Basic Research grant no. 05–02–39028-NSFC-a*
[25] *STFC Advanced Fellow*
[26] *nee Korcsak-Gorzo*
[27] *This material was based on work supported by the National Science Foundation, while working at the Foundation.*
[28] *now at University of Kansas, Lawrence, U.S.A.*
[29] *now at West Valley College, Saratoga, CA 95070–5698, U.S.A.*
[30] *now at DESY, group MPY, Hamburg, Germany*
[31] *also at Max Planck Institute, Munich, Germany, Alexander von Humboldt Research Award*
[32] *now at KEK, Tsukuba, Japan*
[33] *now at Nagoya University, Japan*
[34] *member of Department of Radiological Science, Tokyo Metropolitan University, Japan*
[35] *now at SunMelx Co. Ltd., Tokyo, Japan*
[36] *also at Hamburg University, Inst. of Exp. Physics, Alexander von Humboldt Research Award and partially supported by DESY, Hamburg, Germany*
[37] *also at Łódź University, Poland*
[38] *member of Łódź University, Poland*
[39] *also at University of Podlasie, Siedlce, Poland*
[40] *now at Lund Universtiy, Lund, Sweden*
[†] *deceased*
[a] *supported by the Natural Sciences and Engineering Research Council of Canada (NSERC)*
[b] *supported by the German Federal Ministry for Education and Research (BMBF), under contract numbers 05 HZ6PDA, 05 HZ6GUA, 05 HZ6VFA and 05 HZ4KHA*
[c] *supported in part by the MINERVA Gesellschaft für Forschung GmbH, the Israel Science Foundation (grant no. 293/02–11.2) and the U.S.-Israel Binational Science Foundation*
[d] *supported by the Israel Science Foundation*
[e] *supported by the Italian National Institute for Nuclear Physics (INFN)*
[f] *supported by the Japanese Ministry of Education, Culture, Sports, Science and Technology (MEXT) and its grants for Scientific Research*
[g] *supported by the Korean Ministry of Education and Korea Science and Engineering Foundation*
[h] *supported by the Netherlands Foundation for Research on Matter (FOM)*
[i] *supported by the Polish State Committee for Scientific Research, project no. DESY/256/2006 - 154/DES/2006/03*
[j] *partially supported by the German Federal Ministry for Education and Research (BMBF)*
[k] *supported by RF Presidential grant N 1456.2008.2 for the leading scientific schools and by the Russian Ministry of Education and Science through its grant for Scientific Research on High Energy Physics*

JHEP06(2009)074

[l] *supported by the Spanish Ministry of Education and Science through funds provided by CICYT*

[m] *supported by the Science and Technology Facilities Council, UK*

[n] *supported by the US Department of Energy*

[o] *supported by the US National Science Foundation. Any opinion, findings and conclusions or recommendations expressed in this material are those of the authors and do not necessarily reflect the views of the National Science Foundation.*

[p] *supported by the Polish Ministry of Science and Higher Education as a scientific project (2006–2008)*

[q] *supported by FNRS and its associated funds (IISN and FRIA) and by an Inter-University Attraction Poles Programme subsidised by the Belgian Federal Science Policy Office*

[r] *supported by an FRGS grant from the Malaysian government*

References

[1] R.P. Feynman, *Very high-energy collisions of hadrons*, *Phys. Rev. Lett.* **23** (1969) 1415 [SPIRES].

[2] M. Basile et al., *The 'leading' particle effect in hadron physics*, *Nuovo Cim.* **A 66** (1981) 129 [SPIRES]; *The 'leading' baryon effect in strong, weak and electromagnetic interactions*, *Lett. Nuovo Cim.* **32** (1981) 321 [SPIRES].

[3] V.N. Gribov et al., *The creation of QCD and the effective energy*, L.N. Lipatov ed., World Scientific Series in 20$^{\text{th}}$ Century Physics, Vol. 25, World Scientific, Singapore (2001).

[4] J. Whitmore and M. Derrick, *Multiplicity distributions in the reaction $p + p \to p+$ anything*, *Phys. Lett.* **B 50** (1974) 280 [SPIRES].

[5] A.E. Brenner et al., *Experimental study of single particle inclusive hadron scattering and associated multiplicities*, *Phys. Rev.* **D 26** (1982) 1497 [SPIRES].

[6] M. Aguilar-Benitez et al., *Inclusive particle production in 400 GeV/c p p interactions*, *Z. Phys.* **C 50** (1991) 405 [SPIRES].

[7] ZEUS collaboration, S. Chekanov et al., *Leading proton production in e+ p collisions at HERA*, *Nucl. Phys.* **B 658** (2003) 3 [hep-ex/0210029] [SPIRES].

[8] H1 collaboration, C. Adloff et al., *Measurement of leading proton and neutron production in deep inelastic scattering at HERA*, *Eur. Phys. J.* **C 6** (1999) 587 [hep-ex/9811013] [SPIRES]; *Photoproduction with a leading proton at HERA*, *Nucl. Phys.* **B 619** (2001) 3 [hep-ex/0106070] [SPIRES].

[9] J.D. Sullivan, *One pion exchange and deep inelastic electron-nucleon scattering*, *Phys. Rev.* **D 5** (1972) 1732 [SPIRES].

[10] V.R. Zoller, *Peripheral structure of nucleon in probing with high Q^2 photons*, *Z. Phys.* **C 53** (1992) 443 [SPIRES].

[11] H. Holtmann, G. Levman, N.N. Nikolaev, A. Szczurek and J. Speth, *How to measure the pion structure function at HERA*, *Phys. Lett.* **B 338** (1994) 363 [SPIRES].

[12] B. Kopeliovich, B. Povh and I. Potashnikova, *Deep-inelastic electroproduction of neutrons in the proton fragmentation region*, *Z. Phys.* **C 73** (1996) 125 [hep-ph/9601291] [SPIRES].

JHEP06(2009)074

[13] A. Szczurek, N.N. Nikolaev and J. Speth, *Leading proton spectrum from DIS at HERA*, *Phys. Lett.* **B 428** (1998) 383 [hep-ph/9712261] [SPIRES].

[14] A. Edin, G. Ingelman and J. Rathsman, *Soft color interactions as the origin of rapidity gaps in DIS*, *Phys. Lett.* **B 366** (1996) 371 [hep-ph/9508386] [SPIRES].

[15] L. Trentadue and G. Veneziano, *Fracture functions: an improved description of inclusive hard processes in QCD*, *Phys. Lett.* **B 323** (1994) 201 [SPIRES];
D. Graudenz, *One particle inclusive processes in deeply inelastic lepton-nucleon scattering*, *Nucl. Phys.* **B 432** (1994) 351 [hep-ph/9406274] [SPIRES];
L. Trentadue, *Fracture functions*, *Nucl. Phys. Proc. Suppl.* **B 39** (1995) 50 [hep-ph/9506324] [SPIRES]; *Fracture functions*, *Nucl. Phys. Proc. Suppl.* **B 64** (1998) 152 [SPIRES];
D. de Florian and R. Sassot, *Phenomenology of forward hadrons in DIS: fracture functions and its Q^2 evolution*, *Phys. Rev.* **D 56** (1997) 426 [hep-ph/9703228] [SPIRES]; *QCD analysis of diffractive and leading proton DIS structure functions in the framework of fracture functions*, *Phys. Rev.* **D 58** (1998) 054003 [hep-ph/9804240] [SPIRES].

[16] ZEUS collaboration, M. Derrick et al., *Study of elastic ρ^0 photoproduction at HERA using the ZEUS leading proton spectrometer*, *Z. Phys.* **C 73** (1997) 253 [hep-ex/9609003] [SPIRES].

[17] ZEUS collaboration, S. Chekanov et al., *Dissociation of virtual photons in events with a leading proton at HERA*, *Eur. Phys. J.* **C 38** (2004) 43 [hep-ex/0408009] [SPIRES].

[18] M.T. Dova and S. Ferrari, *Confronting models on cosmic ray interactions with particle physics at LHC energies*, *Eur. Phys. J.* **C 52** (2007) 673 [hep-ph/0702238] [SPIRES].

[19] R.S. Fletcher, T.K. Gaisser, P. Lipari and T. Stanev, *SIBYLL: an event generator for simulation of high-energy cosmic ray cascades*, *Phys. Rev.* **D 50** (1994) 5710 [SPIRES].

[20] N.N. Kalmykov, S.S. Ostapchenko and A.I. Pavlov, *Quark-gluon string model and EAS simulation problems at ultra-high energies*, *Nucl. Phys. Proc. Suppl.* **52B** (1997) 17 [SPIRES].

[21] ZEUS collaboration, U. Holm ed., *The ZEUS detector*, status report (unpublished), available on http://www-zeus.desy.de/bluebook/bluebook.html, DESY, Germany (1993).

[22] N. Harnew et al., *Vertex triggering using time difference measurements in the ZEUS central tracking detector*, *Nucl. Instrum. Meth.* **A 279** (1989) 290 [SPIRES];
ZEUS collaboration, B. Foster et al., *The performance of the ZEUS central tracking detector z-by-timing electronics in a transputer based data acquisition system*, *Nucl. Phys. Proc. Suppl.* **B 32** (1993) 181 [SPIRES]; *The design and construction of the ZEUS central tracking detector*, *Nucl. Instrum. Meth.* **A 338** (1994) 254 [SPIRES].

[23] M. Derrick et al., *Design and construction of the ZEUS barrel calorimeter*, *Nucl. Instrum. Meth.* **A 309** (1991) 77 [SPIRES];
ZEUS Calorimeter Group collaboration, A. Andresen et al., *Construction and beam test of the ZEUS forward and rear calorimeter*, *Nucl. Instrum. Meth.* **A 309** (1991) 101 [SPIRES];
A. Caldwell et al., *Design and implementation of a high precision readout system for the ZEUS calorimeter*, *Nucl. Instrum. Meth.* **A 321** (1992) 356 [SPIRES].

[24] A. Bernstein et al., *Beam tests of the ZEUS barrel calorimeter*, *Nucl. Instr. Meth.* **A 336** (1993) 23 [SPIRES].

JHEP06(2009)074

[25] A. Dwuraźny et al., *Experimental study of electron-hadron separation in calorimeters using silicon diodes*, *Nucl. Instrum. Meth.* **A 277** (1989) 176 [SPIRES].

[26] S. Bhadra et al., *Test of a forward neutron calorimeter for the ZEUS experiment at HERA*, *Nucl. Instrum. Meth.* **A 354** (1995) 479 [SPIRES];
ZEUS FNC Group collaboration, S. Bhadra et al., *Design and test of a forward neutron calorimeter for the ZEUS experiment*, *Nucl. Instrum. Meth.* **A 394** (1997) 121 [hep-ex/9701015] [SPIRES];
S. Bhadra et al., *The calorimetry of single particles with energies up to* 820 *GeV using the ZEUS forward neutron calorimeter*, in *Proceedings of the Seventh International Conference on calorimetry in High Energy Physics*, E. Cheu et al. eds., Tucson Arizona U.S.A. (1997), pg. 295 [SPIRES].

[27] ZEUS Luminosity Group collaboration, J. Andruszków et al., *First measurement of HERA luminosity by ZEUS lumi monitor*, Preprint DESY-92-066, DESY, Germany (1992) [SPIRES];
ZEUS collaboration, M. Derrick et al., *Measurement of total and partial photon proton cross-sections at* 180 *GeV center-of-mass energy*, *Z. Phys.* **C 63** (1994) 391 [SPIRES];
ZEUS Luminosity Group collaboration, J. Andruszków et al., *Luminosity measurement in the ZEUS experiment*, *Acta Phys. Polon.* **B 32** (2001) 2025 [SPIRES].

[28] H. Abramowicz, A. Caldwell and R. Sinkus, *Neural network based electron identification in the ZEUS calorimeter*, *Nucl. Instrum. Meth.* **A 365** (1995) 508 [hep-ex/9505004] [SPIRES].

[29] ZEUS collaboration, J. Breitweg et al., *Measurement of the diffractive structure function* $F_2^{D(4)}$ *at HERA*, *Eur. Phys. J.* **C 1** (1998) 81 [hep-ex/9709021] [SPIRES]; *Measurement of the diffractive cross-section in deep inelastic scattering using ZEUS* 1994 *data*, *Eur. Phys. J.* **C 6** (1999) 43 [hep-ex/9807010] [SPIRES];
G. Briskin, *Diffractive dissociation in e p deep inelastic scattering*, Ph.D. Thesis, report DESY-THESIS-1998-036, Tel Aviv University, Tel-Aviv Israel (1998) [SPIRES].

[30] ZEUS collaboration, S. Chekanov et al., *Study of deep inelastic inclusive and diffractive scattering with the ZEUS forward plug calorimeter*, *Nucl. Phys.* **B 713** (2005) 3 [hep-ex/0501060] [SPIRES].

[31] ZEUS collaboration, J. Breitweg et al., *Measurement of the proton structure function* F^2 *and* $\sigma_{\rm tot}(\gamma^* p)$ *at low* Q^2 *and very low* x *at HERA*, *Phys. Lett.* **B 407** (1997) 432 [hep-ex/9707025] [SPIRES].

[32] S. Bentvelsen, J. Engelen and P. Kooijman, *Reconstruction of* (x, Q^2) *and extraction of structure functions at HERA*, in *Proceedings of the Workshop on Physics at HERA*, Volume 1, W. Buchmüller and G. Ingelman eds., DESY, Germany (1991), pg. 23;
K.C. Höger, *Measurement of* x, y *and* Q^2 *in neutral current events*, in *Proceedings of the Workshop on Physics at HERA*, Volume 1, W. Buchmüller and G. Ingelman eds., DESY, Germany (1991), pg. 43.

[33] F. Jacquet and A. Blondel, *Detectors for charged current events*, in *Proceedings of the Study of an ep Facility for Europe*, U. Amaldi ed., Hamburg Germany (1979), pg. 391 [DESY-79-48] [SPIRES].

[34] W.H. Smith, K. Tokushuku and L.W. Wiggers, *The ZEUS trigger system*, in *Proc. of Int. conference "Computing in High Energy Physics" (CHEP'92)*, Annecy, France (1992) [DESY-92-150] [SPIRES].

JHEP06(2009)074

[35] L. Rinaldi, *Measurement of leading-proton production cross section in DIS with the ZEUS detector at HERA*, Ph.D. Thesis, report DESY-THESIS-2006-028, University of Bologna, Bologna Italy (2006) [SPIRES].

[36] ZEUS collaboration, S. Chekanov et al., *Leading neutron energy and p_T distributions in deep inelastic scattering and photoproduction at HERA*, *Nucl. Phys.* **B 776** (2007) 1 [hep-ex/0702028] [SPIRES].

[37] G.A. Schüler and H. Spiesberger, *DJANGO: the interface for the event generators HERACLES and LEPTO*, in *Proceedings of the Workshop on Physics at HERA*, Volume 3, W. Buchmüller and G. Ingelman eds., DESY, Germany (1991), pg. 1419 [SPIRES];
H. Spiesberger, *DJANGOH*, http://wwwthep.physik.uni-mainz.de/~hspiesb/djangoh/djangoh.html.

[38] A. Kwiatkowski, H. Spiesberger and H.-J. Möhring, *HERACLES: an event generator for ep interactions at HERA energies including radiative processes*, *Comput. Phys. Commun.* **69** (1992) 155 [SPIRES].

[39] T. Sjöstrand et al., *High-energy-physics event generation with PYTHIA* 6.1, *Comput. Phys. Commun.* **135** (2001) 238 [hep-ph/0010017] [SPIRES].

[40] G. Ingelman, A. Edin and J. Rathsman, *LEPTO* 6.5 — *a Monte Carlo generator for deep inelastic lepton-nucleon scattering*, *Comput. Phys. Commun.* **101** (1997) 108 [hep-ph/9605286] [SPIRES].

[41] T. Sjöstrand and M. Bengtsson, *The Lund Monte Carlo for jet fragmentation and e^+e^- physics — jetset version* 6.3 — *an update*, *Comput. Phys. Commun.* **43** (1987) 367 [SPIRES];
T. Sjöstrand, *High-energy-physics event generation with PYTHIA* 5.7 *and JETSET* 7.4, *Comput. Phys. Commun.* **82** (1994) 74 [SPIRES].

[42] R. Brun et al., *GEANT*3, Technical Report CERN DD/EE/84-1, CERN, Geneva Switzerland (1987) [SPIRES].

[43] G. Bruni et al., *Leading proton production in ep and pp experiments: how well do high-energy physics Monte Carlo generators reproduce the data?*, in *Proceedings of the HERA-LHC workshop*, H. Jung and A. de Roeck eds., CERN-2005-014, (2005), pg. 605 [hep-ph/0601013] [SPIRES].

[44] N.N. Nikolaev, W. Schafer, A. Szczurek and J. Speth, *Do the E*866 *Drell-Yan data change our picture of the chiral structure of the nucleon?*, *Phys. Rev.* **D 60** (1999) 014004 [hep-ph/9812266] [SPIRES];
U. D'Alesio and H.J. Pirner, *Target fragmentation in pp, ep and γp collisions at high energies*, *Eur. Phys. J.* **A 7** (2000) 109 [hep-ph/9806321] [SPIRES];
A.B. Kaidalov, V.A. Khoze, A.D. Martin and M.G. Ryskin, *Leading neutron spectra*, *Eur. Phys. J.* **C 47** (2006) 385 [hep-ph/0602215] [SPIRES];
V.A. Khoze, A.D. Martin and M.G. Ryskin, *Information from leading neutrons at HERA*, *Eur. Phys. J.* **C 48** (2006) 797 [hep-ph/0606213] [SPIRES].

[45] ZEUS collaboration, S. Chekanov et al., *An NLO QCD analysis of inclusive cross-section and jet-production data from the zeus experiment*, *Eur. Phys. J.* **C 42** (2005) 1 [hep-ph/0503274] [SPIRES].

[46] E.M. Levin and L.L. Frankfurt, *The quark hypothesis and relations between cross-sections at high-energies*, *JETP Lett.* **2** (1965) 65 [SPIRES].

JHEP06(2009)074

[47] H. Jung, *Hard diffractive scattering in high energy ep collisions and the Monte Carlo generator RAPGAP*, *Comput. Phys. Commun.* **86** (1995) 147 [SPIRES].

[48] L. Lönnblad, *Ariadne version 4 — a program for simulation of QDC cascades implementing the colour dipole model*, *Comput. Phys. Commun.* **71** (1992) 15 [SPIRES].

JHEP06(2009)074